

MAGNETOM FLASH

Content

ABDOMEN AND PELVIS

New Perspectives and
Challenges in Abdominal
Imaging with the
MAGNETOM Trio, A Tim System

Page 12

CARDIAC

Advances in Cardiac MRI
at 3T – Benefits of
Multi-Channel MR Systems

Page 30

MR ANGIOGRAPHY

An Overview of
Three Dimensional
Contrast-Enhanced MRA
at 3.0 Tesla

Page 40

NEUROLOGY

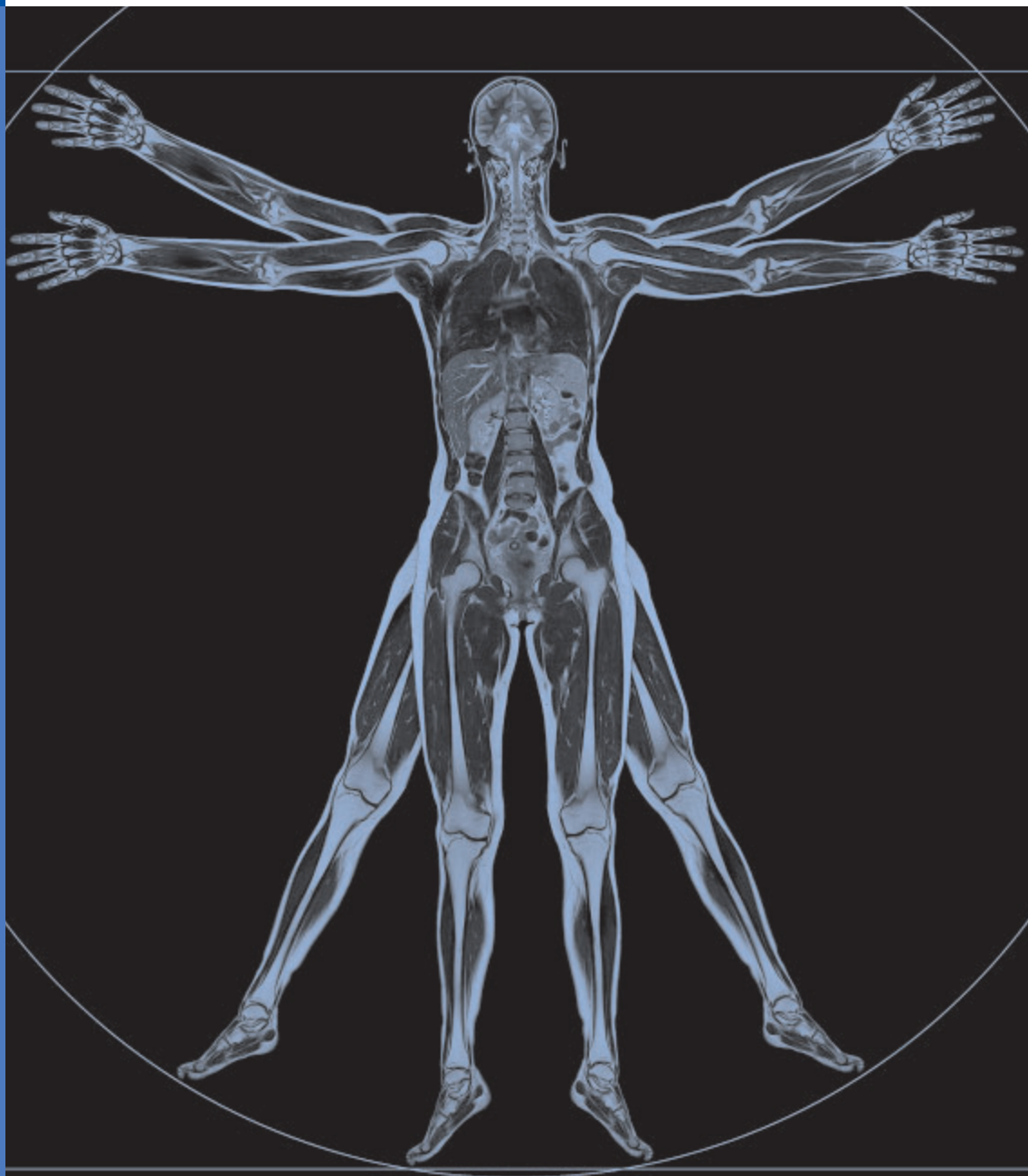
Neuroimaging at
MAGNETOM Trio, A Tim System

Page 54

TIM@3T

Tim at 3T: Highlights

Page 96



Dear MAGNETOM User,

At Siemens MR our constant goal is to provide you with better, earlier, faster, easier and more comprehensive medical diagnoses. This requires the development and implementation of the most advanced medical imaging technology. One such development is the availability of Tim (Total Imaging Matrix) – our revolutionary MR technology – at 3T. Siemens' constantly growing range of Tim products now includes MAGNETOM Trio.

3T MR systems – initially of interest mainly in research areas due to their higher image resolution – have enjoyed steadily increasing popularity in clinical routine over the last few years, and industry analysts predict that by 2008, 3T MRI will emerge as a mainstream investment for a majority of hospitals of all specializations. Siemens is the only manufacturer offering receiver coils for all applications in the 3T range, from abdominal, cardiological or orthopedic applications, whole-body scans or examinations of the whole spine. Thanks to its revolutionary acquisition ability to breakthrough applications, Tim has opened up new possibilities for 3T MRI.

The core of Tim technology is the revolutionary matrix coil concept. Up to 102 coil elements can be combined with up to 32 independent radio-frequency channels – providing much higher image quality. Tim allows parallel image acquisition along all three axes over the entire body up to a length of 182 cm (6 ft). The physician can choose any area relevant to the clinical question at hand – from individual sub-areas of the body to the entire anatomy – without having to limit the number of coils that can be connected.

iPAT (integrated Parallel Acquisition Techniques) technology makes the Trio the only 3T system on the market to perform parallel high-speed imaging with up to 16 PAT factors. Massive iPAT improves acquisition speed and image quality even further – a particular advantage for examining moving organs, such as the heart or the intestines, or for improved patient throughput. MAGNETOM Trio and Tim have turned pioneering medical research into daily clinical routine. Examples include:

- Virtual bone biopsy for the early diagnosis of osteoporosis with down to 0.3 mm³ image resolution. Early detection of osteoporosis could help by enabling early treatment that will delay the onset of symptoms, such as fractures.
- Potential early diagnosis of Alzheimer's disease as well as mental diseases (schizophrenia, depression, epilepsy etc). Accurate and early diagnosis will enable preventive treatment that could help very large numbers of patients.



Ioannis Panagiotelis, Ph.D Ultra High Field Segment Manager

- Potential prostate cancer diagnosis without endorectal coil (differentiation of benign and malignant tumours in the prostate without biopsy). This spares the patient from an invasive and painful examination.
- Resolution similar to digital mammography (image resolution 0.2 mm) for breast MR without radiation. This will help reduce repetitive breast scans with higher capability to differentiate between tumours and cysts.
- Accurate diagnosis of microscopic joint injuries, e.g. finger/toe joint injuries of football/basketball players, musicians, golfers and climbers. Imaging at this resolution could make the use of invasive diagnostic approaches like arthroscopy unnecessary.

Other articles cover a summary of 3T MRI's main clinical applications, highlight their benefits and limitations, analyze trends in 3T MRI utilization and outline future directions in MRI technology.

We hope you will enjoy this special edition of MAGNETOM FLASH, dedicated to 3T.

J. Panagiotelis

Ioannis Panagiotelis, Ph.D
Ultra High Field Segment Manager

The Editorial Team

We appreciate your comments.

Please contact us at magnetomworld.med@siemens.com



*Lisa Reid,
US Installed Base Manager,
Malvern, PA*



*Dagmar Thomsik-Schröpfer, Ph.D.
MR Marketing-Products, Erlangen*



*Antje Hellwich
Associate Editor*



*A. Nejat Bengi, M.D.
Editor in Chief*



*Heike Weh,
Clinical Data Manager,
Erlangen*



*Bernhard Baden,
Clinical Data Manager,
Erlangen*



*Tony Enright, Ph.D.
Asia Pacific Collaborations,
Australia*



*Milind Dhamankar, M.D.
Manager Clinical MR
Research Collaborations,
Siemens Medical
Solutions USA*



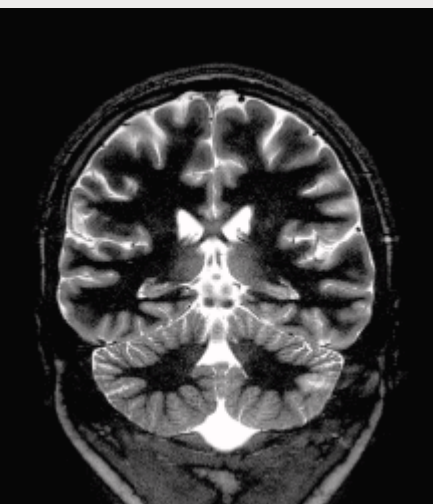
*Peter Kreisler, Ph.D.
Collaborations & Applications,
Erlangen*



*Gary R. McNeal, MS (BME)
Advanced Application Specialist,
Cardiovascular MR Imaging
Siemens Medical Solutions USA*



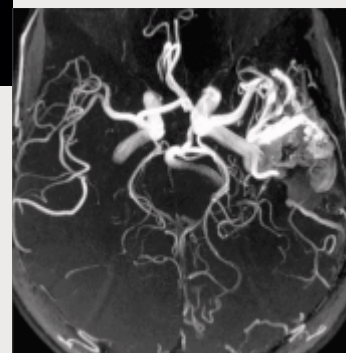
*Cécile Mohr, Ph.D.
Head of Market Segment
Management, Erlangen*



High Resolution T2 weighted 3T head imaging. **Page 54**



3D Volume rendered image of pulmonary venous anatomy at 3T. **Page 43**



Left temporal AVM with superior small vessel delineation at 3T. **Page 39**

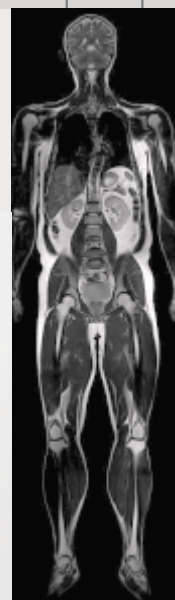
CLINICAL

- 8 ABDOMEN AND PELVIS**
MR Cholangiopancreatography at 3.0 Tesla – Initial Experience and Future Outlook
- 12 ABDOMEN AND PELVIS**
New Perspectives and Challenges in Abdominal Imaging with the MAGNETOM Trio, A Tim System
- 22 ABDOMEN AND PELVIS**
Accurate Prostate Cancer Staging with MR
- 26 ABDOMEN AND PELVIS**
Accurate Staging of Prostate Cancer with MR
- 30 CARDIAC**
Advances in Cardiac MRI at 3T – Benefits of Multi-Channel MR Systems
- 36 MR ANGIOGRAPHY**
Comparison of Intracranial 3D-ToF-MRA with and without Parallel Acquisition Techniques at 1.5T and 3.0T: Preliminary Results
- 40 MR ANGIOGRAPHY**
An Overview of Three Dimensional Contrast-Enhanced MRA at 3.0 Tesla
- 46 NEUROLOGY**
CSI-Measurements of the Human Brain at 3T
- 54 NEUROLOGY**
Neuroimaging at MAGNETOM Trio, A Tim System
- 60 NEUROLOGY**
SPACE Case Reports: Brain Imaging with MAGNETOM Trio
- 64 ORTHOPEDICS**
3T Cartilage Imaging in the Knee Joint
- 66 ORTHOPEDICS**
3T Imaging in the Hip
- 68 ORTHOPEDICS**
3T MRI in Orthopedics



3D Neuro taskcard showing functional activation. **Page 58**

The new Peripheral Angiography Coil of MAGNETOM Trio a Tim System. **Page 98**



Whole Body Imaging at 3T **Page 100**

- 72 ORTHOPEDICS**
Case Report: Comparison of Acetabular Labrum Lesion and Corresponding Cartilage
- 74 PEDIATRICS**
3T Neuropediatric Imaging, Initial Experience at the Children's Hospital of Philadelphia
- 77 SPACE**
SPACE (Clinical Practice)


TECHNOLOGY

- 82 MULTINUCLEAR MRS**
Multinuclear MR Spectroscopy at 3 Tesla
- 86 OPEN ARCHITECTURE**
University of Utah uses Siemens MAGNETOM Open Architecture for Applications from Carotid Wall Imaging to Image Guided Thermal Therapy
- 92 SPACE TECHNICAL**
SPACE: An Innovative Solution to Rapid, Low SAR, T2-Weighted Contrast in 3D Spin Echo Imaging
- 96 TIM@3T**
Tim at 3T: Highlights

LIFE

- 100 HONG KONG**
Initial Results from MAGNETOM Trio, A Tim System in Asia Pacific Hong Kong Sanatorium and Hospital
- 104 IMPRINT**

The information presented in MAGNETOM Flash is for illustration only and is not intended to be relied upon by the reader for instruction as to the practice of medicine. Any health care practitioner reading this information is reminded that they must use their own learning, training and expertise in dealing with their individual patients. This material does not substitute for that duty and is not intended by Siemens Medical Solutions to be used for any purpose in that regard. The drugs and doses mentioned in MAGNETOM Flash are consistent with the approval labeling for uses and/or indications of the drug. The treating physician bears the sole responsibility for the diagnosis and treatment of patients, including drugs and doses prescribed in connection with such use. The Operating Instructions must always be strictly followed when operating the MR System. The source for the technical data is the corresponding data sheets.



We see a way to change coils with a single mouse click

We see a way to increase patient throughput by 50%

Tim proves it.


SIEMENS

We see a way to do MRI with an increased signal-to-noise of up to 100%

www.siemens.com/medical

Results may vary. Data on file.

M-2934-1-7600

 **Proven Outcomes with Tim (Total imaging matrix technology).** In hundreds and hundreds of installations around the world, Tim® is proving that a new era in MRI is here. With Tim's unmatched 32 independent RF channels and up to 102 Matrix coil elements, you can combine coils in any way, for multi-organ exams, all in a single patient set-up. Offering incredible flexibility and accuracy.

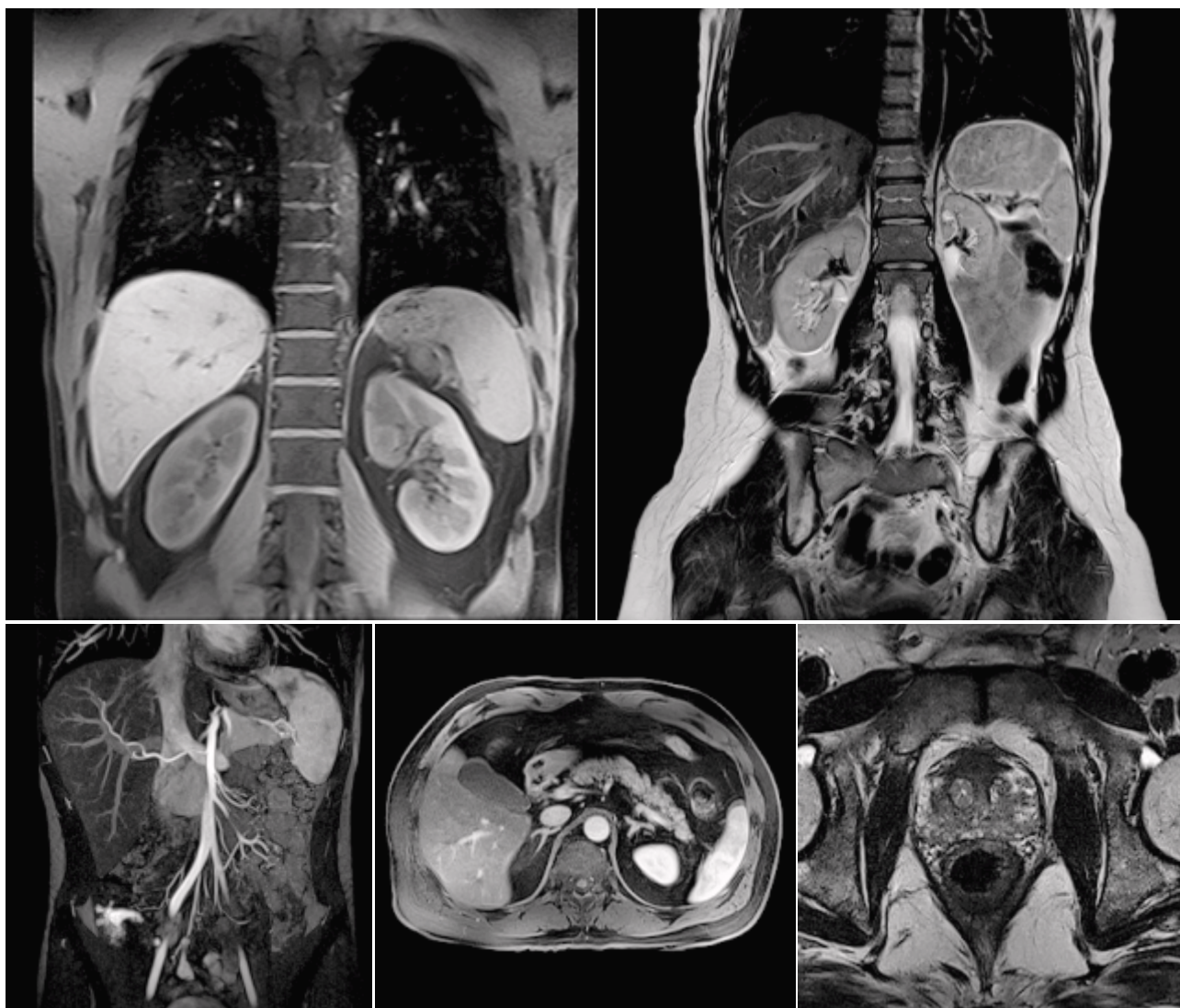
Ensuring no detail is lost — from the smallest lesions to a large organ or extended anatomical region. And with iPAT in all directions, you can actually reduce image time, yet scan at a higher resolution. Visit us at www.siemens.com/Tim and let Tim prove it to you.

Siemens **Medical Solutions** that help

SIEMENS
medical

Abdomen and Pelvis

MAGNETOM Trio, A Tim System enables for the first time comprehensive clinical abdominal imaging at 3T. The use of parallel imaging in combination with the Matrix coil technology helps overcome 3T related technical challenges like SAR limitations as well as physiological motion artefacts. In addition, the largest Field of View (FoV) and the best magnet homogeneity at 3T delivered with the system enable abdominal imaging with excellent fat saturation capable of delineating the finest abdominal structures.



MR Cholangiopancreatography at 3.0 Tesla – Initial Experience and Future Outlook

Elmar M. Merkle, M.D.¹ and Brian M. Dale, Ph.D.²

¹ Duke University Medical Center, Department of Radiology, Durham, NC, USA

² Siemens Medical Solutions, Cary, NC, USA

Introduction

Since its original description in 1991 by Wallner et al. [1], magnetic resonance cholangiopancreatography (MRCP) has gained general acceptance along with transabdominal ultrasound as the non-invasive imaging method of choice for diseases of the biliary system. It has replaced endoscopic retrograde cholangiography (ERC), particularly in those cases in which an endoscopic intervention seems unlikely at the outset [2]. While transabdominal ultrasound seems to be superior for gallbladder imaging, MRC is favored for evaluation of extrahepatic biliary ductal disease [3]. Unfortunately, both imaging modalities are of limited use for evaluating the intrahepatic biliary anatomy, particularly if the biliary system is not dilated. The underlying reasons are mainly limitations in spatial resolution and/or signal-to-noise. However, a detailed anatomical depiction of the 'non-distended' intrahepatic biliary ductal system is occasionally needed, e.g. for the preoperative evaluation of potential living liver donors. The introduction of whole body 3.0-Tesla MR systems in combination with a dedicated receive-only torso coil array is an appealing concept with the potential to overcome these limitations.

State-of-the-art MRCP imaging protocol

A current MRCP protocol at ultra-high field MR imaging is very similar to a standard 1.5 Tesla MRCP protocol and includes several steps. Following the acquisition of a multiplanar localizer, a HASTE sequence in coronal orientation and a Gradient Echo in and opposed phase sequence in axial orientation through the liver and pancreas are performed. These imaging data sets are primarily used to optimize the positioning of the subsequent 'dedicated' MRCP sequences. In particular the opposed phase imaging data set has been shown to be helpful as it allows the identification of the

pancreas with a high level of confidence even for inexperienced MR technologists due to the chemical shift artifact of the second kind (also known as India ink artifact). The dedicated MRCP sequences include single-slice breath hold RARE* (Rapid Acquisition with Relaxation Enhancement) in various angulations, multi-slice breath hold HASTE (Half Fourier Acquisition Single-Shot Turbo Spin Echo), and a respiratory triggered 3D Turbo Spin Echo sequence. A more detailed description is provided as follows:

Sequence 1: Triplanar localizer

TR/TE/FA/NSA = 15/5/40/1, 96 x 192 matrix, ST 10 mm

Sequence 2: Coronal T2-weighted HASTE

TR/TE/FA/NSA = 1000/83/136/1, 256 x 256 matrix, 17 slices, ST 8 mm

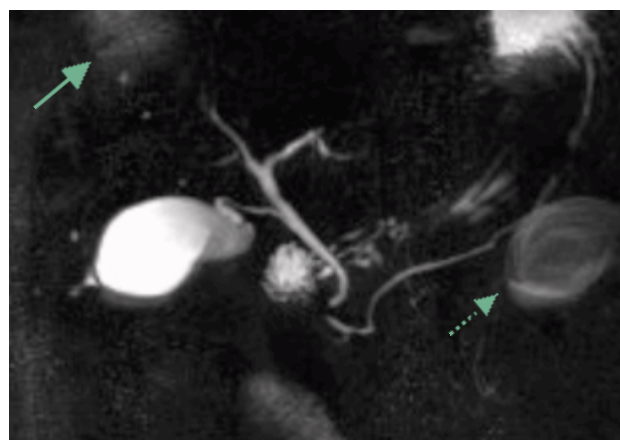


[Figure 1] Maximum intensity projection of a respiratory triggered coronal 3D T2-weighted TSE dataset showing a normal biliary and pancreatic ductal anatomy. Note ghosting artifacts from the stomach (solid arrow) and gallbladder (dashed arrow).

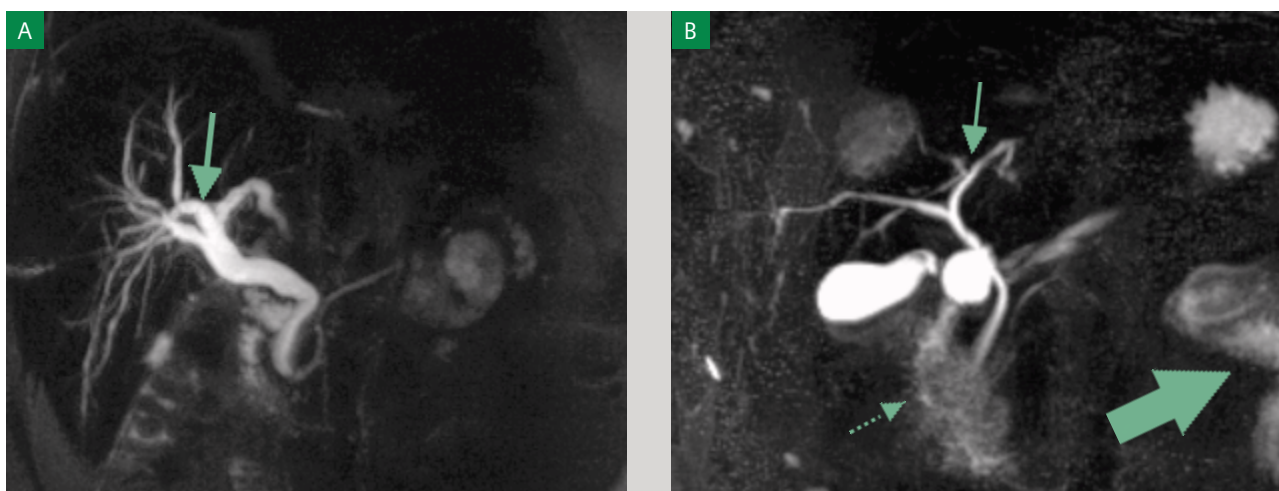


[Figure 2] Maximum intensity projections of a SPACE (A) and a respiratory triggered coronal 3D T2-weighted TSE (B) dataset showing two normal variants of the biliary ductal anatomy. (A), Trifurcation variant where the right posterior segmental branch (arrow), the right anterior segmental branch and left hepatic duct join at the same point. (B), Cross-over variant where the right posterior segmental branch (arrow) drains into the left hepatic duct. Note ghosting artifacts (dashed arrow) from fluid filled small bowel loops (large arrow) obscuring the area of the papilla of Vater.

Sequence 3: Axial T1-weighted gradient recalled echo in- and opposed phase

TR/TE1/TE2/FA/NSA = 216/1.52/4.9/71/1, iPAT 2, 192 x 256 matrix, 2 x 19 slices, ST 8 mm

Sequence 4–6: Coronal single slice T2-weighted RARE with fat saturation, coronal and ± 20 oblique coronal
TR/TE/FA/NSA = 2120/964/150/1, 256 x 256 matrix, ST 50 mm, 30 x 30 cm² FoV, TA 2 s

Sequence 7: Coronal T2-weighted HASTE with fat saturation
TR/TE/FA/NSA = 3000/106/123/1, 256 x 256 matrix, 16 slices, ST 3 mm, 35 x 35 cm² FoV, 2 concatenations, TA 2 x 24 s

Sequence 8: Respiratory triggered coronal 3D T2-weighted TSE with fat saturation utilizing a navigator technique for detection of the diaphragm position
TR/TE/FA/NSA = 1 x respiratory cycle/645/180/1, 240 x 256 matrix, 60 slices, ST 1 mm, 30 x 30 cm² FoV, TA 3 – 6 min depending on the respiratory frequency

Normal biliary anatomy

Accurate preoperative radiological imaging with a high level of confidence is essential in order to assess the vascular and biliary anatomy of patients prior to liver resection or potential living related liver donors. It is the unique ability of MR imaging to delineate the biliary system without the need for biliary excreted contrast agents. This allows a fast preoperative workup using a single imaging approach. Visualization and classification of the intrahepatic biliary variants repre-

sent the most challenging part of the preoperative evaluation with variants in as many as 45% of cases [4]. A correct understanding of the biliary anatomy is crucial in order to achieve safe hepatic resections and to minimize biliary complications [5].

The 'classic' biliary anatomy is known as a left hepatic duct and a short right hepatic duct which together form the common hepatic duct. The right hepatic duct itself is formed by the anterior and posterior right hepatic segmental branches (Figure 1). Unfortunately, this classic anatomy is seen in only two-thirds of all cases. The most common variants are so-called cross-over anomalies where the right posterior segmental branch either joins together with the right anterior segmental branch the left hepatic duct or the right posterior segmental branch crosses over to drain into the left hepatic duct. These cross-over variants are seen in approximately 30% of cases (Figure 2). Depiction of these variants is important for the hepatic surgeon to optimize patient outcome. Preliminary data suggest that MRCP at 3.0 Tesla offers improved CNR and a higher level of confidence for depicting intrahepatic variants compared to MRCP at 1.5 Tesla [6].

Remaining challenges at ultra-high field MRCP

The RARE and HASTE sequences are very robust and reliable. However, they are orientation-dependent and have a relatively coarse through-plane resolution. The respiratory triggered sequence, on the other hand, is a nearly isotropic 3D

high resolution sequence. It can be used to generate a high resolution MIP in any orientation and detect small structures with a high degree of confidence [6], but it is less robust and occasionally suffers from certain artifacts. In particular, it is common to see a FoV/2 ghost (Figure 1 arrows and Figure 2B

dashed and large arrows) because each partition is acquired over two separate respiratory cycles. Additionally, this sequence is quite long, requiring 3–6 minutes depending on the respiratory cycle of the patient.

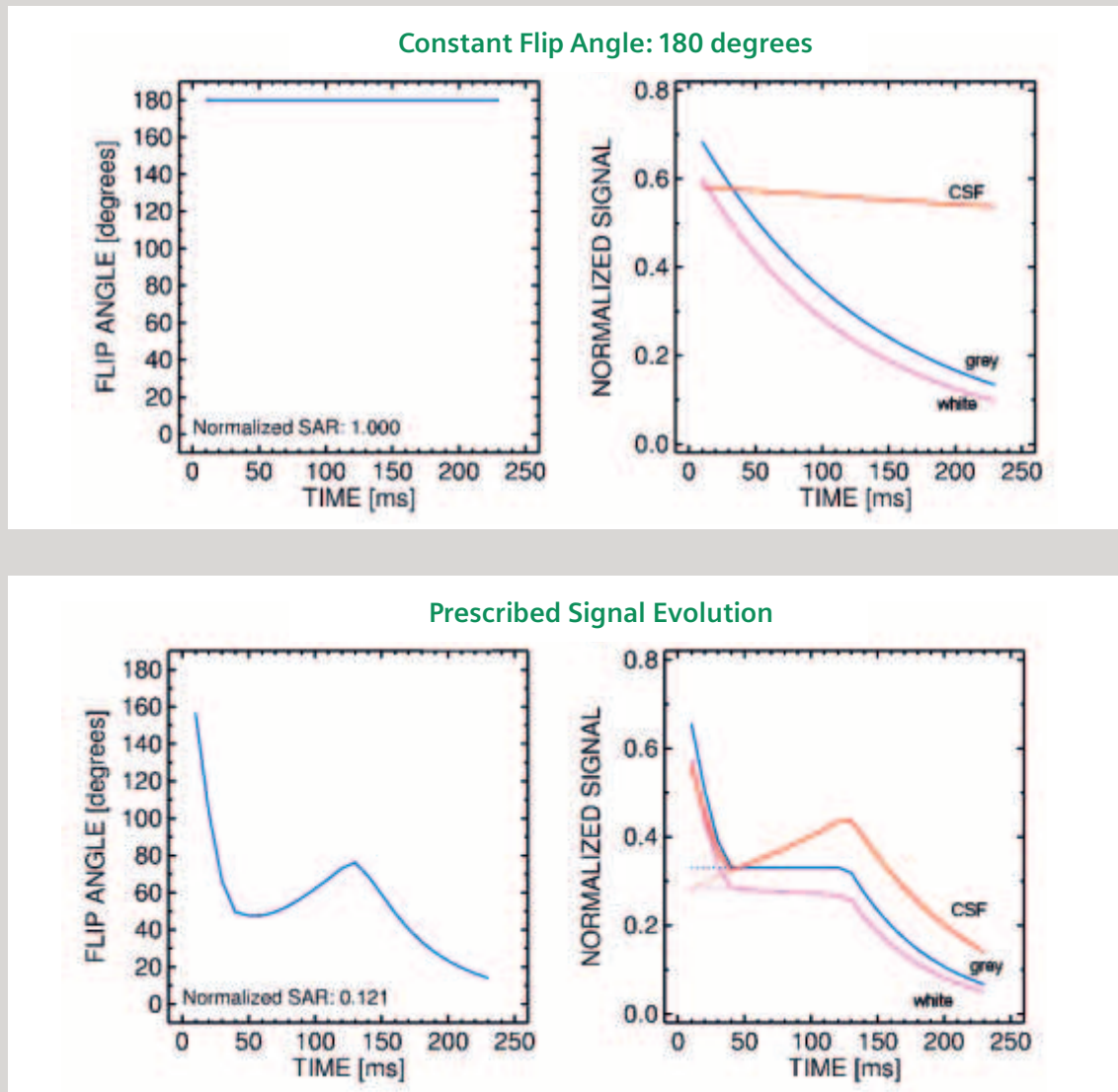


[Figure 3] Plots of signal evolution during the echo train with a standard TSE sequence (top) and the SPACE sequence (bottom). In each case the flip angles used during the echo train are shown (left), as well as the resulting MR signal during the echo train (right). The standard TSE sequence uses a constant train of 180° pulses while the SPACE sequence varies the flip angle during the echo train. Due to SAR restrictions, the 180° train is oftentimes not possible at 3.0T leading to degraded contrast and signal properties. With the SPACE sequence SAR is dramatically reduced and the desirable signal properties, especially late in the train, are maintained. Because longer echo trains can be used, an entire partition is acquired in a single TR with SPACE, which effectively eliminates the FoV/2 ghosts present with the standard sequence.

Potential solutions and further outlook

One potential solution to the ghosting is to use the SPACE sequence. Instead of using a constant train of 180° refocusing pulses, the SPACE sequence uses a varying train. These carefully designed refocusing pulse trains allow the use of very large Turbo-factors while maintaining desired contrast and even reducing SAR (Figure 3) [7]. With these large Turbo-factors an entire partition may be acquired in a single respiratory cycle, thereby eliminating the FoV/2 ghost artifacts and improving resolution (Figure 4 and Figure 2A). Image quality with this sequence is generally high with high resolution isotropic 3D datasets allowing a high-resolution MIP (Maximum Intensity Projection) in any direction.

The SPACE sequence is a respiratory-triggered sequence, which therefore requires a substantial amount of time for acquisition, just like the original respiratory-triggered TSE sequence suggested above. Whilst it is possible that the higher SNR and iPAT factors available on the MAGNETOM Trio, A Tim System will allow for a more rapid acquisition with similarly high image quality, this possibility, however, remains to be validated clinically.

Summary

MRCP is an important and effective imaging technique that benefits significantly from the additional SNR available at 3.0T. A state of the art protocol is presented including RARE, HASTE, and respiratory triggered 3D T2-weighted TSE. The new SPACE sequence can eliminate some of the artifacts encountered with the suggested TSE sequence without compromising resolution or contrast.

Literature

- [1] Wallner BK, Schumacher KA, Weidenmaier W, Friedrich JM. Dilated biliary tract: evaluation with MR cholangiography with a T2-weighted contrast-enhanced fast sequence. *Radiology* 1991;181:805–8.
- [2] Barish MA, Yucel EK, Ferrucci JT. Magnetic resonance cholangiopancreatography. *N Engl J Med* 1999;341:258–264.
- [3] Varghese JC, Liddell RP, Farrell MA, Murray FE, Osborne H, Lee MJ. The diagnostic accuracy of magnetic resonance cholangiopancreatography and ultrasound compared with direct cholangiography in the detection of choledocholithiasis. *Clin Radiol* 1999;54:604–14.
- [4] Gazelle GS, Lee MJ, Mueller PR. Cholangiographic segmental anatomy of the liver. *Radiographics* 1994;14:1005–13.
- [5] Goldman J, Florman S, Varotti G, et al. Noninvasive preoperative evaluation of biliary anatomy in right-lobe living donors with mangafodipir trisodium-enhanced MR cholangiography. *Transplant Proc* 2003;35:1421–2.
- [6] Merkle EM, Haugan PA, Thomas J, Jaffe TA, Gullotto C. MR Cholangiography: 3.0 Tesla versus 1.5 Tesla – A Pilot Study. *Am J Roentgenol*, in press.
- [7] Mugler JP. Variable-Flip-Angle Strategies for T2-Weighted 2D TSE: A Preliminary Theoretical Comparison. *Radiology and Biomedical Engineering*, University of Virginia, presented at Siemens Medical Solutions, Erlangen. 2002.

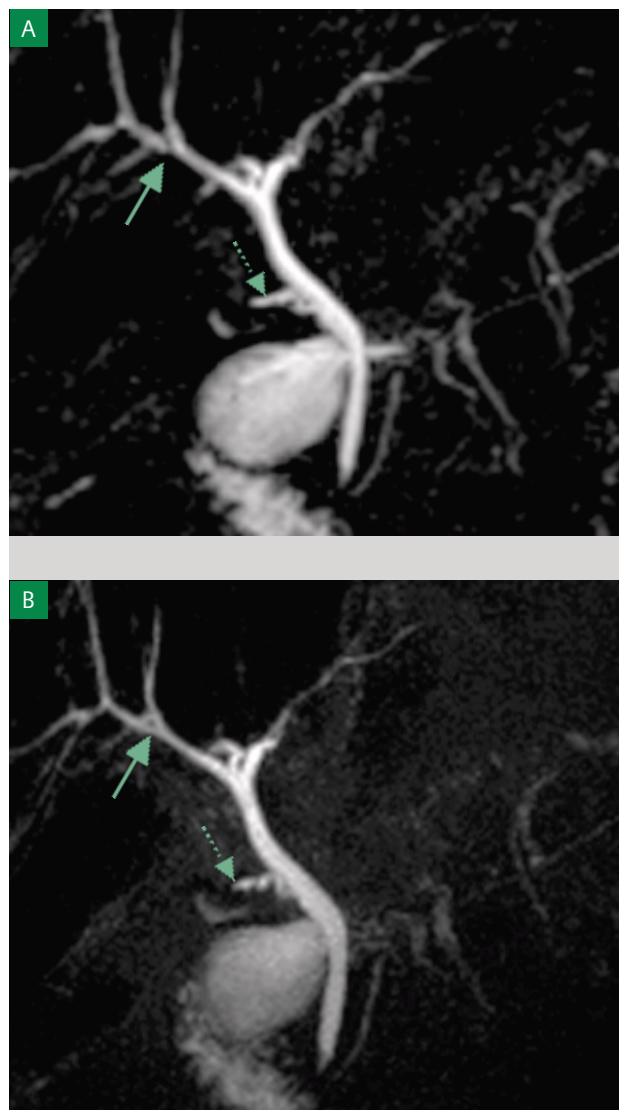


[Figure 4] Maximum intensity projections from the T2-weighted respiratory navigated standard TSE (A) and abdominal SPACE (B) sequences. Patient is status post cholecystectomy. Note the generally sharper edges and better detail with the SPACE sequence (B). The SPACE sequence does not show a pseudo obstruction (solid arrow) and the remnant of the cystic duct (dashed arrow) is more clearly defined for the SPACE sequence.

*The information about this product is preliminary. The product is under development and is not commercially available in the US. and its future availability cannot be assured.

New Perspectives and Challenges in Abdominal Imaging with the MAGNETOM Trio, A Tim System

Christoph J. Zech¹, M.D., Stefan O. Schoenberg¹, M.D., Olaf Dietrich¹, Ph.D., Wilhelm Horger³, Gerhard Laub, Ph.D.³, Ioannis Panagiotelis Ph.D.³, Paul J. Finn², M.D., Maximilian F. Reiser, M.D.¹

¹Institute of Clinical Radiology, University Hospitals-Grosshadern, Ludwig-Maximilians-University Munich

²Cardiovascular Research, Department of Radiology, University of California at Los Angeles, USA

³Siemens Medical Solutions, Malvern PA, USA

Introduction

In general, the challenges for abdominal magnetic resonance imaging (MRI) are confined to the three-fold issues of spatial resolution, signal-to-noise ratio, and artifacts from respiratory motion or vascular pulsation. Within the last few years, a number of strategies have been developed to overcome these limitations. The use of parallel acquisition techniques on MRI systems with multiple receiver channels now allows the increase of the spatial resolution at almost no cost in scan time [Heidemann RM et al., 2003; Zech et al., JMRI 2004]. Motion artifacts can be successfully avoided by the application of navigator-based correction techniques thereby synchronizing the image acquisition with the position of the diaphragm [Zech et al., JMRI 2004; Pauleit et al., 2001]. Lastly, signal-to-noise constraints can now be effectively overcome by the introduction of 3 Tesla (T) MRI systems into the clinical routine. To truly assess the additional value of 3T systems for abdominal MR imaging one has to ensure that a fair comparison is made to current state-of-the-art 1.5T MRI systems, in order to evaluate the benefit of 3T in view of the higher hardware costs.

At the present time, state-of-the-art 1.5T MRI scanners are equipped with between 8 and 32 independent receiver channels allowing the use of parallel acquisition techniques (PAT) in all three directions with acceleration factors of up to 16. For PAT, essentially two different algorithms are applied, which perform the reconstruction either in the image domain (SENSE-based algorithms) [Pruessmann et al., 1999] or k-space domain (SMASH-based algorithms) [Sodickson et Manning, 1997; Jakob et al., 1998; Griswold et al., 2000; Griswold et al., 2002]. Dependent on the vendor-specific implementation, the information of the coil sensitivity profiles is either acquired within a separate breath-hold-scan (SENSE) or by acquisition of additional reference lines within the

same scan (mSENSE, GRAPPA) [Griswold et al., 2004]. The latter implementation is known as integrated parallel acquisition techniques (iPAT).

Current state-of-the-art imaging at 1.5 Tesla

With 1.5T state-of-the-art scanners, a slice thickness for abdominal imaging of 4 to 6 mm can be routinely applied with 2D-sequences and 2 to 4 mm with 3D-sequences. Acquisition of a $(320)^2$ matrix at a $(350 \text{ mm})^2$ field-of-view allows the routine obtaining of an in-plane resolution of approximately 1 mm^2 . By the combination of parallel acquisition techniques with prospective navigator correction e.g. in T2-weighted (w) turbo-spin-echo (TSE) sequences, the image acquisition of larger organs such as the liver is feasible in three breath-holds with a breath-hold time of only 13 seconds [Zech et al., JMRI 2004]. For free-breathing acquisitions, the total acquisition time can be effectively reduced by parallel acquisition techniques to around 4 minutes. Studies have shown that the use of PAT does not result in a substantially larger number of artifacts from aliasing, while at the same time motion artifacts are decreased due to the shorter overall scan times [Zech et al., JMRI 2004]. With these techniques liver lesions can now be reliably detected with T2-w sequences at a size of 4 to 5 mm or less after administration of superparamagnetic iron oxides (SPIO). It has been shown that the combination of dynamic gadolinium-enhanced imaging using thin-slice 3D T1-w gradient-echo (GRE) sequences with SPIO-imaging further improves the detection of small lesions $< 10 \text{ mm}$ [Kwak et al, 2004].

In sequence types that have an intrinsically high signal-to-noise ratio (SNR), such as steady-state free precession techniques (TrueFISP, balanced FFE, FIESTA), higher PAT acceleration factors can be applied. These techniques are particularly

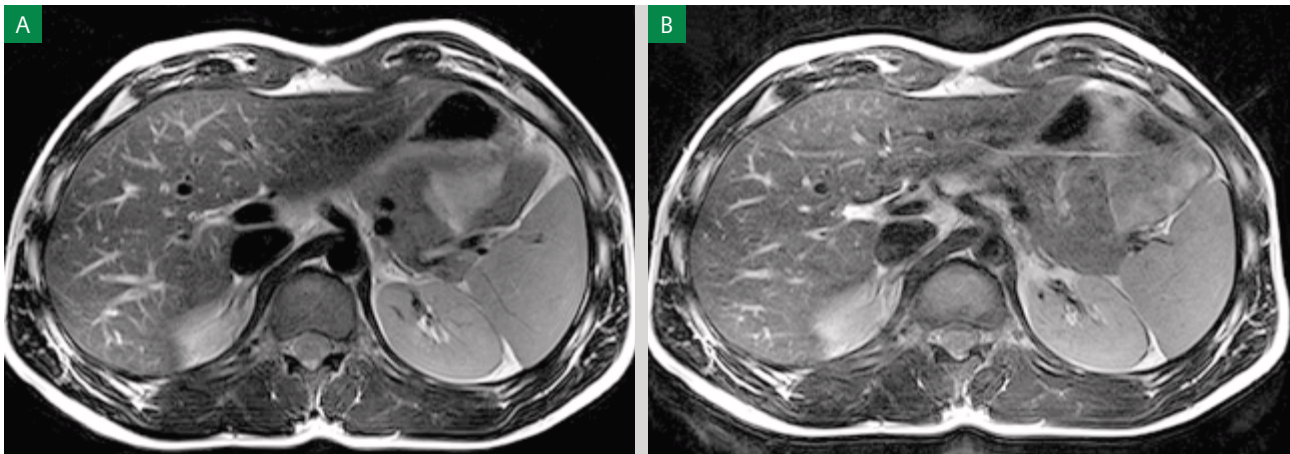


[Figure A-1] Comparison of a navigator-triggered T2-weighted TSE sequence of the liver on a 3T system (MAGNETOM Trio, Siemens Medical Solutions). The time of acquisition is decreased from 1:52 min without (A) parallel imaging to 1:11 min with (B) parallel imaging with an acceleration factor of 2. Same parameter settings were used for both sequences: TR: > 1900 ms, depending on the respiratory cycle; TE: 109 ms; 27 slices with 6 mm thickness; $(384)^2$ matrix with a rectangular field of view ($360 \times 270 \text{ mm}^2$).

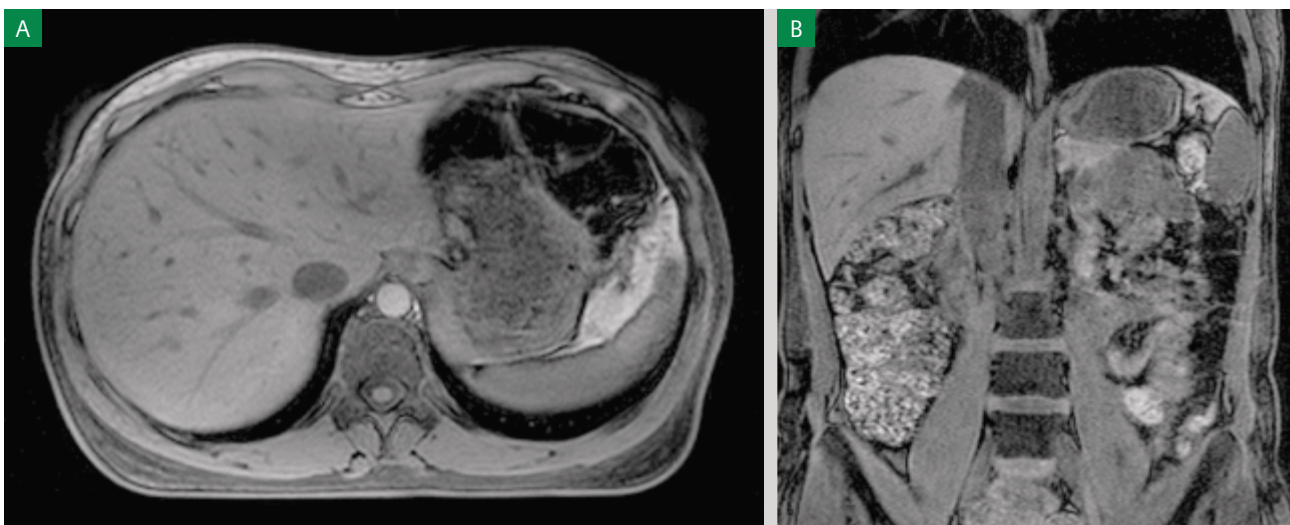


[Figure A-2] Transversal (A) and coronal (B) VIBE fat-sat T1-weighted 3D GRE images acquired on a 3T system (MAGNETOM Trio, Siemens Medical Solutions) with a novel whole-body coil concept (total imaging matrix) and parallel imaging with an acceleration factor of 2 for the transversal study and 3 for the coronal study. Note the excellent image homogeneity and fat suppression. The whole liver can be covered with 2 mm slices within a single breath-hold of 18 s.

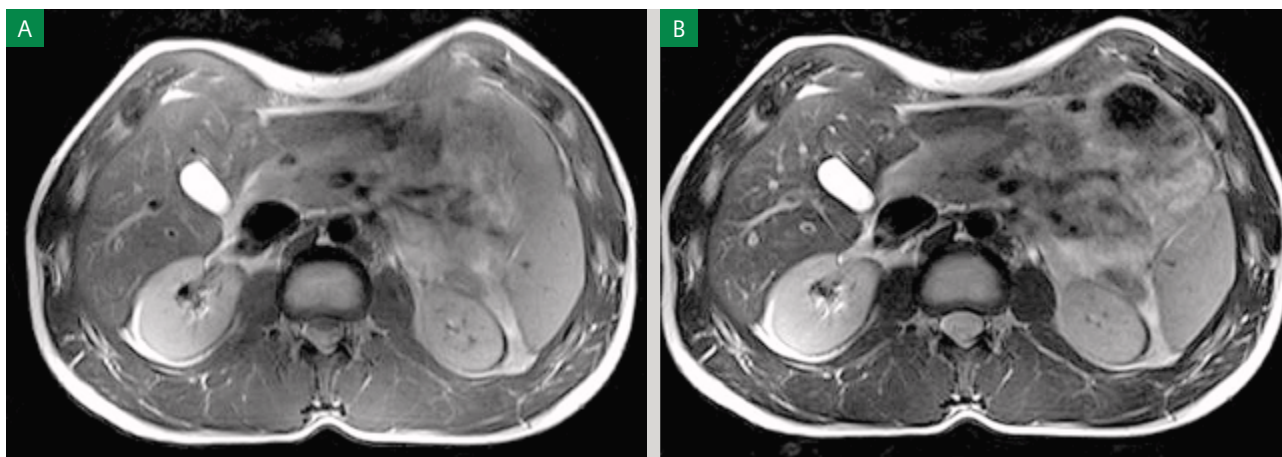


[Figure B] Comparison of a navigator-triggered T2-weighted TSE sequence of the liver on a 3T system using the hyper-echo technique (MAGNETOM Trio, Siemens Medical Solutions). Each two sections at different levels with a flip angle of 60° (A) and 120° (B). The other parameter settings were the same for both sequences: TR: > 1900 ms, depending on the respiratory cycle; TE: 109 ms; 27 slices with 6 mm thickness; $(384)^2$ matrix with a rectangular field of view ($360 \times 270 \text{ mm}^2$).

favorable for single-breath-hold 3D imaging of the small and large bowel after intra-luminal water distension with acceleration in two phase-encoding directions. A total PAT factor of six allows the acquisition of an entire data set with 1.5 mm isotropic voxel length in a single breath-hold of less than 20 seconds. This data can be individually reformatted to show the exact extent of small or large bowel pathology. Imaging of the pancreas can nowadays also be done at very high resolution by the use of PAT, $(320)^2$ to $(384)^2$ matrix size and a slice thickness of 4 mm after administration of manganese-containing contrast agents such as Teslascan™ (Amersham Health, Ismaning, Germany) [Schima et al., 2002]. Similarly, the advent of PAT has revolutionized the use of contrast-enhanced 3D MR-angiography (MRA) in the abdomen. Voxel sizes of less than 1 mm^3 are now achievable within a single breath-hold [Schoenberg et al., SemUltrasCTMR 2003; Schoenberg et al., NDT 2003; Schoenberg et al., Radiology 2005]. These isotropic data sets can also be reformatted in any plane, which offers the possibility of assessing the area stenosis rather than only the diameter stenosis. These area stenosis measurements have shown good correlation to intravascular ultrasound in preliminary studies on renal arteries and appear to be significantly more accurate in terms of the measurement of the true degree of stenosis [Schoenberg et al., Radiology 2005].

Capabilities at 3 Tesla

As already outlined, the current achievements at 1.5T apply a high standard in abdominal MRI. Thus, the initial step at 3T was to reproduce similar image parameters to those at 1.5T.

The problem is that there are a number of challenges for abdominal MRI at 3T despite the obvious advantage of a higher SNR. First, the specific absorption rate (SAR) increases quadratically with field strength, resulting in a major limitation particularly for turbo-spin-echo sequences [Kangarlou et al, 1999]. The shorter wavelength at 3T results in substantial dielectric resonance-effects, causing significant signal inhomogeneities due to eddy currents in the tissue with the result of focal field cancellation [Kangarlou et al, 1999]. Relaxation times are substantially longer, which necessitates the adjustment of several imaging parameters (e.g. TR, TE). The second step for abdominal imaging at 3T has therefore been to effectively address these limitations by new technical strategies. The signal inhomogeneities due to the dielectric resonance effects can be substantially reduced by the application of external gel pads placed on the surface of the patient. These RF homogenisation pads are not visible in the images, but nevertheless alter the dielectric properties of the imaging volume, improving signal homogeneity [Schmitt M et al., 2004]. The SAR can be effectively reduced by new techniques such as the hyper-echo technique and the variable flip angle technique [Mugler JP et al., 1992; Hennig et Scheffler, 2001; Hennig et al., 2003], or parallel imaging [Pruessmann, 2004]. In the third step, these new techniques have been effectively implemented on clinical scanners to extend the limits even further. Currently, matrix sizes of $(512)^2$ and slice thicknesses of less than 4 mm appear feasible, while at the same time breath-hold scans of less than 12 seconds or total scan times for free-breathing acquisitions of less than 2 minutes can be achieved using PAT.

Image optimization

In the following, the individual steps for the optimization of image acquisition for abdominal MRI at 3T are discussed:

- **Optimization of image contrast:** As the T1 relaxation time increases with the field strength B_0 (with a typical increase of 30% to 50% of T1 at 3T compared to 1.5T), the sequence parameters, particularly the repetition time (TR) has to be adapted [de Bazelaire et al, 2004]. The effects on the T2 relaxation are less prominent; T2 is effectively unchanged at 3T, but T2* is shortened [Norris DG, 2003]. The adjustment of the TR strongly depends on the flip angle. Therefore, GRE sequences with small flip angles might require only minor changes in TR compared to sequences with a full 90° flip angle [de Bazelaire et al, 2004].
- **Changes of echo times for in-phase/opposed-phase imaging at 3 Tesla:** Due to the change of the resonance frequency the echo times for in-phase and opposed-phase conditions at 3T have to be adjusted accordingly. The values are almost inverted compared to the conditions at 1.5T. In-phase conditions are found at echo times of 2.3 ms and 4.6 ms, while opposed-phase conditions are present at 1.1 ms, 3.5 ms and 5.75 ms. Therefore, dual echo sequences are problematic, since the echo spacing between the initial opposed-phase echo at 1.1 ms and the following in-phase echo of 2.3 ms are too close for acquisition within a single read-out.
- **Optimization of fat suppression at 3 Tesla:** There are opposite effects at 3T that improve as well as deteriorate the quality of fat suppression. The different resonance frequency at 3T produces a stronger chemical shift between fat and water, thus facilitating the use of spectral fat suppression. At the same time B1 homogeneity decreases with B0 field strength, which results in a more pronounced variation of the flip angle over the field-of-view. This might result in a less optimal fat suppression, which is particularly problematic for TSE sequences, while this effect is less problematic with GRE techniques. In addition, as the field increases stronger eddy currents are generated, that further reduce the quality of fat suppression. Solutions for these limitations are improved gradient-coil design (generating less eddy currents) as well as an alternative, non-radiofrequency-dependent type of fat suppression. This includes, for example, the Dixon method, using several in-phase and opposed-phase images or inversion recovery-type techniques [Wang Y et al, 1998].
- **Increased chemical shift at 3 Tesla:** As mentioned above, the different resonance frequency at 3T produces a stronger chemical shift between fat and water. This can be

advantageous for the use of spectral fat suppression and for MR spectroscopy or chemical shift imaging; however, chemical-shift artifacts are also more pronounced at fat/water interfaces. This increase of chemical-shift artifacts can be addressed by using a higher receiver bandwidth with the consequence of losing some of the SNR advantages gained by 3T.

- **Reduction of specific absorption rate (SAR):** As mentioned earlier the three most important techniques for reduction of SAR are new pulse sequences applying the variable flip angle-technique (VFA) or the hyper-echo technique, which is a modification of the former, and parallel imaging that is discussed below. The VFA technique was initially described by Mugler et al. [Mugler JP et al, 1992] and is particularly used for SSFP sequences that offer high SNR efficiency, if large flip angles are applied ($\alpha = 60^\circ$). However, the SAR also increases quadratically with the flip angle. Since the image contrast is mainly affected by the center of k-space, the flip angle is varied along the phase-encoding direction ensuring a large flip angle in the central parts of k-space, while for the other segments of k-space the flip angle is continuously decreased. This results in a reduction of SAR by at least 50%. The main disadvantage of this technique is that SNR is also reduced by approximately 30%, thus limiting the benefit of the normally two-fold SNR gain at 3T compared to 1.5T. A further refinement of the VFA technique is the so-called hyper-echo technique, which is used for multi-echo sequences such as TSE sequences with long echo trains or single-shot acquisitions (HASTE, RARE). In this technique magnetization can be completely rewound after any arbitrary sequence of RF pulses [Henning et Scheffler, 2001; Henning et al, 2003]. Only the echoes encoding for the center of k-space are refocused by 180° RF pulses. Due to a series of RF pulses with low flip angles stimulated echoes are also obtained, which are used for the image reconstruction together with the conventional echoes as long as they are in-phase with the latter. This technique results in the reduction of SAR by 60% to 80%, while the reduction of SNR is virtually negligible. Simpler techniques to reduce the SAR include the global decrease of the refocusing flip angle in TSE sequences from 180° to a value between 120° and 160°; however, compared to the hyper-echo approach, a larger SNR decrease must be accepted. In fast GRE sequences, the SAR can be reduced by choosing a longer RF pulse, since the RF pulse power scales inversely with the square of the pulse length.
- **Reduction of dielectric resonance effects:** Dielectric resonance effects are caused by local eddy currents because

of the increased conductivity of the tissue. These effects are more enhanced at 3T, since the radio-frequency waves have a shorter length as compared to 1.5T. This causes local inhomogeneities particularly in larger anatomic areas such as the abdomen, where the wavelength is approximately only half the diameter of the body, particularly for patients with low fat content. In the MR images dielectric effects are predominantly noticeable in the ventral aspects of the abdomen as focal areas of varied signal intensity. They can be effectively reduced by placement of an external dielectric gel pad (see above) on the anterior body surface, which increases the resistance for focal eddy currents [Schmitt M et al., 2004]. For standard abdominal imaging this improvement is usually sufficient; however there are certain conditions, in which substantial artifacts with non-diagnostic image quality are virtually unavoidable. These include physiologic or pathologic conditions with large amounts of intraabdominal or intrapelvic fluid, such as pregnancy with a large amount of amniotic fluid or intraabdominal ascites. In those cases, images can be almost non-diagnostic due to focal signal intensity drop-outs [von Falkenhausen et al, 2004].

■ **Parallel acquisition techniques:** With PAT, the SNR is reduced by the square root of the acceleration factor times the so-called g-factor, which represents a measure of the local noise amplification, mostly related to array coil design characteristics [Pruessmann et al., 1999; Griswold et al., 2000 and 2002]. Thus with higher acceleration factors of e.g. three, the SNR is reduced to at least 58% of the original value. This causes a visible increase of image noise in the images at 1.5T. Due to the higher SNR at 3T, image noise at comparable acceleration factors is barely visible in the images. Further development can be expected from dedicated multi-channel MR systems such as the MAGNETOM TRIO, A Tim System (Siemens Medical Solutions, Erlangen). Initial results with new multi element array (matrix) coils allow to apply acceleration factors of up to four without noticeable loss of image quality from increased image noise [Pruessmann, 2004].

With all these optimization strategies at 3T, a robust image quality can be obtained in the majority of patients with slice thickness between 4 and 6 mm, matrix sizes between $(320)^2$ and $(384)^2$ and PAT acceleration factors between 2 and 3. With multi-breath-hold imaging the larger abdominal organs, such as the liver, can be covered in 3 breath-holds each lasting 11 seconds using PAT. For single-shot TSE techniques such as HASTE the effective reduction of SAR by the hyper-echo technique allows to acquire 15 to 20 slices in a

single breath-hold with a $(384)^2$ matrix without exceeding the SAR limitations. Slice thicknesses of down to 4 mm are feasible even when PAT is used. **The overall results for high-resolution images with a decreased amount of blurring is better with the hyper-echo technique, as it allows the use of higher flip angles compared to the standard VFA technique with reduced flip angles (down to 60°) for the refocusing pulse and, therefore, alternated image contrast (Figure B). For free-breathing techniques, the use of PAT for high resolution images with matrix sizes of $(384)^2$ allows for total acquisition times of less than 1.5 minutes (Figure A).**

The combination of several of these described techniques can be used to optimize dedicated techniques for abdominal imaging such as 3D-TSE MRCP. For this type of sequence a free-breathing acquisition is performed with navigator correction. To effectively reduce SAR in view of the long echo trains, a variable flip angle technique is applied. For maintaining high SNR, the remaining magnetization after the read-out is restored into the longitudinal direction by a dedicated 90° restore pulse. The SNR gain from those restore-pulses in combination with the higher field-strengths allows to apply PAT factors of up to 4. Thus three-dimensional data-sets with an isotropic voxel size of $(0.9 \text{ mm})^3$ can be acquired in only 2 minutes, allowing 3D-assessment of the entire biliary tree by a variety of post-processing possibilities such as multi-planar reformats (MPR), maximum intensity projections (MIP), surface-shading techniques (SSD) or volume-rendering techniques (VRT).

For high-resolution MRA at 3T, voxel sizes of $0.7 \times 0.7 \times 0.7 \text{ mm}^3$ are now feasible with a PAT acceleration factor of 3 within a breath-hold of less than 20 seconds. Despite the small voxel sizes and the use of PAT, sufficient SNR is still present due to the higher field strength [Leiner et al, 2003]. The problems for MRA at 3T are two-fold: first the typically short TRs of less than 4 ms result in a high RF power deposition, which easily exceeds the SAR limits. One approach is to lengthen the RF pulse and the TR and to use PAT to compensate for the consecutive increase in scan time; however, this changes the contrast of the image since a longer repetition time increases the background signal. An increased background signal might limit the use of MIPs for the diagnostic evaluation of the MRA. A second problem is the decrease of the flip angle, which is necessary to stay within the SAR limits, which also increases the background signal. Nevertheless in the clinical routine a compromise can usually be found by carefully adjusting these parameters, such that high resolution sub-millimeter MRA is feasible with good image quality [Leiner et al, 2003].

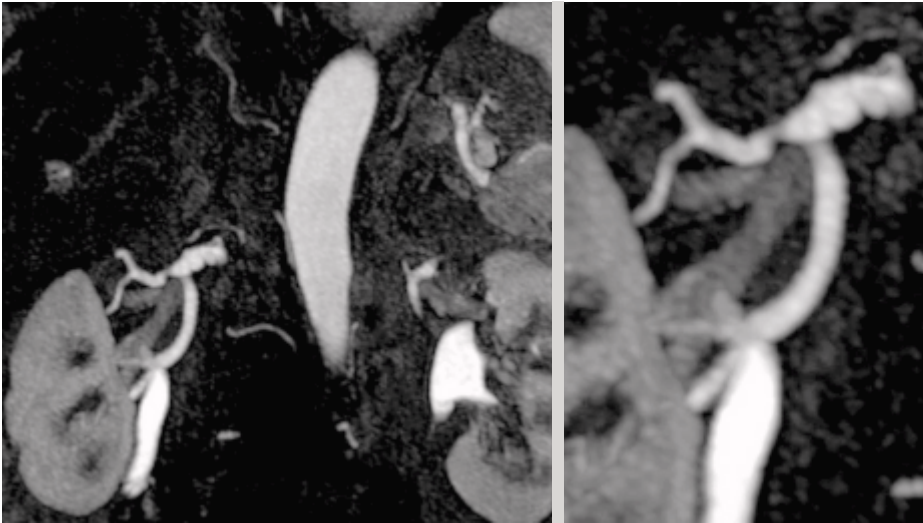


[Figure C-1] Female patient with fibromuscular dysplasia. MR angiography on MAGNETOM Trio with submillimeter spatial resolution ($0.8 \times 0.8 \times 0.8 \text{ mm}^3$) clearly demonstrating the string-of-beads appearance of the FMD lesions. The sequence can be acquired in 18 s with help of parallel imaging (GRAPPA; acceleration factor 3).

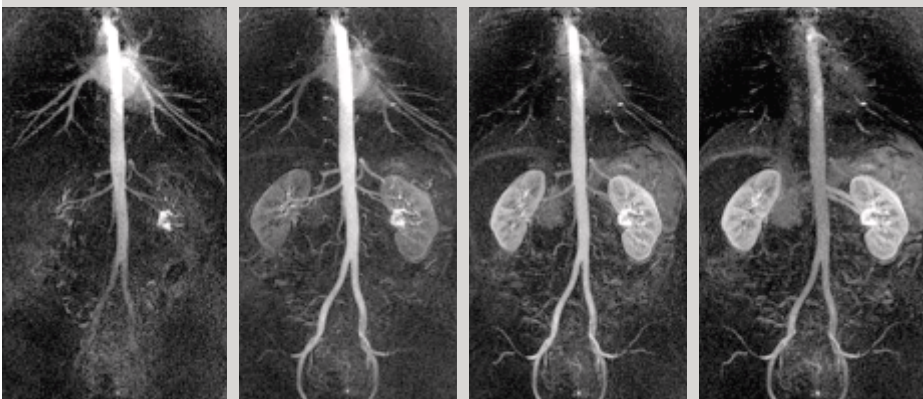


[Figure C-2] Time-resolved MR angiography on a 3T system (MAGNETOM Trio) with a novel whole-body coil concept (total imaging matrix). At a voxel size of $2 \times 2 \times 2 \text{ mm}^3$, one 3D data set is acquired every 2 s using parallel imaging (GRAPPA; acceleration factor 2).

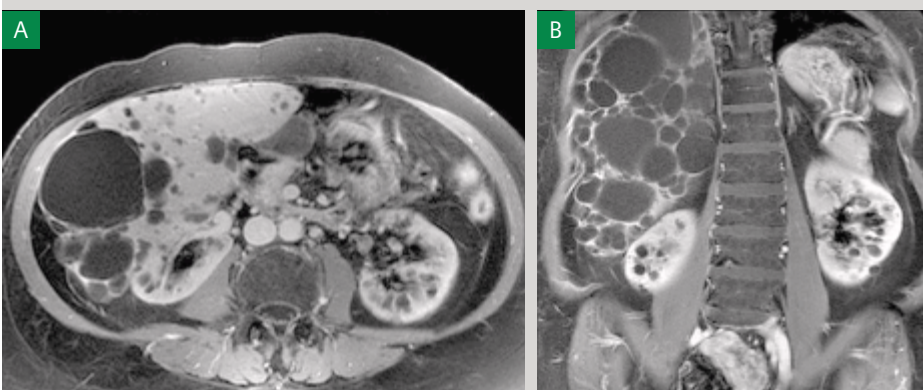


[Figure D] T1-weighted FLASH 2D sequence on a MAGNETOM Trio, 120 s after injection of Gadolinium in a 54-year-old female patient with polycystic kidney disease. Excellent depiction of the innumerable small cysts, which have to be differentiated from cystic renal cell carcinoma. Although a high spatial resolution is maintained with a $(384)^2$ matrix, 23 slices can be acquired in 18 s.

Clinical value of 3 Tesla for abdominal MRI

In general, those applications for abdominal MRI seem to profit from the higher field strength that critically depend on spatial resolution. One promising application appears to be the assessment of multi-cystic abdominal masses, in which the delineation of enhancing septa is important for the detection of malignancy [Israel et al; 2004]. This includes multi-cystic masses of the kidney and ovaries, in which small nodular thickening of the septa with increased enhancement after gadolinium administration is indicative of early malignancy [Israel et al; 2004]. With an optimal spatial resolution the differentiation between cysts and renal cell carcinoma in von-Hippel-Lindau disease, differentiation between cystadenoma and cystadeno-carcinoma in cystic ovarian lesions as well as early detection of renal cell carcinoma in acquired polycystic disease can be facilitated [Israel et al, 2004; Granata et al, 2004; Mosetti et al, 2004] (Figure D). For the assessment of focal liver lesions there is still no consensus on whether the high resolution truly converts into a better detection of small lesions of less than 1 cm. However, it has been already demonstrated in small non-controlled studies that a high spatial resolution, e.g. with 3D-GRE sequences, helps to improve the detection of small lesions and the characterization of lesions in terms of better delineation of morphological features such as the vascular architecture or a central scar [Burrell et al, 2003; Heim et al, 2003].

As high-field MRI with a high spatial resolution is not limited by a decreased liver-to-lesion contrast, such as computer tomography, it can be expected that the high resolution should improve overall lesion detection [Mc Kenzie et al, 2004; Zech et al, Radiologe 2004]. The dilemma at this point, however, is that due to the reduced availability of 3T in the clinical routine, no larger systematic studies with comparison between 1.5 and 3T in correlation to an invasive gold standard such as biopsy or surgery have been performed. An area that holds great promise is the staging of malignant lesions of the uterine cervix and the rectum [Morakkabati-Spitz et al; 2004]. MRI at 1.5T has been notoriously weak in differentiation between stage IIa cervical carcinoma and stage Ib with an accuracy of only around 80% [Sheu et al, 2001]. This question is highly relevant, since differentiation between those two stages affects the decision for either radical hysterectomy or primary radiation therapy. Since extension of the tumor beyond the cervical stroma, which is sometimes less than 1 mm in width, is the discriminator between those two stages, one might expect an improved staging with matrix sizes higher than 512^2 . Similar improved performance could be expected for staging of rectal carcinoma, where MRI is known to over-stage lesions of TNM-stage T1 in T2, since reliable differentiation between the submucosa and muscularis propria layers is difficult at current maximum

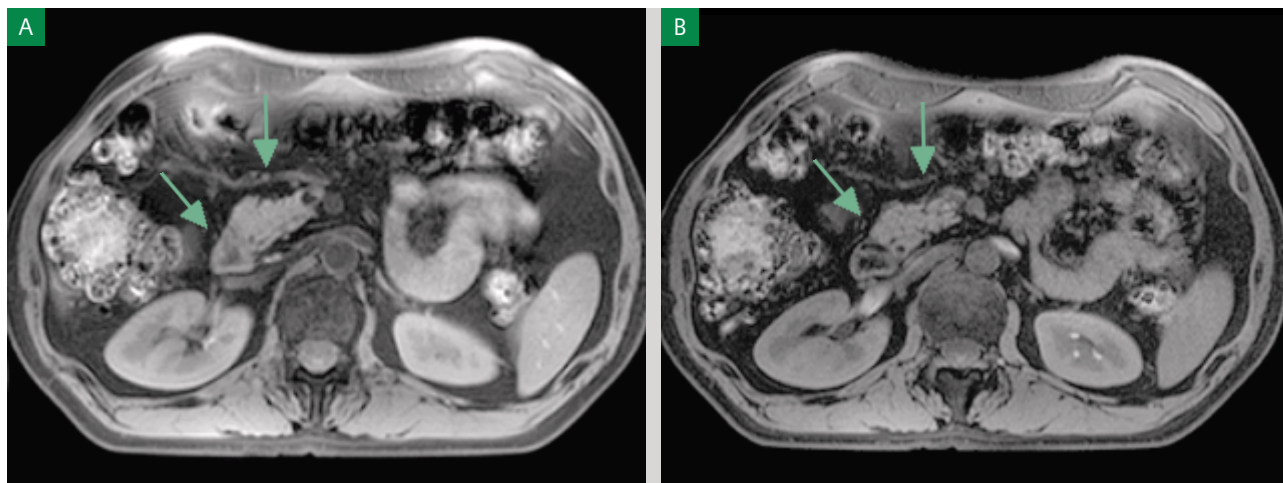


[Figure E] T1-weighted FLASH 2D sequence with fat-saturation on a 3T system (MAGNETOM Trio, Siemens Medical Solutions) in a healthy volunteer. The sequence with 5 mm slice thickness and a 320 x 256 matrix shows already a very good visualization of the anatomical area of the pancreatic head. However, on the 3T system a substantial increase in spatial resolution with 3 mm slice thickness and a 384 x 320 matrix is still possible without a visible loss of signal (B). Note the superior visualization of the pancreatic head in (B).

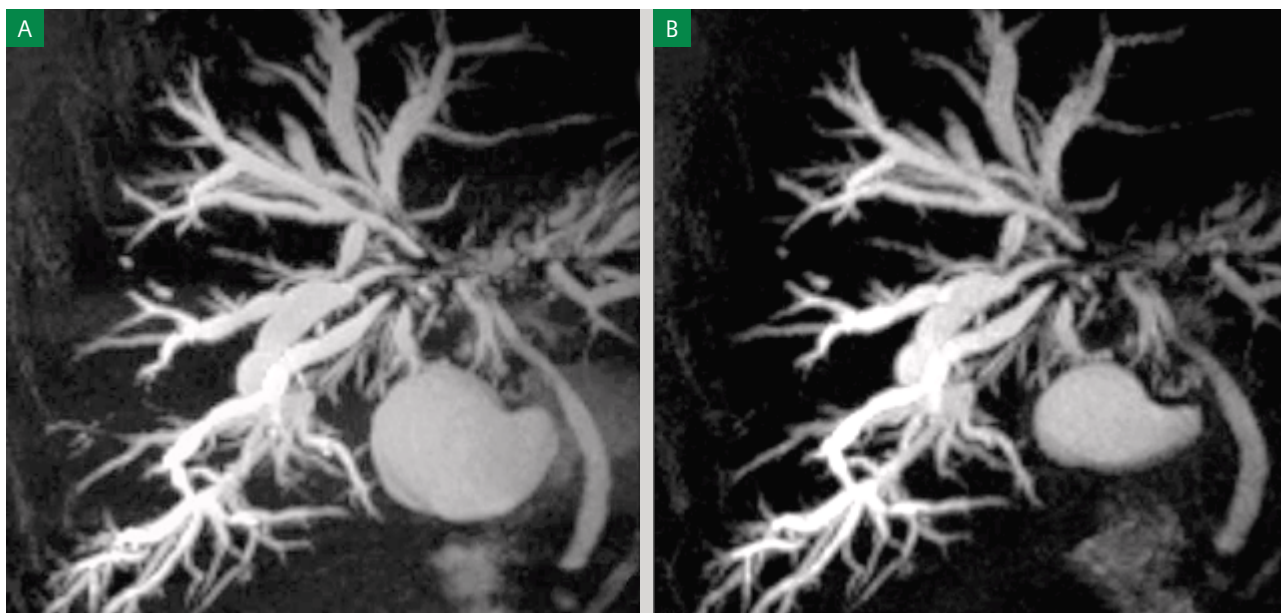


[Figure F] Submillimeter ($0.9 \times 0.9 \times 0.9 \text{ mm}^3$) T2-weighted 3D TSE sequence with variable flip angle technique on a MAGNETOM Trio in a patient with PSC (Primary Sclerosing Cholangitis), suffering from a severe stenosis at the confluence of the left and right hepatic duct. Due to the high SNR at 3T there is no significant difference of image quality between A (parallel imaging; acceleration factor 2) and B (parallel imaging; acceleration factor 4), although the time of acquisition of the respiratory triggered sequence in free-breathing is decreased from around four (A) to two (B) minutes.

matrix size of 512^2 [Branagan et al, 2004; Beets-Tan et al, 2001]. Recent publications do also report that increased spatial resolution is helpful for the evaluation of the nodal staging in colorectal cancer, because of the better visualization of morphologic features that help to distinguish malignant from benign lymph-nodes [Kim et al, 2004].

Probably one of the most promising applications is high-resolution 3D MRCP for diseases of the biliary tree that predominantly manifest in the high-order branches in their early stages, such as primary sclerosing cholangitis (PSC) [Schmitz S et al., 2004]. Reliable visualization of the biliary tree with MRCP at 1.5T is only possible up to the second order branches with current techniques [Fulcher et al., 2000]. Therefore, despite proven cost effectiveness of MRCP compared to ERCP due to its lack of any side effects and complete non-invasiveness, it has not established its role for the initial detection of PSC disease manifestation [Talwalkar et al, 2004]. However this patient group particularly benefits from the non-invasive techniques, since they are frequently young patients and early treatment can substantially affect the course of their disease. Untreated patients may experience severe complications such as multiple strictures of the intra- and extrahepatic bile ducts, which ultimately may

progress to cirrhosis and liver failure [Porayko et al, 1990]. Moreover, in these patients, ERCP for initial diagnosis can lead to substantial side effects such as pancreatitis or common bile duct perforation, which is observed more frequently than in other patients undergoing ERCP [Beuers et al, 1992]. With voxel sizes of $0.9 \times 0.9 \times 0.9 \text{ mm}^3$ spatial resolution and images free of motion artifacts with scan times of about 2 minutes, 3D MRCP at 3T now allows the detection of high-order branches of the biliary tree already in volunteers without biliary disease. Preliminary results show that focal dilations and stenoses of third and fourth-order branches, which are often the early manifestation of PSC, can be well detected with good correlation to ERCP [own preliminary data]. The acceleration of the acquisition by a PAT factor up to 4 makes this an easily feasible technique for these patients (Figure F). MRCP can be also combined with high-resolution liver imaging at 3T with a slice thickness of only 3 mm, which may hold out the promise of earlier detection of malignant tumors of the bile duct such as cholangiocarcinoma.

Ultrahigh-resolution contrast-enhanced breath-hold MRA with 0.7 to 0.8 mm isotropic resolution might eliminate the need for diagnostic DSA of the mesenteric and renal arteries (Figure C). A recent publication in the Annals of Internal

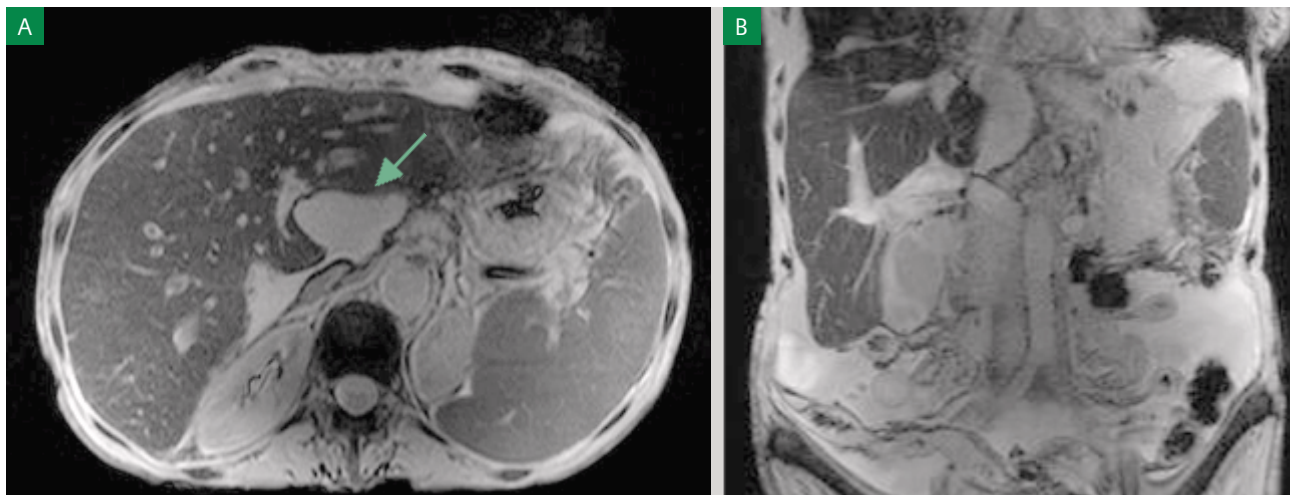


[Figure G] T2*-weighted 2D GRE sequence in the liver-specific phase after injection of ferucarbotran (Resovist®, Schering Germany, Berlin) in a 68-year-old female patient after liver transplantation. The examination was able to rule out a focal liver lesion (e.g. a hepatocellular carcinoma) with high confidence due to the excellent signal loss in the normal liver parenchyma after injection of the SPIO-contrast agent and due to the high spatial resolution. Sequence parameters are TR/TE/ α 132/732/30 with 5 mm slice thickness and a 320 x 256 matrix. The whole liver with 37 slices was covered in 4 x 17 seconds breathhold.

Medicine has shown that MRA at 1.5T with a current spatial resolution of only 1.5 mm or even worse is not sufficient to accurately diagnose and stage the degree of renal artery stenosis [Vasbinder et al., 2004]. Initial results at 1.5T with submillimeter ($0.8 \times 0.8 \times 0.9 \text{ mm}^3$) isotropic spatial resolution and reformats of the vessel area perpendicular to the vessel axis show that assessment of the area stenosis is a much more reliable parameter for exact grading of the degree of stenosis than grading the diameter stenosis in-plane [Schoenberg et al, 2005]. It is expected that this improvement will further increase at 3T.

Conclusion

One has to accept that imaging of the abdomen at 1.5T on a state-of-the-art-system with parallel imaging, navigator correction, and an advanced sequence design is a tough competitor for the evolving field of 3T. Nevertheless, it is now clearly feasible to acquire single-shot TSE images with PAT and hyper-echo technique at a very high resolution with minimal blurring and within the SAR limits. Those images appear to be superior to those currently acquired at 1.5T. PAT is generally applicable without major SNR constraints allowing the use of higher acceleration factors for shorter breathholds. The fat suppression appears acceptable despite problematic dielectric resonance effects. For techniques such as

3D-TSE MRCP, ultra high-resolution submillimeter studies with minimal acquisition times are feasible and may also eliminate the use of diagnostic ERCP for diseases such as primary sclerosing cholangitis in the future. No larger systematic studies have been yet performed for the detection and characterization of small focal liver lesions. It appears, however, that there is improvement at 3T, since in MRI the lesion delineation is primarily limited by the spatial resolution rather than by the liver-to-lesion contrast because of the excellent soft-tissue contrast. The resolution of contrast-enhanced 3D MRA approximates that of DSA for the first time, which should eliminate the use of diagnostic renal or mesenteric DSA other than for rare diseases such as small vessel vasculitis. In the pelvis ultra high-resolution imaging with SE and TSE sequences might further improve the staging of early T1 and T2 tumors of the cervix, uterus and rectum. However, it needs to be pointed out the true gain in clinical value is still speculative at the present time, since no large comparative studies have yet been performed or published.

References

- [1] Heidemann RM, Ozsarlak O, Parizel PM, et al. A brief review of parallel magnetic resonance imaging. *Eur Radiol.* 2003;13:2323–2337.
- [2] Zech CJ, Herrmann KA, Huber A, Dietrich O, Stemmer A, Herzog P, Reiser MF, Schoenberg SO. High-resolution MR-imaging of the liver with T2-weighted sequences using integrated parallel imaging: Comparison of prospective motion correction and respiratory triggering. *J Magn Reson Imaging* 2004;20:443–450.
- [3] Pauleit D, Textor J, Bachmann R, et al. Improving the detectability of focal liver lesions on T2-weighted MR images: ultrafast breath-hold or respiratory-triggered thin-section MRI? *J Magn Reson Imaging* 2001;14:128–133.
- [4] Pruessmann KP, Weiger M, Scheidegger MB, Boesiger P. SENSE: sensitivity encoding for fast MRI. *Magn Reson Med* 1999;42:952–962.
- [5] Sodickson DK, Manning WJ. Simultaneous acquisition of spatial harmonics (SMASH): fast imaging with radiofrequency coil arrays. *Magn Reson Med.* 1997;38:591–603.
- [6] Jakob PM, Griswold MA, Edelman RR, et al. AUTO-SMASH: a self-calibrating technique for SMASH imaging. *MAGMA* 1998;7:42–54.
- [7] Griswold MA, Jakob PM, Nittka M, et al. Partially parallel imaging with localized sensitivities (PILS). *Magn Reson Med* 2000;44:602–609.
- [8] Griswold MA, Jakob PM, Heidemann RM, et al. Generalized auto-calibrating partially parallel acquisitions (GRAPPA). *Magn Reson Med* 2002;47:1202–1210.
- [9] Griswold MA, Kannengiesser S, Heidemann RM, Wang J, Jakob PM. Field-of-view limitations in parallel imaging. *Magn Reson Med.* 2004;52:1118–1126.
- [10] Kwak HS, Lee JM, Kim CS. Preoperative detection of hepatocellular carcinoma: comparison of combined contrast-enhanced MR imaging and combined CT during arterial portography and CT hepatic arteriography. *Eur Radiol* 2004;14:447–457.
- [11] Schima W, Fugger R. Evaluation of focal pancreatic masses: comparison of mangafodipir-enhanced MR imaging and contrast-enhanced helical CT. *Eur Radiol.* 2002;12:2998–3008.
- [12] Schoenberg SO, Rieger J, Nittka M, Dietrich O, Johannson LO, Reiser MF. Renal MR angiography: current debates and developments in imaging of renal artery stenosis. *Semin Ultrasound CT MR.* 2003;24:255–267.
- [13] Schoenberg SO, Rieger J, Johannson LO, Dietrich O, Bock M, Prince MR, Reiser MF. Diagnosis of renal artery stenosis with magnetic resonance angiography: update 2003. *Nephrol Dial Transplant.* 2003;18:1252–1256.
- [14] Schoenberg SO, Rieger J, Weber C, Michael HJ, Waghershauser T, Dietrich O, Reiser MF. High-resolution MR-angiography of the renal arteries using Integrated Parallel Acquisition Techniques (iPAT): value of isotropic cross-sectional reformats compared to digital subtraction angiography and intravascular ultrasound. *Radiology.* 2005 (in press).
- [15] Kangarlu A, Baertlein BA, Lee R, et al. Dielectric resonance phenomena in ultra high field MRI. *J Comput Assist Tomogr.* 1999;23:821–831.
- [16] Schmitt M, Feiweier T, Horger W, et al. Improved uniformity of RF-distribution in clinical whole body-imaging at 3T by means of dielectric pads. *Proc Int Soc Magn Reson Med* 2004;12:197.
- [17] Mugler JP 3rd, Epstein FH, Brookeman JR. Shaping the signal response during the approach to steady state in three-dimensional magnetization-prepared rapid gradient-echo imaging using variable flip angles. *Magn Reson Med.* 1992;28:165–185.
- [18] Hennig J, Scheffler K. Hyperchoes. *Magn Reson Med.* 2001;46:6–12.
- [19] Hennig J, Weigel M, Scheffler K. Multiecho sequences with variable refocusing flip angles: optimization of signal behavior using smooth transitions between pseudo steady states (TRAPS). *Magn Reson Med.* 2003;49:527–35.
- [20] Pruessmann KP. Parallel imaging at high field strength: synergies and joint potential. *Top Magn Reson Imaging.* 2004;15:237–244.
- [21] de Bazelaire CM, Duhamel GD, Rofsky NM, Alsop DC. MR imaging relaxation times of abdominal and pelvic tissues measured in vivo at 3.0 T: preliminary results. *Radiology.* 2004;230:652–659.
- [22] Norris DG. High field human imaging. *J Magn Reson Imaging.* 2003;18:519–29. (Erratum in: *J Magn Reson Imaging.* 2004;19:513.)
- [23] Wang Y, Li D, Haacke EM, Brown JJ. A three-point Dixon method for water and fat separation using 2D and 3D gradient-echo techniques. *J Magn Reson Imaging.* 1998;8:703–710.
- [24] von Falkenhausen M, Gieseke J, Morakkabati N, et al. 3T MRI of the Liver. Establishing a Comprehensive Highfield Clinical Imaging Protocol and Comparison to 1.5T. *Proc Int Soc Magn Reson Med* 2004;12:902.
- [25] Leiner T, de Vries M, Hoogeveen R, Vasbinder GB, Lemaire E, van Engelshoven JM. Contrast-enhanced peripheral MR angiography at 3.0 Tesla: initial experience with a whole-body scanner in healthy volunteers. *J Magn Reson Imaging.* 2003;17:609–614.
- [26] Israel GM, Hindman N, Bosniak MA. Evaluation of cystic renal masses: comparison of CT and MR imaging by using the Bosniak classification system. *Radiology* 2004;231:365–371.
- [27] Granata A, Sessa A, Righetti M, et al. Juvenile renal cell carcinoma as first manifestation of von Hippel-Lindau disease. *J Nephrol.* 2004;17:306–310.
- [28] Mosetti MA, Leonardou P, Motohara T, Kanematsu M, Armao D, Semelka RC. Autosomal dominant polycystic kidney disease: MR imaging evaluation using current techniques. *J Magn Reson Imaging.* 2003;18:210–215.
- [29] Burrell M, Llovet JM, Ayuso C, et al. Barcelona Clinic Liver Cancer Group. MRI angiography is superior to helical CT for detection of HCC prior to liver transplantation: an explant correlation. *Hepatology.* 2003;38:1034–1042.
- [30] Heim P, Steiner P, Schoder V, Dieckmann C, Kuhlencordt R, Adam G. Detection of liver lesions with gadolinium-enhanced VIBE sequence in comparison with SPIO-enhanced MRI. *Rofo.* 2003;175:1376–1383.
- [31] McKenzie CA, Lim D, Ransil BJ, et al. Shortening MR image acquisition time for volumetric interpolated breath-hold examination with a recently developed parallel imaging reconstruction technique: clinical feasibility. *Radiology.* 2004;230:589–594.
- [32] Zech CJ, Schoenberg SO, Herrmann KA, Dietrich O, Menzel MI, Lanz T, Wallnofer A, Helmberger T, Reiser MF. Modern visualization of the liver with MRI. Current trends and future perspectives. *Radiologe.* 2004;44:1160–1169.
- [33] Morakkabati-Spitz N, Gieseke J, Kuhl C, et al. 3.0-T high-field magnetic resonance imaging of the female pelvis: preliminary experiences. *Eur Radiol.* 2004; [Epub ahead of print].
- [34] Sheu MH, Chang CY, Wang JH, Yen MS. Preoperative staging of cervical carcinoma with MR imaging: a reappraisal of diagnostic accuracy and pitfalls. *Eur Radiol.* 2001;11:1828–1833.
- [35] Branagan G, Chave H, Fuller C, McGee S, Finnis D. Can magnetic resonance imaging predict circumferential margins and TNM stage in rectal cancer? *Dis Colon Rectum.* 2004;47:1317–22.
- [36] Beets-Tan RG, Beets GL, Vliegen RF, et al. Accuracy of magnetic resonance imaging in prediction of tumour-free resection margin in rectal cancer surgery. *Lancet.* 2001;357:497–504.
- [37] Kim JH, Beets GL, Kim MJ, Kessels AG, Beets-Tan RG. High-resolution MR imaging for nodal staging in rectal cancer: are there any criteria in addition to the size? *Eur J Radiol.* 2004;52:78–83.
- [38] Schmitz S, Allsop J, Zeka J, et al. MRCP, Initial Experience at 3Tesla. *Proc Int Soc Magn Reson Med.* 2004;12:899.
- [39] Fulcher AS, Turner MA, Franklin KJ, et al. Primary sclerosing cholangitis: evaluation with MR cholangiography—a case-control study. *Radiology.* 2000; 215:71–80.
- [40] Talwalkar JA, Angulo P, Johnson CD, Petersen BT, Lindor KD. Cost-minimization analysis of MRC versus ERCP for the diagnosis of primary sclerosing cholangitis. *Hepatology.* 2004;40:39–45.
- [41] Porayko MK, Wiesner RH, LaRusso NF, et al. Patients with asymptomatic primary sclerosing cholangitis frequently have progressive disease. *Gastroenterology.* 1990;98:1594–1602.
- [42] Beuers U, Spengler U, Sackmann M, Paumgartner G, Sauerbruch T. Deterioration of cholestasis after endoscopic retrograde cholangiography in advanced primary sclerosing cholangitis. *J Hepatol.* 1992;15:140–143.
- [43] Vasbinder GB, Nelemans PJ, Kessels AG, et al. Renal Artery Diagnostic Imaging Study in Hypertension (RADISH) Study Group. Accuracy of computed tomographic angiography and magnetic resonance angiography for diagnosing renal artery stenosis. *Ann Intern Med.* 2004;141:674–682.

Accurate Prostate Cancer Staging with MR

Tom Scheenen, Ph.D.; Stijn Heijmink, M.D.; Jelle Barentsz, M.D., Ph.D.

Radboud University Nijmegen Medical Centre, Dept. of Radiology

Patient History

A 65-year-old patient with prostate cancer was referred to MR for clinical staging of the disease. The PSA level was 25 µg/l and the biopsy of the prostate had shown a Gleason grade 5.

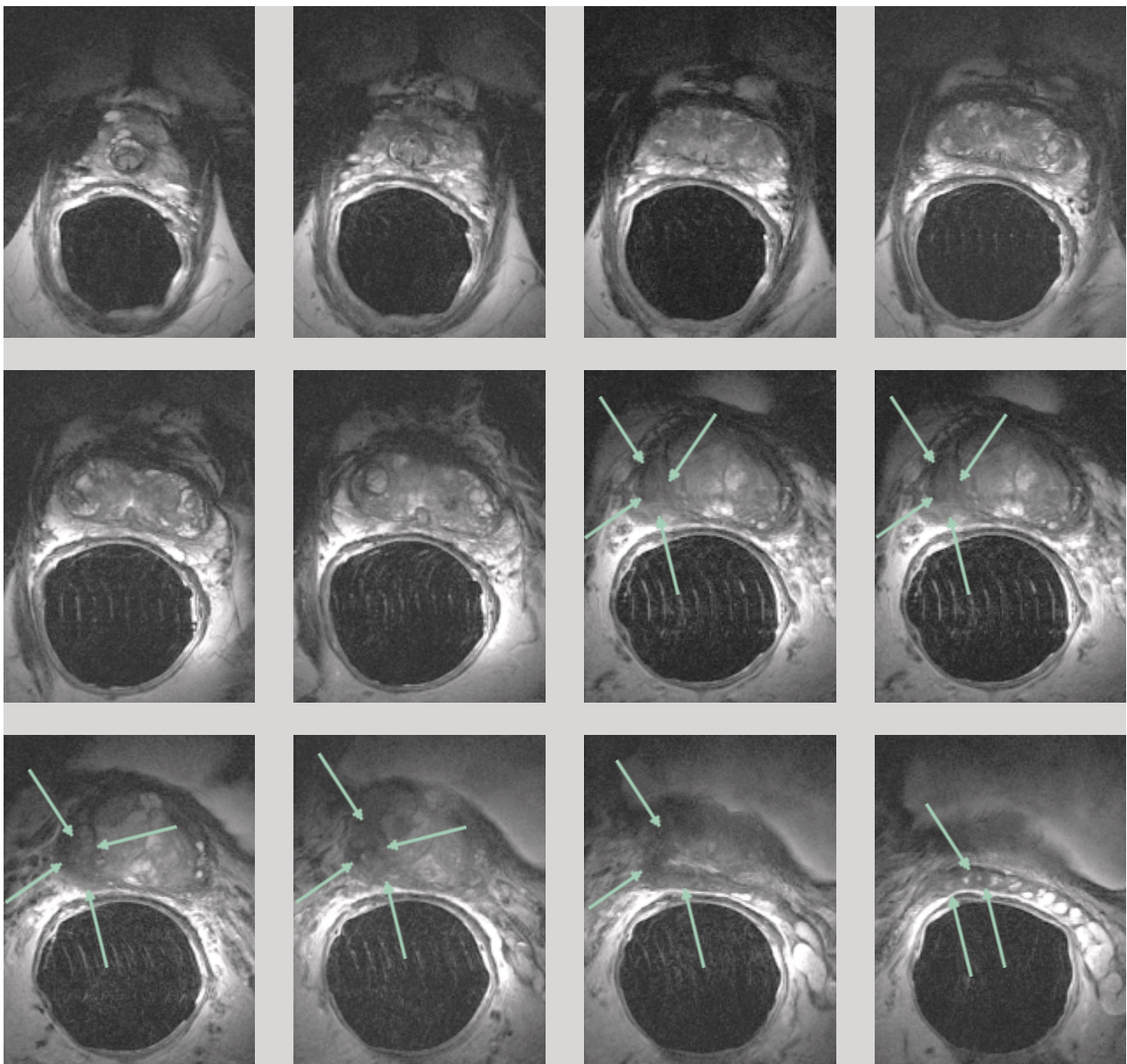


[Figure 1] T2-weighted axial images of the prostate of a 65-year-old patient with prostate cancer. The complete prostate is visualized from apex to base. The large tumor is visible in the right base of the prostate extending into the seminal vesicles (arrows).

Measurement Details

- A prototype of an endorectal coil and interface for 3T (Medrad, Pittsburgh, USA) was used for signal reception. The body coil was used for signal excitation.
- **Multislice axial T2-weighted TSE sequence:**
15 axial slices, TR 4490 ms, TE 153 ms, turbo factor 17, FoV 200 x 100 mm, matrix 768 x 384, slice thickness 2.5 mm. Hyperechoes were used to decrease SAR.
- **Multislice coronal T2-weighted TSE sequence:**
13 coronal slices, TR 4000 ms, TE 116 ms, turbo factor 17, FoV 180 x 90 mm, matrix 512 x 256, slice thickness 4 mm. Hyperechoes were used to decrease SAR.
- **T1-weighted 3D sequence:**
Axial reconstruction of 32 partitions, TR 8.6 ms, TE 4.0 ms, flip angle 15 degrees, FoV 130 x 65 x 48 mm, matrix 256 x 128 x 32, slice thickness 2.5 mm.
- **MAGNETOM Trio, software syngo MR 2004A**

Results & Discussion

On axial and coronal T2-weighted imaging (Fig. 1 and 2) a large hypo-intense region is visible on the right side in the base of the prostate, extending into the seminal vesicles. After contrast agent administration this lesion, including seminal vesicle invasion, enhances on T1-weighted images (Fig. 3). Based on these findings the diagnosis is stage T3b. The histopathological analysis of biopsy material from the seminal vesicles confirmed the presence of cancer with Gleason grade 3+4. After a negative lymph node dissection the prostate was resected. The resected prostate was cut, stained and studied (Fig. 4), confirming the clinical stage of the disease: T3b. Because of medication before the prostatectomy the Gleason score was difficult to assess.

This is an example of accurate prostate cancer staging. The combination of an endorectal coil and a magnetic field strength of 3T provides enough SNR for high resolution imaging of the complete prostate. In this case the MRI findings made the urologist decide to take biopsies from the seminal vesicles. Since these were positive for cancer, lymph nodes around the prostate were dissected. With no signs of cancer in the lymph nodes, the next step was to resect the prostate itself.

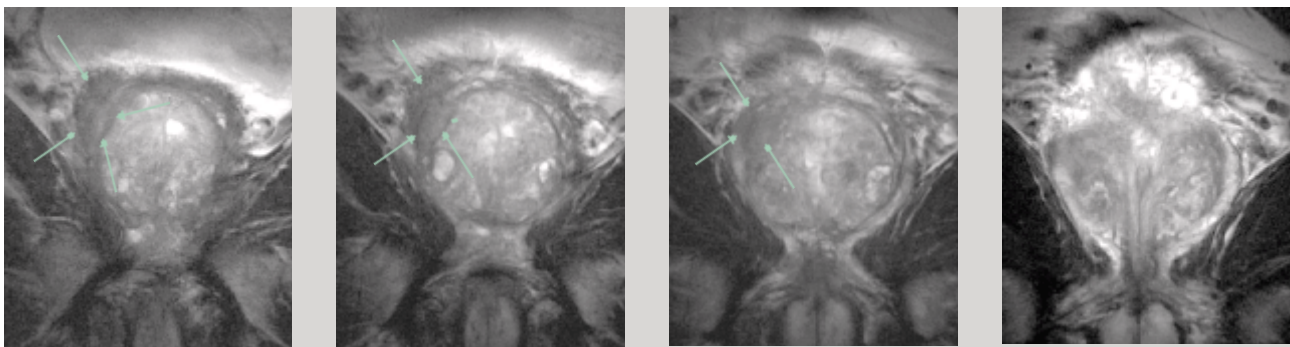


[Figure 2] Four out of 13 T2-weighted coronal images of the prostate. As the images move towards the endorectal coil (from ventral to dorsal) the SNR of the images increases. Again the tumor with seminal vesicle invasion is indicated with the arrows.

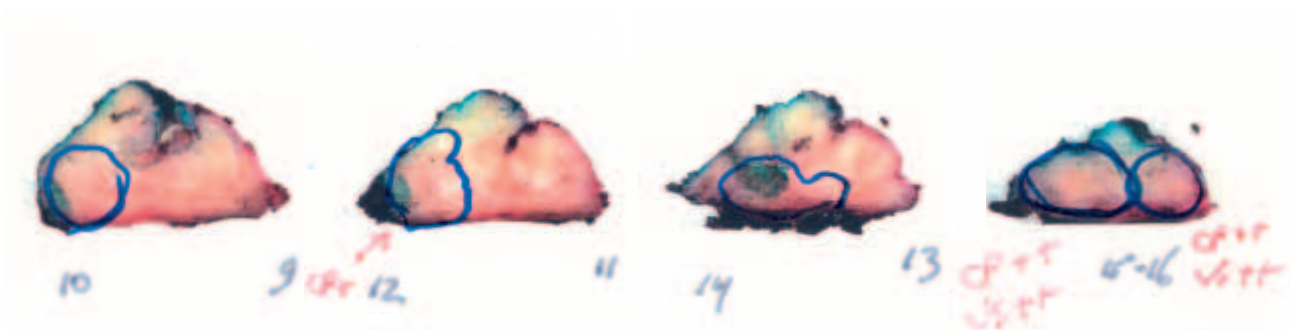
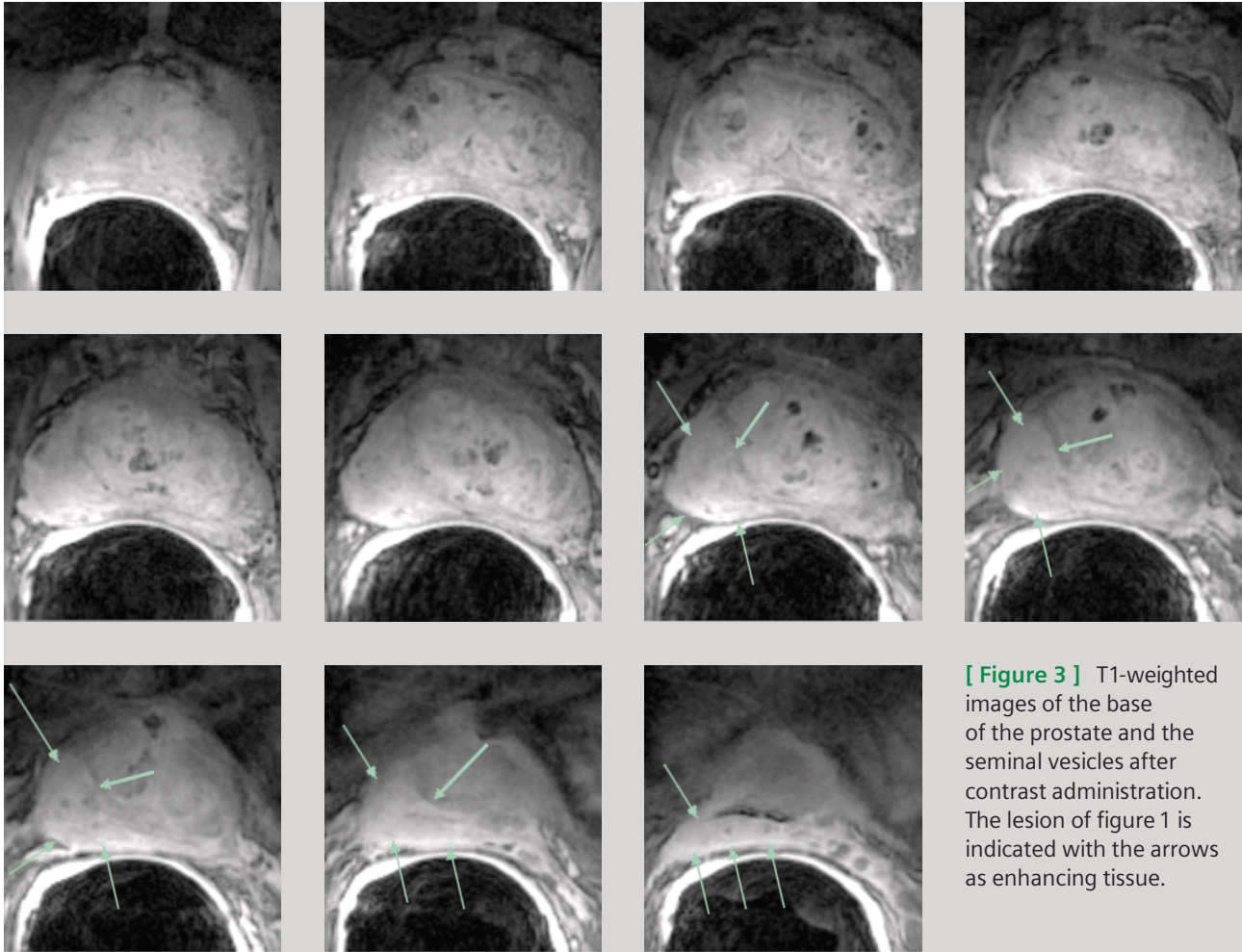


[Figure 4] Histopathology of four cuts through the base of the resected prostate. The tumor is indicated with a blue line. Extra capsular extension is indicated as CP+ and CP++, seminal vesicle invasion is indicated as VS++.



We see a way to increase patient throughput by 50%

We see a way to do MRI with an increased signal-to-noise of up to 100%


From a revolutionary
to the world leader in two years.

Tim

www.siemens.com/medical

Results may vary. Data on file.

M-Z928-1-7600

 **Proven Outcomes with Tim (Total imaging matrix technology).** Around the world, Tim[®] has become the new standard in MRI. With hundreds and hundreds of installations, Tim is proving every day that a new era has begun. Now, with just one mouse click you can change Tim's coils and perform a comprehensive assessment of an entire disease, not

just a single body region. You can scan the smallest lesions or the entire central nervous system without a detail lost. And you can do it all at the highest speed without sacrificing resolution. Let Tim prove it to you at www.siemens.com/Tim.

Siemens **Medical Solutions** that help

SIEMENS
medical

Accurate Staging of Prostate Cancer with MR

Tom Scheenen, Ph.D.; Stijn Heijmink, M.D.; Jelle Barentsz, M.D., Ph.D.

Radboud University Nijmegen Medical Centre, Dept. of Radiology

Patient History

51 year old patient with prostate cancer. Clinical stage T2 based on digital rectal examination. For accurate staging of the disease, this patient was called for an MRI exam at 3T. With his stage, PSA and Gleason score (PSA = 1.0 µg/l Biopsy: Gleason 6/10) the pretest probability of having limited disease (confined to the prostate) is between 52 and 64%, according to the Partin coefficient tables.

Measurement Details

■ **A prototype of an endorectal coil and interface for 3T** (Medrad, Pittsburgh, USA) was used for signal reception. The body coil was used for signal excitation.

■ **Multislice T2-weighted TSE sequence:**
15 axial slices, TR 4490 ms, TE 153 ms, turbo factor 17, FOV 200 x 100 mm, matrix 768 x 384, slice thickness 2.5 mm. Hyperechoes were used to decrease SAR.

■ **T1-weighted 3D sequence:**

Axial reconstruction of 32 partitions, TR 8.6 ms, TE 4.0 ms, flip angle 15 degrees, FOV 130 x 65 x 48 mm, matrix 256 x 128 x 32, slice thickness 2.5 mm.

■ **MAGNETOM Trio, software syngo MR 2004A**

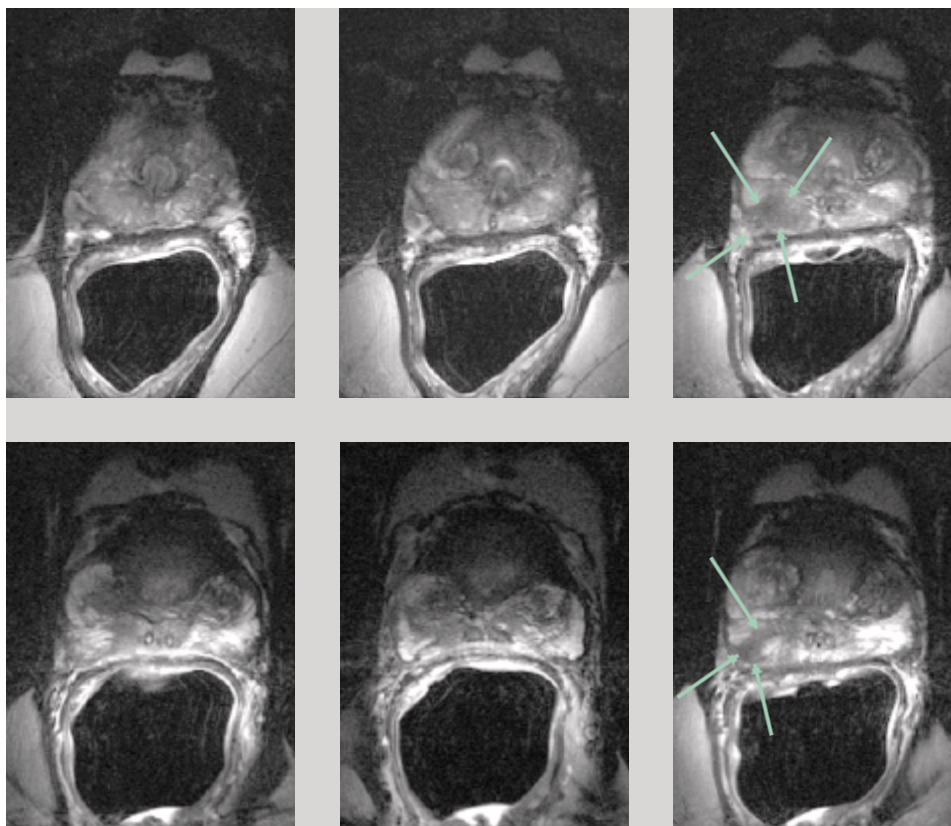


[Figure 1] Six out of 15 T2-weighted axial images of the prostate of a 51-year-old patient with prostate cancer. The endorectal coil balloon is visible as a large void below the prostate. The arrows indicate the tumor lesion.

Results & Discussion

On T2-weighted imaging a hypo-intense area is clearly visible in the peripheral zone of the right side of the prostate gland (arrows Fig. 1). This region enhances after administration of contrast agent (Fig. 2). There are no clear signs of extracapsular spread or seminal vesicles invasion of the disease. Based on these findings the diagnosis is stage T2a.

After staging of the disease, the patient was treated with a prostate and seminal vesicles resection. The resected prostate was cut, stained and investigated at the department of pathology (Fig. 3). The pathological stage confirmed the clinical stage of the disease but found a higher Gleason score: T2a with Gleason grade 3+5.

The attainable spatial resolution with an endorectal coil at 3T provides excellent opportunities for accurate staging of prostate cancer. In this case the MRI-examination confirms the existence of the cancerous tissue, and provides valuable information on local disease stage.

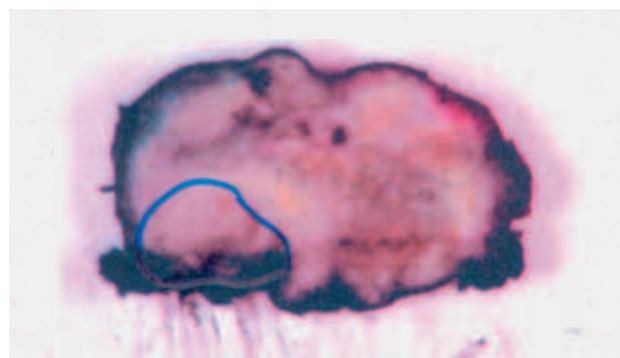


[Figure 3] Histopathology of the corresponding cut through the resected prostate on which the tumor is indicated with a blue line.

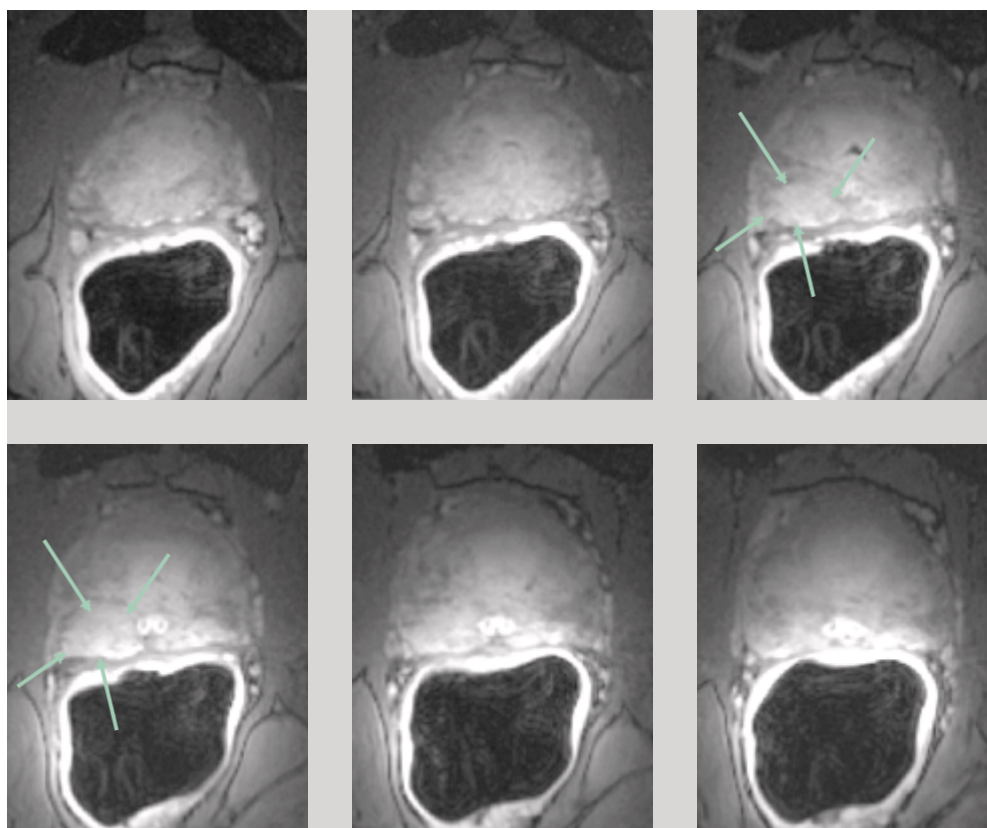


[Figure 2] Six out of 32 T1-weighted images after contrast administration. The thickness of slices and partitions do not coincide, so the slice positions do not exactly match with T2-weighted imaging. The lesion of figure 1 is indicated with the arrows as enhancing tissue.

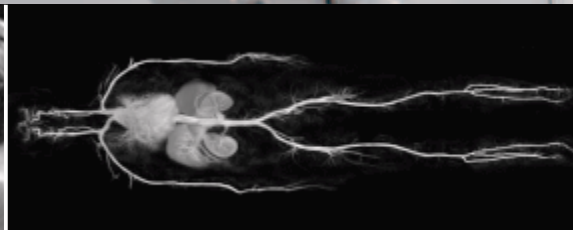
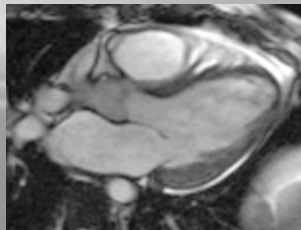
We see a way to evaluate myocardial infarct and vascular disease within one exam without any patient repositioning

Tim won't let you miss a beat.

We see a way to determine regional ventricular function in real time allowing free-breathing using 12 matrix coil elements

Results may vary. Data on file.

www.siemens.com/medical



M-2906-1-7600

Proven Outcomes in Cardiology with Tim® (Total imaging matrix technology). Tim offers unmatched MRI capabilities for all cardiovascular exams without repositioning the patient. Ideal not only in diagnosing subendocardial infarct and congenital heart disease, but also systemic diseases like diabetes and atherosclerosis. With its 76 matrix coil elements and up

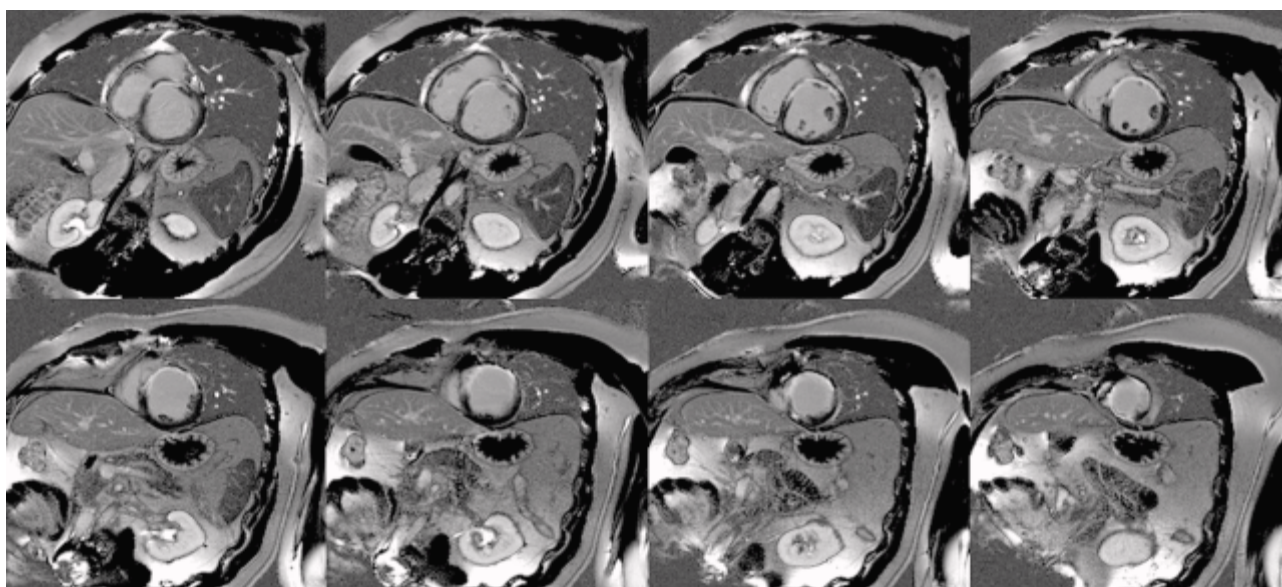
to 32 RF channels, you enjoy revolutionary acquisition speed with virtually unlimited Parallel Imaging even in double oblique slice orientations. Tim transforms workflow from an exam limited by the dimensions of local RF-coils to one determined by the disease. Tim. Very heart smart.

Siemens **Medical Solutions** that help

SIEMENS
medical

Cardiac

CMR particularly benefits from the high SNR of MAGNETOM Trio, A Tim System. Applications like myocardial viability and cardiac perfusion improve significantly. This is also due to synergies between new advanced parallel imaging techniques like T-SENSE and the high element density of the MAGNETOM Trio Matrix coils.



Advances in Cardiac MRI at 3T – Benefits of Multi-Channel MR Systems

Bernd J. Wintersperger, M.D.; Stefan O. Schoenberg, M.D.; Olaf Dietrich, Ph.D; Maximilian F. Reiser, M.D.

Department of Clinical Radiology, University Hospitals-Grosshadern,
Ludwig-Maximilians-University, Munich, Germany

Introduction

The challenges for cardiac MR imaging are three-fold: spatial and temporal resolution, signal-to-noise ratio and the limitations induced by the need for breath-hold imaging (Figure 1). With the advance of multi-channel whole-body MRI systems at 3T, all these limitations can now be effectively overcome. Parallel acquisition techniques (PAT) allow increasing temporal or spatial resolution at virtually no costs in acquisition time. The higher field strength at 3T makes up for the loss of signal-to-noise ratio (SNR) induced by fast scanning with PAT. With the combination of PAT and 3T, real-time acquisitions have now become feasible without obviating the need for breath-hold cardiac MRI (Figure 1).

Different Aspects of MR imaging

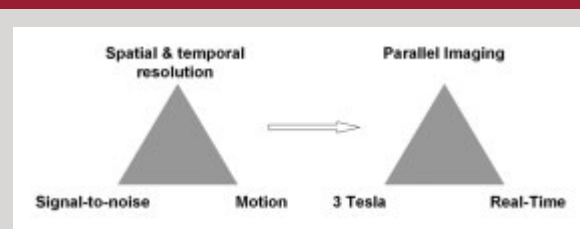


[Figure 1] Relationship of different aspects of MR imaging specially in respect to resolution, SNR and motion (left); possible solutions to the problems as offered by 3T multi-channel MRI.

Basic Concepts of Parallel Imaging at 3T

The concept of parallel imaging is the under-sampling of k-space by sampling only every n^{th} line in k-space compared to a full k-space acquisition. This reduces the acquisition time to $1/n$ of the non-accelerated acquisition and is typically referred to as imaging with an acceleration or reduction factor R . However, parallel imaging requires multi-element coils for spatially resolved signal detection. The so-called coil sensitivity profiles are then used to reconstruct an image

equivalent to a full k-space acquisition without increase in acquisition time and without aliasing artifacts caused by under-sampling. Parallel imaging and 3T have a unique synergistic effect. One limitation of 3T MRI is the higher specific absorption rate (SAR) induced by the higher Larmor frequency of the RF pulses, which is effectively compensated by parallel imaging where fewer RF pulses are required to sample an equivalent data set. Nevertheless, the lower SNR induced by the use of PAT which decreases the SNR by at least a factor of one over the square root of the acceleration factor ($1/\sqrt{R}$) is nicely compensated by the higher SNR at 3T. Looking at the performance of PAT at 3T compared to 1.5T, it is easy to see that the loss of SNR introduced by an acceleration factor of $R=4$ with parallel imaging is approximately compensated by the SNR increase of a factor of 2 from 1.5 to 3.0T. Therefore a four-fold gain in acquisition speed is feasible at 3 Tesla with virtually no penalty in SNR compared to 1.5T.

These methodological advantages result in a number of shifts of paradigms in cardiac MRI at 3T:

- Multi-breath-hold imaging becomes single breath-hold imaging.
- 128 matrix becomes 256 matrix.
- Gated breath-hold CINE MRI becomes free breathing real-time CINE MRI.
- 2D CINE cardiac MRI becomes 3D CINE cardiac MRI.

Cardiac CINE MRI @ MAGNETOM Trio with Tim

It has already effectively been shown that single breath-hold multi-slice cardiac MRI is feasible already at 1.5T. In a study by Wintersperger et al., 11 short axis slices using TrueFISP cardiac functional analysis have been feasible within a single breath-hold of ~20 heart beats (1). As other studies have shown that temporal resolution is more critical for the accuracy of cardiac function analysis than spatial resolution (2), a temporal resolution of <50ms could have been maintained in this study with an acquisition matrix of 128 (1). For those

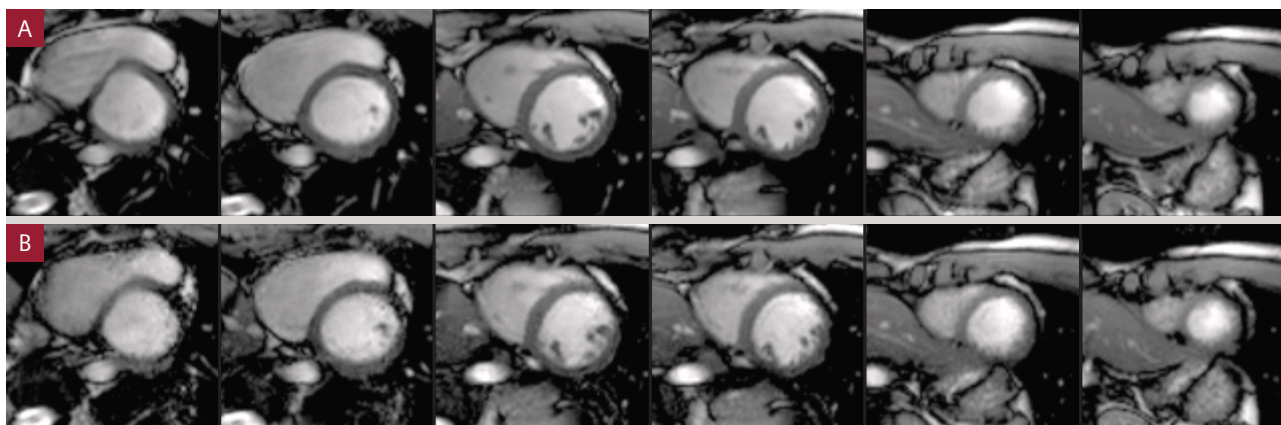


[Figure 2] Comparison of (a) segmented CINE TrueFISP acquiring a single slice per breath-hold and (b) fourfold ($R=4$) TSENSE accelerated CINE TrueFISP with whole short axis data acquired in just 2 breath-holds on a MAGNETOM Trio, A Tim System. Note that the slightly increased noise does not interfere with depictability of subtle details.

studies typically an acceleration factor of $R=2$ was used with a GRAPPA (generalized auto-calibrating partially parallel acquisition) reconstruction algorithm. A limitation of the integrated auto-calibration in the GRAPPA algorithm in CINE imaging is caused by the fact that within each image frame additional central lines in k-space (reference lines) have to be acquired for auto-calibration of the coil sensitivity profiles. This results in a net loss of the effective acceleration factor R which is typically reduced by approximately 20–40%, depending on the number of reference lines. More recent reconstruction algorithms such as TSENSE or TGRAPPA effectively overcome this limitation by eliminating the need for additional reference line or ACS (auto-calibration signal) measurements by exploiting the data of an interleaved k-space line sampling covering the full k-space in subsequent dynamic CINE frames (3, 4). These techniques allow for a marked acceleration of CINE TrueFISP imaging as already shown at 1.5T by Reeder et al. with no significant loss in image quality and accuracy for cardiac functional analysis at $R=3$ (5). The combination of the TSENSE algorithm with higher field strengths and multi-channel MRI at 3T exceeds this performance by far.

On a MAGNETOM Trio, A Tim System, four-fold faster cardiac acquisitions at full 256 matrix size with no loss in diagnostic accuracy compared to the unaccelerated images have been successfully demonstrated in clinical applications. In a study of 10 patients with myocardial infarction, an excellent visualization of regional wall motion abnormalities and evaluation of global ventricular function was possible due to the high spatial and temporal resolution of a full 256 matrix and 50 ms temporal resolution in a multi-slice approach (Figure 2). This is a clear gain in diagnostic accuracy for single breath-hold

cardiac MRI compared to 1.5T, since it has been shown earlier that with real-time CINE regional function analysis is not reliably feasible at 1.5T due to the limits in spatial resolution. Another advantage of the combination of parallel imaging with a multi-channel MAGNETOM Trio, A Tim System compared to conventional 3T MRI scanner is that the under-sampling of k-space with parallel acquisition techniques results in the possible use of higher flip angles for TrueFISP imaging. Due to the square relationship between the excitation angle and the specific absorption rate (SAR), cardiac MRI at 3T was traditionally limited to lower flip angles within the range of $\sim 40^\circ$ to 50° . Using TSENSE in combination with a MAGNETOM Trio, A Tim System, flip angles of 60° or even higher could be realized resulting in a better blood-to-myocardium contrast. The contrast of multi-slice acquisitions at 3T accelerated by T-SENSE is therefore comparable to unaccelerated images at 1.5T.

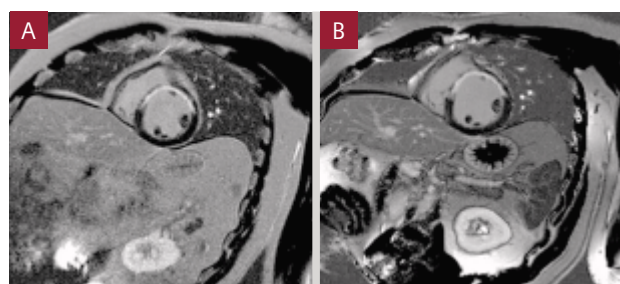


[Figure 3] PSIR single-shot TrueFISP in a patient with extensive LAD infarction; while this technique at 1.5T (a) comes along with a considerable level of noise, at 3T (b) image quality improves also based on the substantial lower noise level.

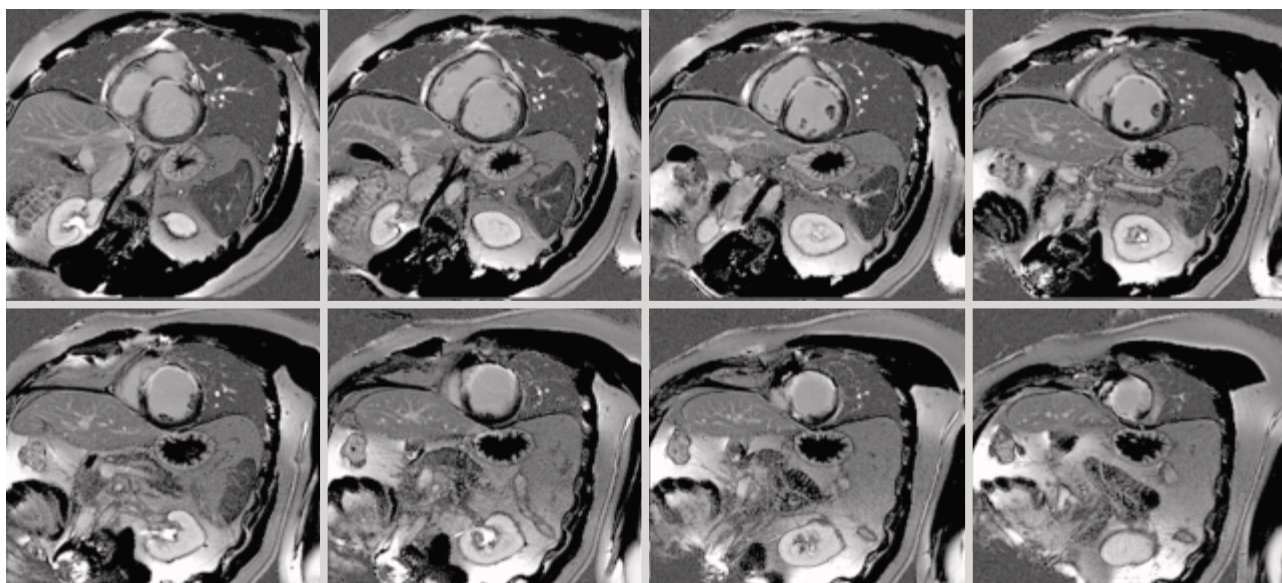


[Figure 4] MAGNETOM Trio, A Tim System short axis data set acquired in multiple breath-holds using a segmented PSIR TrueFISP technique showing the whole extent of the LAD infarction in the same patient as shown in figure 3.

Delayed Enhancement* @ MAGNETOM Trio, A Tim System

Additionally, for use in delayed enhancement (DE) imaging assessing myocardial infarction and viability, multi-channel 3T MRI allow for new possibilities and options. Despite all the effectiveness and value of DE imaging for assessment of myocardial infarction, this technique remains quite time-intensive in clinical routine due to the need for inversion time adjustments to allow optimized contrast between the infarcted and normal myocardium. Already at 1.5T it had been shown that a new technique termed phase sensitive IR (PSIR) reconstruction obviates the need for exact optimization of the inversion time (6).

Huber et al. demonstrated that PSIR allows an accurate assessment of the area of infarcted myocardium at virtually any arbitrary chosen inversion time (7). The combination with TrueFISP based acquisition speeds up data sampling allowing single breath-hold multi-slice coverage of the entire left ventricle for the exact assessment of the extent of myocardial infarction (8). However at 1.5T these images are somewhat noisy and sometimes influenced by artifacts due to the ambiguousness of the phase information at low signal-to-noise ratios (Figure 3). At 3T the higher SNR allows for excellent multi-slice single breath-holds TrueFISP PSIR imaging of the entire left ventricle with high image quality (Figure 4). The combination with PAT techniques like GRAPPA again allows preventing possible SAR limitations using TrueFISP at 3T.

If TSENSE TrueFISP acquisitions of cardiac function and PSIR TrueFISP acquisition of delayed contrast enhancements are combined at multi-channel 3T MRI, a complete assessment of function and viability with high temporal and spatial resolution is feasible with only a few breath-holds.

At 3T the contrast-to-noise ratio of the TrueFISP based PSIR technique even exceeds the SNR of the best technique at hand used 1.5T, e.g. segmented TurboFLASH magnitude reconstruction. Comparing the accuracy of single breath-hold multi-slice acquisitions to time intensive multi-breath-hold single slice acquisitions, it has been shown that the limits of agreement between both are smaller at 3T compared to 1.5T.

Myocardial Perfusion* @ MAGNETOM Trio with Tim

While CINE MRI and viability imaging have already been daily clinical routine techniques on 1.5T with sufficient high SNR levels, myocardial perfusion imaging has been a promising tool for the evaluation of coronary artery disease for years but never really took off for widespread use. This has been mainly based on limited SNR performance, artifacts and variable coexisting sequence techniques. At 3T one can envision that due the higher SNR the quality of TurboFLASH techniques, the best evaluated standard in myocardial perfusion imaging, will dramatically improve therefore enabling a reliable time-signal analysis and accurate assessment of myocardial perfusion (Figure 5). The gain in SNR could par-

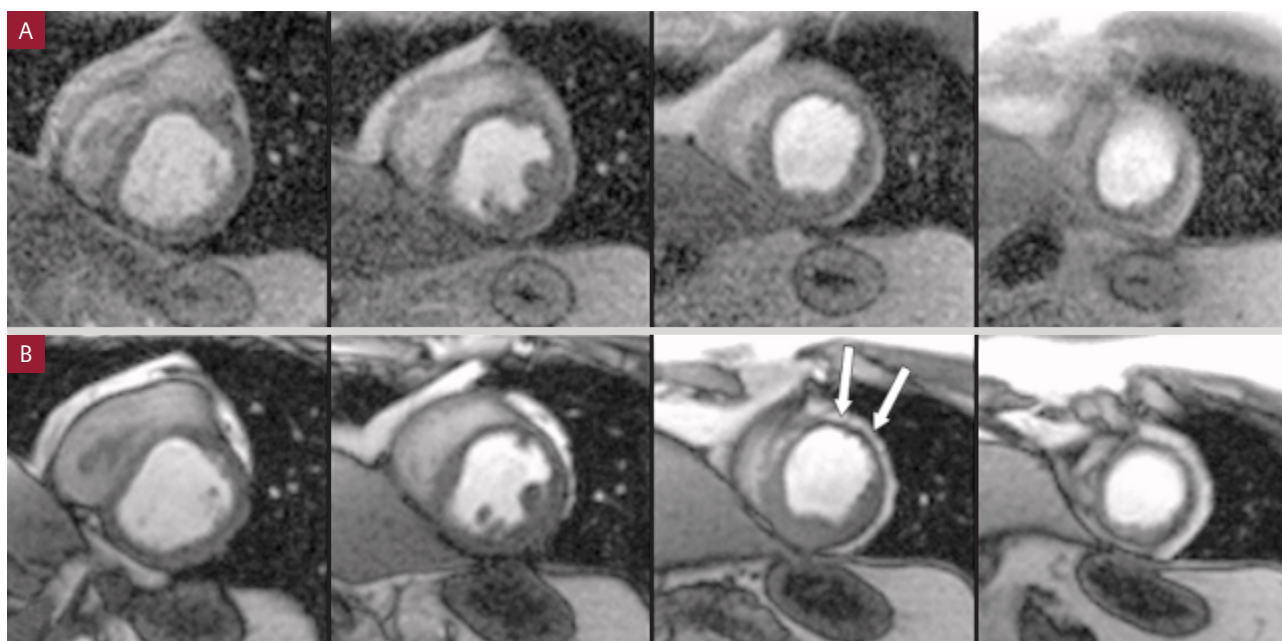


[Figure 5] IR TurboFLASH myocardial perfusion imaging: (a) four slice data set acquired at 1.5T shows a considerable high noise level possibly interfering with quantitative analysis. (b) Data set of same patient acquired with MAGNETOM Trio, A Tim System using the same technique shows markedly reduced noise and allows better delineation of the hypoperfusion in the infarcted anterior wall (arrows).

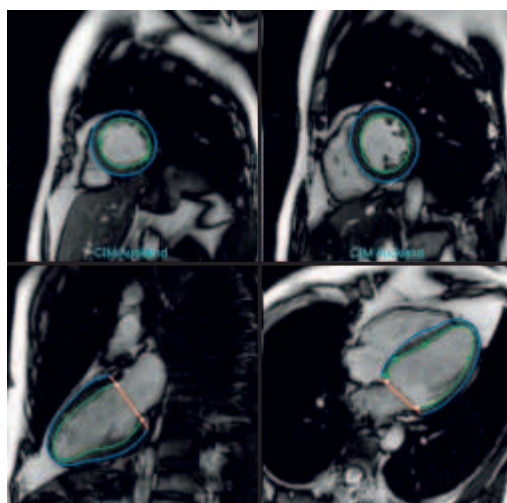


[Figure 6] T-SENSE CINE data set showing the automated contouring of the endo- and epicardial border in multiple planes. This technique allows for better detection of valve planes and therefore increased accuracy. Functional Information of the circumferential contraction though is maintained by incorporated short axis images.

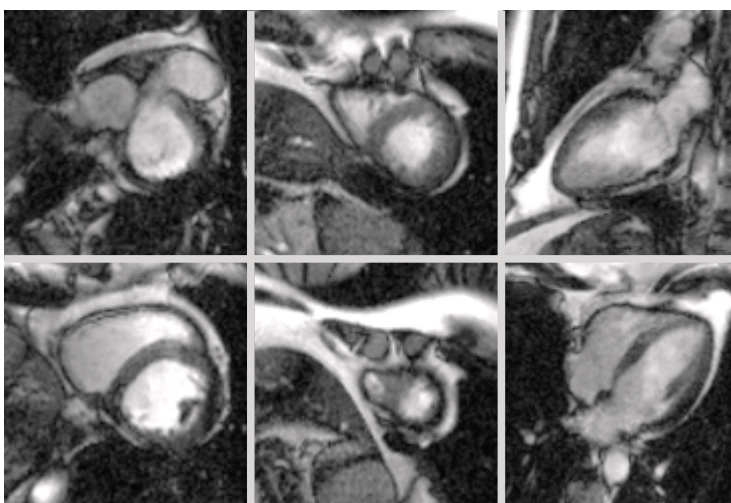


[Figure 7] The data sampling acceleration in CINE imaging of the heart by PAT (T-SENSE) allows not only for fast acquisition of short axis data but also multiplanar data sets without the need of data registration to avoid mismatch of the data.

*The information about this product is preliminary. The product is under development and is not commercially available in the US. and its future availability cannot be assured.

tially be invested in even higher spatial/temporal resolution using higher acceleration factors with PAT (e.g. TENSE) or enabling coverage of the entire short axis during first pass perfusion.

Future Developments

The introduction of 4D function analysis tools allows changing the approach for cardiac functional assessment (9). Although the use of the Simpsons' rule with a contiguous coverage along the entire short axis from the apex to the AV-valve plane has major benefits in terms of accuracy based on its 3D modeling, the valve plane itself could much better be identified in 2- and 4-chamber views. The 4D analysis software allows combining the information of long and short axis cardiac MRI including a computerized LV model thereby reducing the number of required short axis views (Figure 6). This ideally combines with single breath-hold cardiac MRI at 3T accelerated with T-SENSE, since one breath-hold is sufficient to require 5–6 slices with sufficiently high temporal and spatial resolution for this analysis (Figure 7). Therefore one can envision a single breath-hold, highly accurate assessment of the LV function by the combination of MAGNETOM Trio, A Tim System and 4D Argus Software.

With the advent of multi-channel scanner systems, new dedicated coil arrays might be developed that meet the high number of the receiver channels of the MAGNETOM Trio, A Tim System ("32 elements meet 32 channels"). In a preliminary research study in collaboration with RAPID Biomedical, a dedicated flexible cardiac coil was used in close cooperation with the team of Dr. Mark Griswold. Results exceeded those already obtained at 1.5T with a previous prototype of the coil (5). Acceleration factors of 6 for TENSE cine TrueFISP cardiac function analysis were feasible at virtually no loss in diagnostic image quality. In combination with real-time acquisitions instead of segmented CINE techniques, this would allow new three-dimensional insights in the true physiologic cardiac function without hemodynamic changes based on breath-hold induced intrathoracic pressure variations. As already shown in preliminary studies, this has promising clinical applications for the assessment of diseases such as constrictive pericarditis and the differentiation from restrictive cardiomyopathy (10).

Summary

Cardiac MRI was initially not considered the primary application for 3T due to problems with the high SAR and a number of artifacts particularly for the use of steady-state free precession techniques (TrueFISP). The advent of multi-channel cardiac MRI systems in combination with new acquisition

strategies such as TENSE and TGRAPPA now has vastly overcome these limitations and even shown new possibilities for improved diagnosis of cardiac diseases at higher field strengths.

Acknowledgement

The authors also acknowledge the work of the entire cardiac team of the Department of Clinical Radiology: Kerstin Bauner, M.D., Denise Friedrich RT, Armin Huber, M.D., Michele Picciolo, RT, Frank Stadie, RT, and of Siemens Medical Solutions: Andreas Greiser Ph.D., Edgar Müller, Ph.D., Michaela Schmidt, RT, Katrin Sprung, RT.

This work was in part supported by the "Verein zur Förderung der Forschung und Entwicklung der Magnetresonanztomographie e.V."



Authors (left to right): Bernd J. Wintersperger, M.D.; Stefan O. Schoenberg, M.D.; Olaf Dietrich, Ph.D.; Maximilian F. Reiser, M.D.

References

- [1] Wintersperger BJ, Nikolaou K, Dietrich O, et al. Single breath-hold real-time cine MR imaging: improved temporal resolution using generalized auto-calibrating partially parallel acquisition (GRAPPA) algorithm. *Eur Radiol* 2003; 13:1931–1936.
- [2] Miller S, Simonetti OP, Carr J, Kramer U, Finn JP. MR Imaging of the heart with cine true fast imaging with steady-state precession: influence of spatial and temporal resolutions on left ventricular functional parameters. *Radiology* 2002; 223:263–269.
- [3] Kellman P, Epstein FH, McVeigh ER. Adaptive sensitivity encoding incorporating temporal filtering (TENSE). *Magn Reson Med* 2001; 45:846–852.
- [4] Breuer FA, Kellman P, Griswold MA, Jakob PM. Dynamic auto-calibrated parallel imaging using temporal GRAPPA (TGRAPPA). *Magn Reson Med* 2005; 53:981–985.
- [5] Reeder SB, Wintersperger BJ, Dietrich O, et al. Cardiac CINE SSFP imaging with parallel acquisition techniques and a 32-channel cardiac coil: evaluation of SNR performance. *Magn Reson Med* 2005; in press.
- [6] Kellman P, Arai AE, McVeigh ER, Aletras AH. Phase-sensitive inversion recovery for detecting myocardial infarction using gadolinium-delayed hyperenhancement. *Magn Reson Med* 2002; 47:372–383.
- [7] Huber AM, Schoenberg SO, Hayes C, et al. Value of phase-sensitive Inversion Recovery (PSIR) for Detection of Myocardial Infarction. *Radiology* 2005; in press.
- [8] Huber AM, Schoenberg SO, Spannagl B, et al. Single shot inversion recovery TrueFISP for assessment of myocardial infarction. *Am J Roentgenol* 2005; accepted.
- [9] Young AA, Cowan BR, Thrupp SF, Hedley WJ, Dell'Italia LJ. Left ventricular mass and volume: fast calculation with guide-point modeling on MR images. *Radiology* 2000; 216:597–602.
- [10] Francone M, Dymarkowski S, Kalantzi M, Bogaert J. Real-time cine MRI of ventricular septal motion: a novel approach to assess ventricular coupling. *J Magn Reson Imaging* 2005; 21:305–309.

MR Angiography

1024 image acquisition matrix for Time of Flight (TOF) angiography in the head in a few minutes acquisition time as well as submillimeter isotropic resolution for contrast enhanced angiography in all body parts in less than 20 s is now everyday reality with MAGNETOM Trio, A Tim System.



Comparison of Intracranial 3D-ToF-MRA with and without Parallel Acquisition Techniques at 1.5T and 3.0T: Preliminary Results

Jochen Gaa¹, Stefan Weidauer², Martin Requardt³, Berthold Kiefer³, Heinrich Lanfermann², Friedhelm E. Zanella²

¹Department of Radiology, Technische Universität München, Germany

²Department of Neuroradiology, University of Frankfurt, Germany

³Siemens Medical Systems, Erlangen, Germany

Introduction

Magnetic resonance angiography (MRA) has undergone significant developments over the past decade. For imaging intracranial vessels, time-of-flight (ToF) MRA sequences have been widely used (5, 6, 11). With this technique the vessels give high signal intensity related to the inflow effect of blood during its passage through the acquisition volume, whereas the background tissue appears dark because a short repetition time prevents relaxation of stationary tissue.

Present available pulse sequences are well optimized for ToF-MRA at 1.5T. However, one of the principal limitations inherent to ToF-MRA is that they remain signal limited when pushed to the limits of higher resolution and shorter acquisition times. The main advantage of high B-field imaging is a significant improvement in the signal-to-noise-ratio (SNR), which increases in an approximately linear fashion with field strength in the range of 1.5T to 3.0T. Thus, the gain in SNR at 3.0T can be used for either a reduction in imaging time or an increase in resolution. ToF-MRA is a technique that can benefit from the increased SNR available at 3.0T by decreasing voxel size, resulting in improved spatial resolution compared to 1.5T. In addition, advances in coil technology have resulted in further signal gains and multichannel technology has allowed for novel acquisition strategies such as integrated parallel acquisition techniques (iPAT); (3, 4, 7, 8).

Material and Methods

Seven volunteers and 5 patients (4 aneurysms, 1 AVM) underwent 3D-ToF-MRA at 1.5T (MAGNETOM Sonata) and 3.0T (MAGNETOM Trio) with and without parallel acquisition techniques (iPAT) using similarly designed 8-channel phased-array head coils. Imaging time of the pulse sequences was set to 7.15 and 7.35 min, respectively. The pulse sequence parameters for both 1.5T and 3.0T are listed in Table 1.

Images were analyzed quantitatively by calculating signal-to-noise (SNR) and contrast-to-noise (CNR) ratios of proximal M2 segments and qualitatively by using a 5-point scale.

Results

All patients tolerated the MR examination well. No sensory-motor stimulations or signs related to the increased RF deposition (such as increased sweating) particularly at 3.0T were reported. Analysis of the vessel SNR and CNR is summarized in Table 1. The results indicate a significant increase in both vessel SNR and CNR at 3.0T. ToF-MRA without iPAT at 3.0T showed a higher, statistically insignificant SNR and CNR compared with MRA at 3.0T with iPAT. Both SNR and CNR were significantly higher at 3.0T compared with 1.5T.

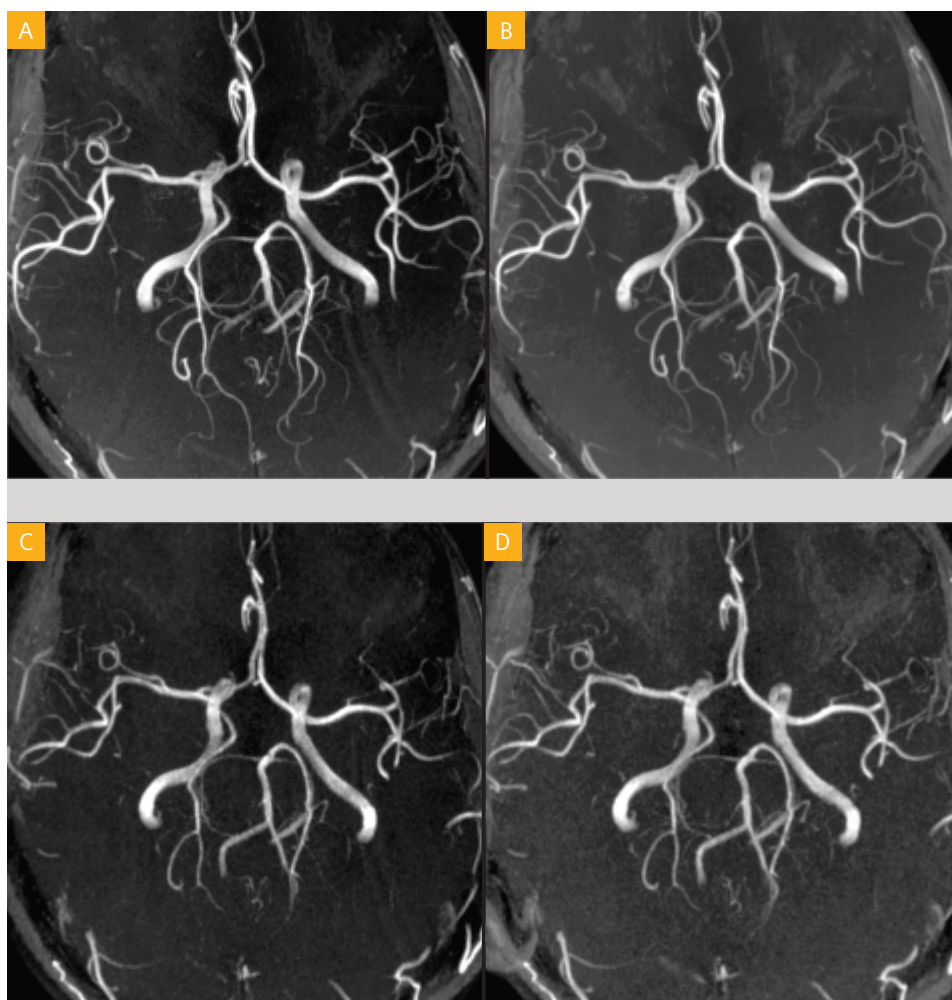
Overall vessel visualization was rated more highly at both MRA sequences with 3T (Table 2). A slightly higher, statistically not significant overall score was obtained for the MRA with iPAT at 3.0T compared with the 3.0T MRA without iPAT. In particular, visualization of smaller vessel segments, such

Table 1

Field Strength	SNR	CNR
3.0T no iPAT	122,6 ± 31,4**	88,9 ± 27,4**
3.0T with iPAT	107,8 ± 26,6*	75,9 ± 24,4**
1.5T no iPAT	67,3 ± 14,2	39,7 ± 13,5
1.5T with iPAT	50,3 ± 10,7	31,6 ± 11,1

* $P < 0.005$, ** $P < 0.001$

SNR and CNR values obtained at 1.5T and 3.0T with and without iPAT. Blood measurements were made on the proximal M2 segments of the MCA.



[Figure 1] Axial collapse 3D-ToF MIP images at 3.0T with (A) and without (B) iPAT and at 1.5T with iPAT (C) and without iPAT (D). Note the better visualization of distal MCA and PCA branches as well as the right AICA at 3.0T (A, B). Minor aliasing artifacts are noticed due to the use of the iPAT reconstruction algorithm (A, C).T.

as M3 and P3 segments as well as delineation of PICA and AICA, was rated significantly superior compared to both MRA sequences at 1.5T (Fig. 1).

Wrap around artifacts in the MRAs with iPAT were minor at both 1.5T and 3.0T and had no noticeable influence on image analysis. The increased susceptibility effects at 3.0T,

especially at air-bone interfaces along the floor of the anterior cranial fossa and adjacent to the petrous portions of the temporal bones had no noticeable effects on the image quality of ToF MRA at 3.0T. Delineation of a left temporal AVM in one patient was slightly better at both MRAs at 3.0T (Fig. 2). One aneurysm of the right MCA (Fig. 3) with a size of 2.8 mm was

Table 2

Field Strength	A2	M2	M3	P2	P3	PICA	AICA	SCA	Overall
3.0T no iPAT	4,8	4,4	3,3*	4,2	3,7**	4,0**	3,8**	4,2**	4,1±0,5**
3.0T with iPAT	4,8	4,8	3,7**	4,6	4,0**	4,0**	4,0**	4,6**	4,3±0,4**
1.5T no iPAT	4,0	3,0	1,3	2,9	1,0	2,3	1,7	2,3	2,3±0,1
1.5T with iPAT	4,0	3,4	1,3	2,9	1,0	1,7	1,3	2,3	2,1±0,1

* $P<0.005$, ** $P<0.001$

Confidence of vessel visualization at 1.5T and 3.0T with and without iPAT. Five-point scale with scores of 1 = unsatisfactory, 2 = fair, 3 = average, 4 = good, and 5 = excellent.



[Figure 2] One aneurysm of the right MCA with a size of 2.8 mm was reliably detected only at 3.0T.

reliably detected only at 3.0T, while the other aneurysms – sized between 6 and 10 mm – were detected at both field strengths.

Discussion

ToF-MRA is commonly used in the evaluation of intracranial vascular pathology. Present available pulse sequences are well optimized for ToF-MRA at 1.5T. However, one of the principal limitations inherent to ToF-MRA is that they remain signal limited when pushed to the limits of higher resolution and shorter acquisition times.

There are various factors which enhance the overall image quality in ToF-MRA at 3.0T compared with MRA at lower field strengths. The increased SNR available at 3.0T was used in our study to increase spatial resolution, which reduces the amount of partial volume artifact. Smaller voxels are less subject to intravoxel dephasing because they contain a smaller heterogeneity of spins, providing further improvements in MRA. In addition, the effects of magnetic-field strength-related T1-lengthening of brain parenchyma and background tissue are beneficial for ToF-MRA at 3.0T, providing better suppression of background signal. Furthermore, there is little change in the T1 relaxation of blood, making in-plane saturation effects similar at 1.5T and 3.0T for ToF techniques (2). The lengthened T1 of background tissue allows

ToFMRA at 3.0T with smaller flip angles, decreasing saturation effects within in-plane blood. Since high resolution scanning increases the total number of phase encoding- and 3D-encoding steps, a prolongation of measurement time will result. Owing to the prolonged T1-relaxation constants it was useful to remove the MT pulse in our measurement protocol. MT pulses increase the TR of a measurement protocol by typically 8-12 ms, depending on field strength. Therefore, by removing the MT pulse, a 30% higher resolution within the same total measurement time can be achieved. In addition, the field strength of 3.0T allows an echo time of 3.8 ms to be used as the opposed phase condition. This echo time is shorter than the corresponding 7 ms at 1.5T, which will result in decreased intravoxel dephasing.

In our study, a significantly higher confidence of small vessel visualization was obtained with both ToF-MRA sequences at 3.0T. Despite a lower SNR and CNR, small vessel conspicuity was rated best at 3.0T with iPAT, which was the result of a higher resolution matrix (512 x 640 vs. 296 x 512) and smaller voxel sizes (0.08 vs. 0.13 mm³) compared with the MRA at 3.0T without iPAT.

Main applications of iPAT are the reduction of examination time by faster imaging or the increase of spatial resolution in a given acquisition time. However, the trade-off for reducing the number of acquired k-space lines using iPAT is a decreased

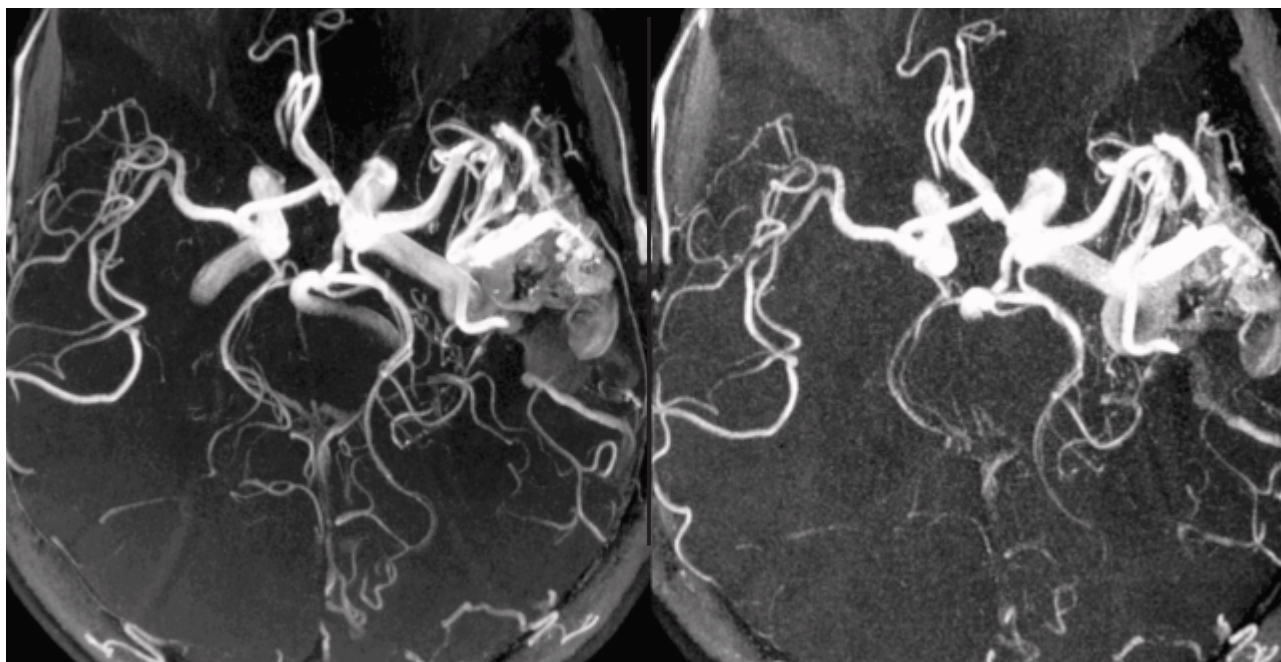


[Figure 3] Patient with left temporal AVM. Note the superior image quality as well as the superior small vessel delineation at 3.0T (left) compared to 1.5T (right).

SNR. Owing to this loss of SNR, parallel acquisition techniques are particularly useful when the corresponding image has a high intrinsic SNR like in 3D-ToF-MRA at 3.0T.

Several techniques have been suggested for the iPAT image reconstruction from the reduced data sets (3, 4, 7, 8). They can be divided into two different groups, such as techniques working on the data in frequency domain (e.g. SMASH, GRAPPA) and techniques working on the Fourier transformed data in the image domain (e.g. SENSE). However, one general limitation of the iPAT approach is the propagation of wrap-around artifacts into the center of the image. We therefore decided to use an AUTO-SMASH-like algorithm such as GRAPPA, since these artifacts are less prominent compared to the SENSE technique (4). In our study, aliasing artifacts were only mild and therefore did not limit the accurate assessment of fine vessel detail.

In conclusion, we have demonstrated that 3D-ToF-MRA at 3.0T is superior to that at 1.5T. The combined use of a multi-channel phased-array head coil in conjunction with iPAT allows for high resolution intracranial vessel imaging with adequate SNR in reasonable imaging times. With continued optimization and refinements, ToF-MRA at 3.0T will further reduce the need for conventional digital subtraction angiography, which is still an invasive method with possible serious complications.

References

- [1] Bernstein MA, Huston J, Lin C, et al. High-resolution intracranial and cervical MRA at 3.0T: technical considerations and initial experience. *Magn Reson Med* 2001;46:955–62.
- [2] Campeau NG, Huston J, Bernstein MA, et al. Magnetic resonance angiography at 3.0 Tesla: initial clinical experience. *Topics Magn Reson Imaging* 2001;12: 183–204.
- [3] Dietrich O, Nikolaou K, Wintersperger BJ, et al. iPAT: applications for fast and cardiovascular MR imaging. *Electromedica* 2002;70:133–46.
- [4] Griswold MA, Jakob PM, Heidemann RM, et al. Generalized autocalibrating partially parallel acquisitions (GRAPPA). *Magn Reson Med* 2002; 47:1202–10.
- [5] Heiserman JE, Drayer BP, Keller PJ, et al. Intracranial vascular stenosis and occlusion: evaluation with three-dimensional time-of-flight MR angiography. *Radiology* 1992;185:667–73.
- [6] Marchal G, Bosmans H, van Fraeyenhoven L, et al. Intracranial vascular lesions: optimization and clinical evaluation of three-dimensional time-of-flight MR angiography. *Radiology* 1990;175:443–8.
- [7] Pruessmann KP, Weiger M, Scheidegger MB, et al. SENSE: sensitivity encoding encoding for fast MRI. *Magn Reson Med* 1999;42:952–62.
- [8] Sodickson DK, Manning WJ. Simultaneous acquisition of spatial harmonics (SMASH): fast imaging with radiofrequency coil arrays. *Magn Reson Med* 1997;38: 591–603.
- [9] Thomas SD, Al-Kwif O, Emery DJ, et al. Application of magnetization transfer at 3.0T in three-dimensional time-of-flight magnetic resonance angiography of the intracranial arteries. *J Magn Res Imag* 2002;15:479–83.
- [10] U.S. Department of Health and Human Services, Food and Drug Administration, Center for Devices and Radiological Health. Guidance for the submission of premarket notifications for magnetic resonance diagnostic devices. Washington, DC: 14 Nov., 1998.
- [11] Wentz KU, Roether J, Schwartz A, et al. Intracranial vertebrobasilar system: MR angiography. *Radiology* 1994;190:105–10.

An Overview of Three Dimensional Contrast-Enhanced MRA at 3.0 Tesla

Kambiz Nael, M.D.¹; Gerhard Laub, Ph.D.²; J. Paul Finn, M.D.¹

¹University of California at Los Angeles, David Geffen School of Medicine, L.A., USA

²Siemens Medical Solutions, USA

Over the past decade, thanks to steady advances in pulse sequences and scanner design, contrast-enhanced MR angiography (CE-MRA) has made significant advances in image quality and reliability. For a variety of applications, 3D CE-MRA has advantages over other modalities such as CTA, or digital subtraction angiography (DSA), and in many institutions it is often the imaging test of first choice.

Recently, whole body, 3.0T MR systems have become available, with the promise of greatly improved signal-to-noise ratio (SNR) in comparison to 1.5T. Also, since the longitudinal relaxation time (T₁) of background increases with field strength, sensitivity to injected gadolinium agents for CE-MRA is heightened, so that smaller contrast doses may be used. Whilst there are also challenges and disadvantages to 3.0T imaging, such as SAR limitations, dielectric resonances and radiofrequency (RF) eddy currents, nevertheless, CE-MRA at 3.0T can often generate spectacular studies, providing very high spatial resolution 3D data over a large field of view (FoV). This article describes existing 3D CE-MRA techniques at 3.0T, as implemented on the Siemens MAGNETOM Trio scanner. We also summarize clinical experience with CE-MRA to date over a variety of vascular territories.

Background

1. Conventional CE-MRA:

CE-MRA relies on the T₁ shortening effect of paramagnetic contrast agents and is performed with a T₁-weighted fast spoiled 3D gradient echo (GRE) pulse sequence. The sequence parameters and the contrast administration scheme should be carefully planned, to achieve the best compromise between the expendable signal-to-noise (SNR) and the required spatial and temporal resolution. With gradient slew rates of up to 200 mT/m/s and up to 45 mT/m gradient amplitudes, TRs of the order of 2.5–3 ms and TE of the order of 1.2 ms are achievable, for 512 matrix acquisitions. Pulse sequence features such as asymmetric echo and different k-space sampling schemes have also improved the performance of CE-MRA. Parallel acquisition has greatly increased

the performance of CE-MRA at 3.0T, where the higher baseline SNR provides a firmer base to support aggressive acceleration factors. Precise contrast administration is an essential prerequisite for CE-MRA, where the center of k-space should be aligned with the peak vascular enhancement. Timing can be easily optimized by use of a test bolus, but real-time triggering algorithms provide an alternative, if less flexible, method. Contrast doses between 0.1 and 0.2 mmol/kg body weight Gd-based contrast agent have been reported to be sufficient for most single-station MRA examinations.

2. Time-resolved CE-MRA:

Advances in ultrafast MR techniques can now generate temporally resolved 3D MRA, which depict the transit of the paramagnetic contrast agent through the vascular system. Time resolved MRA has the ability to provide supplemental functional information about cardiovascular hemodynamics. Other strengths of time resolved MRA include relative insensitivity to motion and the requirement for only very small doses of contrast.

A general limitation of all time-resolved MRA techniques is that the spatial resolution of the individual 3D data set is limited when compared to single-phase MRA acquisitions. Nonetheless, for many applications, in-plane resolution can be preserved while through-plane resolution is traded for rapid temporal sampling. Unless off-axis reconstruction of the time-resolved data is required (in our experience an uncommon requirement), there is little to be gained from spending a lot of time on through-plane phase-encoding. The MIP images are then viewed in a cine format in the plane of acquisition. Temporal resolution of one second or better is readily achieved with this approach.

Recent advances:

The introduction of parallel imaging is one of the most promising recent advances in MR imaging, and it has significantly improved the performance of MRA applications by changing the way that data are acquired and processed. In these tech-

niques, component coil signals in a radiofrequency coil array are used to partially encode spatial information by substituting for phase-encoding gradient steps that have been omitted. Therefore only a subset of the k-space data, defined by the 'acceleration factor' is sampled and then the whole dataset is reconstructed afterward. The major drawback to parallel acquisition is that SNR is diminished, and this represents a fundamental challenge as acceleration factors are increased. Among the strategies to counteract the SNR loss of parallel imaging are the use of higher magnetic field, improvement and adjustment in array coil geometry and sensitivity, and the optimal infusion of contrast agent.

The availability of whole body 3.0T MR systems with higher baseline SNR, promises more efficient use of parallel acquisition. Recently integrated multicoil technology has also become available at 3.0T (Tim, Siemens). Appropriately designed array coils with more optimal sensitivity profiles and more channels, will improve overall SNR and CE-MRA performance. 32-channel MR systems are now available at 3.0T, with 102 coil elements which can be sited simultaneously, if required. These multiple RF receiver coils, with associated multi-RF receiver channel electronics, combine for more effective parallel acquisition strategies. The improved CE-MRA

performance can be used in any combination to increase coverage, speed or spatial resolution.

The clinical application of CE-MRA in different vascular territories:

Head & Neck

3D CE-MRA in craniocervical vasculature is useful for atherosclerotic arterial disease (Fig.1), aneurysms (Fig.2), AVMs, and pre-operational assessment of tumors.



[Figure 1]
Coronal MIP from CE-MRA shows severe stenosis of the left carotid bifurcation and right vertebral artery (arrows) (voxel: 0.8 x 0.7 x 0.7 mm in a 21 second breath hold).



[Figure 2]
Coronal MIP and VR from CE-MRA show an arterial aneurysm at the level of the right cavernous ICA (voxel: 0.8 x 0.7 x 0.7 mm in a 21 seconds breath hold).

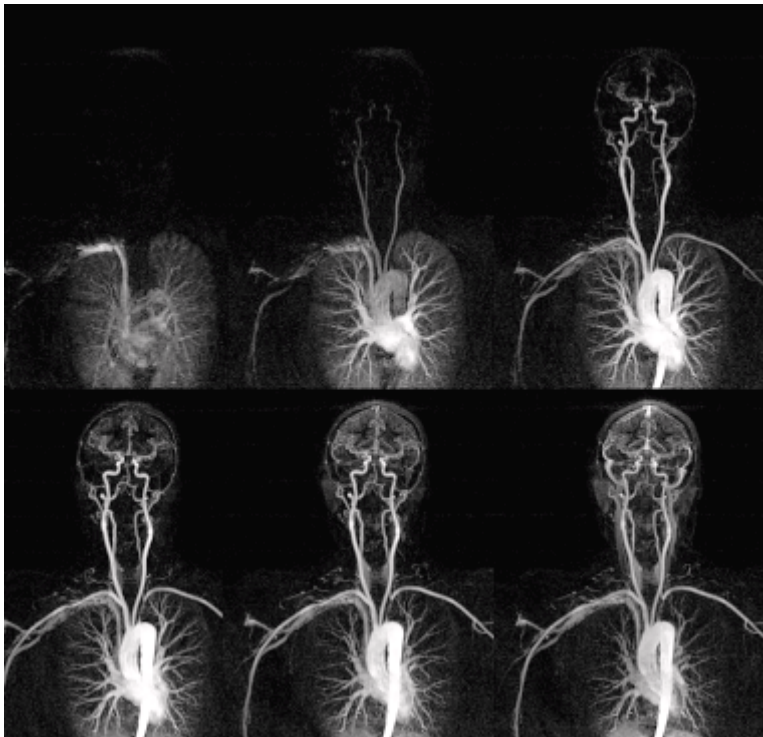


[Figure 3] MIP images from time resolved CE-MRA show subclavian steal syndrome (left side) (voxel: $1 \times 1.2 \times 3$ mm over a 500 mm FOV, 3D volume was updated every 2 seconds, after injection of 6 ml of contrast).

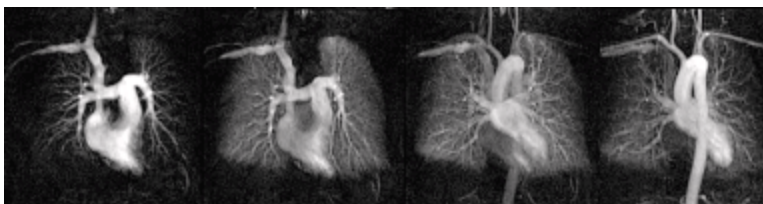


[Figure 5] Coronal MIP images from time resolved MRA at 3.0T demonstrate the sequential filling of the pulmonary and systemic arteries and pulmonary perfusion (voxel size: $1.6 \times 1.2 \times 5$ mm, each 3D volume was updated in 1.5 s).

Pulmonary

Clinical applications for pulmonary CE-MRA include the evaluation of pulmonary embolism, pulmonary perfusion (Fig. 5), pulmonary hypertension (Fig. 6), pulmonary AVM, congenital heart disease, lung tumors, and pulmonary venous mapping (Fig. 7).

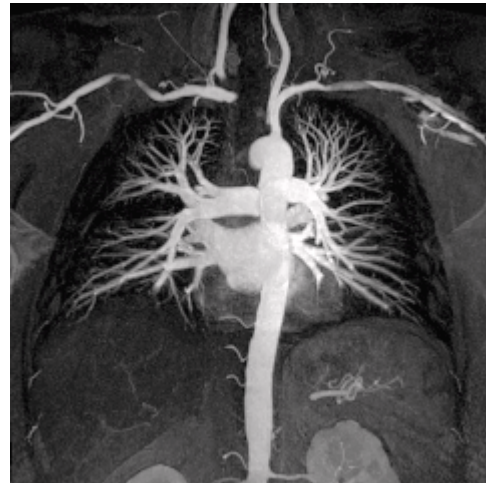


[Figure 4] Coronal partial thickness MIP from high spatial resolution pulmonary CE-MRA at 3.0T, acquired during a 20 seconds breath hold, showing up to 5th order pulmonary arterial branches (voxels $0.8 \times 0.9 \times 1$ mm over a 450 mm FOV).

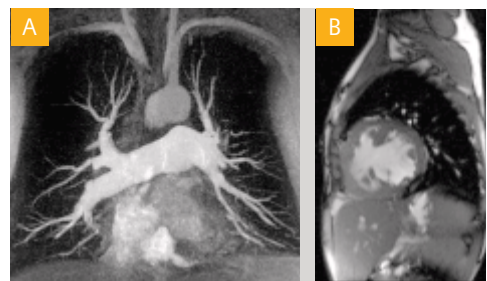


[Figure 6] Coronal MIP image (A) from CE-MRA at 3.0T shows dilatation of central pulmonary vessels and abnormal proximal-to-distal tapering of the pulmonary arteries. These findings are consistent with pulmonary hypertension which is secondary to a large ventricular septal defect (VSD) (B).



[Figure 7] 3D VR image from CE-MRA defines pulmonary venous anatomy, which can improve pre-procedural planning and fluoroscopic procedural time during the ablation treatment for patients with atrial arrhythmias.



[Figure 8] Coronal MIP from CE-MRA at 3.0T showing the irregularity and tortuosity of the abdominal aorta and bilateral renal artery stenosis due to atherosclerosis.



[Figure 9] Sagittal oblique 3D VR from CE-MRA at 3.0T shows aneurysmal dilatation of the superior mesenteric artery (voxel size: $0.8 \times 0.8 \times 1\text{mm}$; 21 second breath hold). The origin of the celiac artery is occluded.

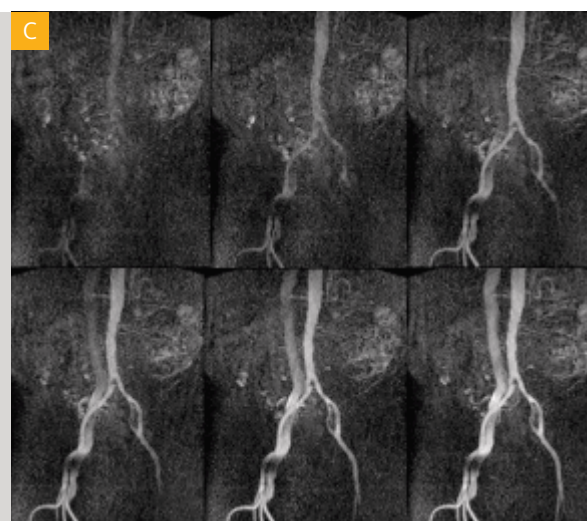
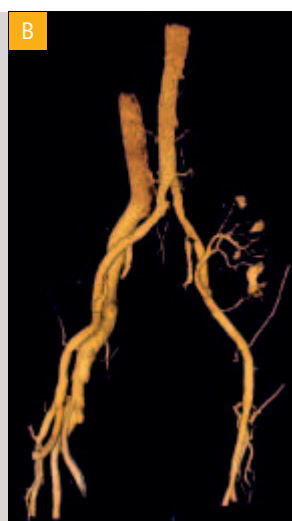
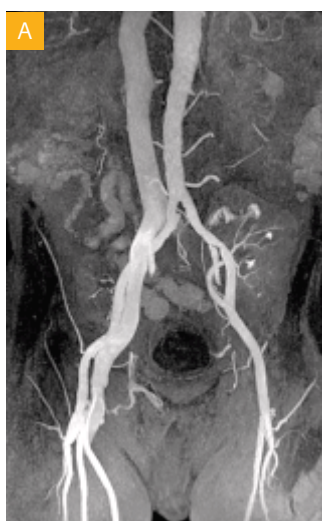


[Figure 10] Coronal MIP (A) and 3D VR (B) from CE-MRA at 3.0T demonstrate widely patent transplant renal artery (voxel size: $0.8 \times 0.8 \times 0.9$, FOV: 440, time: 21 s). Time resolved MRA (C) shows an AV-fistula between the right common iliac artery and vein results in early filling of the inferior vena cava. Metal in the right inguinal region from prior surgery causes focal signal loss.



3TimTM

It was meant to be.

www.siemens.com/medical

M-Z899-1-7600



Proven Outcomes with Clinical 3T MRI.

Now MRI's most innovative new technology, Tim (Total imaging matrix) has been combined with the amazing power of 3T. Together, they go places no 3T has gone before. Now, what was only possible in research can be done daily in clinical practice. You'll see what couldn't be seen. And do things faster than they've ever been done before.

Imagine visualizing 0.4 mm cervical spine nerve roots in less than two minutes. Performing 3-D abdominal imaging with submillimeter resolution in 15 seconds. Or a full head protocol in less than three minutes. With 3T and Tim, the extraordinary will become routine. Everyday.

Siemens **Medical Solutions** that help

SIEMENS
medical

Neurology

Unprecedented image resolutions can be achieved within clinically reasonable acquisition times thanks to the unique capabilities of the 12-channel 3T Head Matrix coil as well as the 24-channel 3T Spine Matrix coil. These coils are capable of massive parallel imaging in all 3 directions providing unique flexibility at 3T.



CSI-Measurements of the Human Brain at 3T

U. Klose^{1,2}, E. Bültmann², F. Jiru^{1,2}, T. Nägele²

¹Section on experimental MR of the CNS, ²Department for Neuroradiology, University Hospital Tübingen

Introduction

One of the advantages of using MR scanners working at higher field strengths is the improvement in MR spectroscopy. In proton spectroscopy, the relevant frequency range for analysis of spectra is increased. In addition, an increased signal-to-noise ratio can be expected if appropriate coils are used. Since both effects contribute to a more reliable data analysis, high field systems are of great interest for the clinical MR spectroscopy. In the systems equipped with a multi-channel receiver, the sensitivity of the measurement can be additionally improved by the use of multi-array coils [1] and by the subsequent combination of the signals from particular channels [2]. A disadvantage of a higher field is, however, the decreased value of T2*-relaxation time compared to the lower field strengths [3, 4]. This fact compromises the signal-to-noise ratio, especially when long echo times are used. Also, more pronounced susceptibility effects in higher field strengths lead to a worse field homogeneity in the examined volume. To evaluate benefits of a 3T MR scanner for the diagnosis of brain diseases, a short echo time proton spectroscopic imaging at a whole body 3T scanner of the newest generation was performed. Spectroscopic imaging (CSI) enables the measurement of both spectral information and a spatial distribution of the spectra. To prevent a contamination of the spectra by unwanted signals originating mainly in the subcutaneous fat tissue, a combination of volume pre-selection (PRESS) and an outer volume saturation [5, 6] was used. Since spatial selective saturation pulses used in outer volume saturation technique may interfere with the measured signal, the advantages and disadvantages of using outer volume saturation was evaluated in a volunteer examination. The quality and the significance of the short echo CSI spectra for clinical diagnostics at 3T are shown in an exemplary patient examination.

Methods and Subjects

All CSI measurements were performed at a whole body 3T scanner (MAGNETOM Trio, A Tim System, Siemens AG) using a twelve-channel Head Matrix coil. A volume pre-selected

PRESS CSI sequence with a repetition time of 1.6 s and an echo time of 30 ms was used in all examinations. For the data acquisition, a 16x16 matrix size was used covering a field of view of 15 cm x 15 cm. The excited cubical volume had a slice thickness of 1.5 cm and in-plane dimensions as adjusted to the brain anatomy, varying between 8 cm x 9 cm and 6 cm x 10.5 cm. Four averages were acquired combined with an elliptic weighted data acquisition [7] (omitting the k-space corners and averaging only data in the center of the k-space). Measurement time was 7.5 minutes for each measurement. The delta frequency (the excitation frequency expressed as a difference from the water frequency) for the spatial selective rf pulses was 2.7 ppm, corresponding to the chemical shift of NAA.

A first evaluation of the acquired data was performed with the spectroscopy software at the host computer of the MR scanner. In a second step, the measured time signals from all calculated voxels were transferred to a separate workstation and evaluated with an own software CULICH [8]. Within this evaluation, the spectral fitting by means of LC Model program [9] was performed. The LC Model decomposed the analysed spectra using 15 base spectra of water solutions of particular metabolites measured in vitro. The base spectra were obtained from the single voxel measurements at 3 T, using a PRESS sequence with an echo time of 30 ms. In addition, calculated base spectra from lipids were included in the evaluation as proposed by Seeger et al. [10].

Measurements were performed in a healthy volunteer (female, 29-years-old) to examine the benefit of the outer volume saturation by spatial selective pulses and in a 45-year-old patient, who was examined routinely at 1.5T and was transferred to a spectroscopic examination at 3T for a further characterization of an unclear diagnostic finding.

Results

In the examination of a healthy volunteer, two CSI measurements from an axial slice of the brain were performed with identical parameters except for the application of six addi-

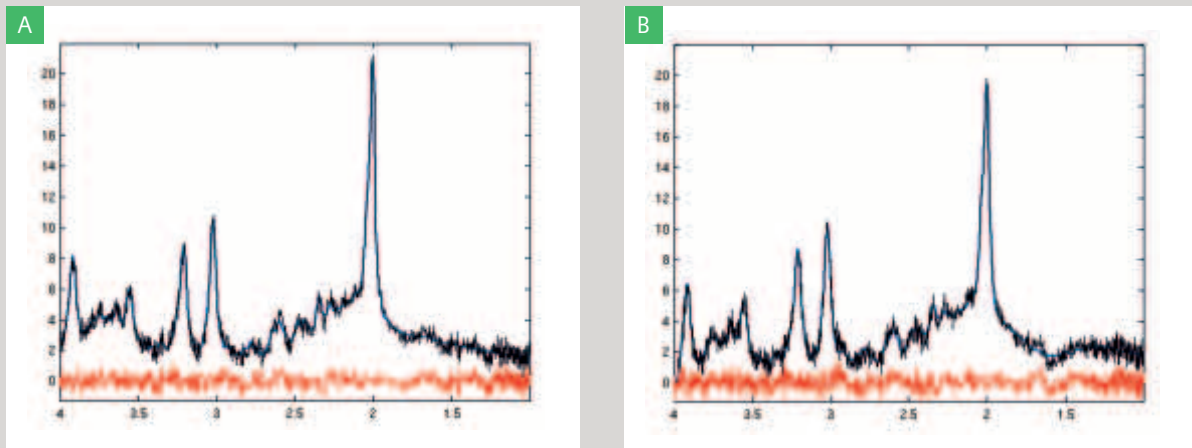


[Figure 1] Spectra of corresponding voxels in two hemispheres of a healthy subject from a measurement without saturation pulses. The measured spectrum (black), the fitted signal (blue) and the residuum (red) is shown.

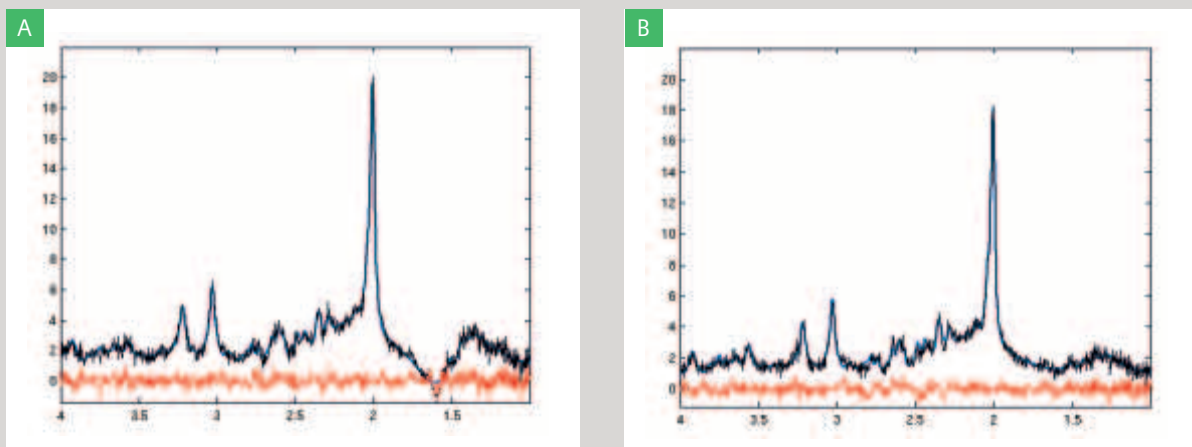


[Figure 2] Spectra from measurements from the same voxel of a healthy subject without (A) and with (B) additional outer volume saturation pulses. Without saturation pulses, artifacts from lipids occur in the frequency range of 1 to 2 ppm. The measured spectrum (black), the fitted signal (blue) and the residuum (red) is shown.

tional spatial saturation pulses (outer volume suppression, OVS, [5]). Even in the measurement without OVS, spectra without any signal contamination in the spectral range of lipids were obtained in most voxels of the CSI data set. As an example, two spectra from the left and right basal ganglia are shown in Fig. 1. In both cases, a very good fit was achieved and both spectra showed a very good congruence. In the frequency range of lipids, only minor signal variations were observed in these spectra. Lipid signals with a higher intensity were found near the edges of the excited volume (Fig. 2A) in the measurement without OVS. The negative

amplitude of the signal was used as a hint indicating the contamination. In the measurement with OVS (Fig. 2B) the erroneous lipid signals are diminished, but the NAA signal is also reduced compared to the measurement without OVS. An additional negative side effect of the measurement with OVS was significantly inferior water saturation in some areas of the excited volume. This effect caused problems with the automatic spectrum evaluation using the LC Model. For these reasons, the measurement without OVS was performed in the patient. The patient was examined due to vertigo and unspecific headache within the last three months.

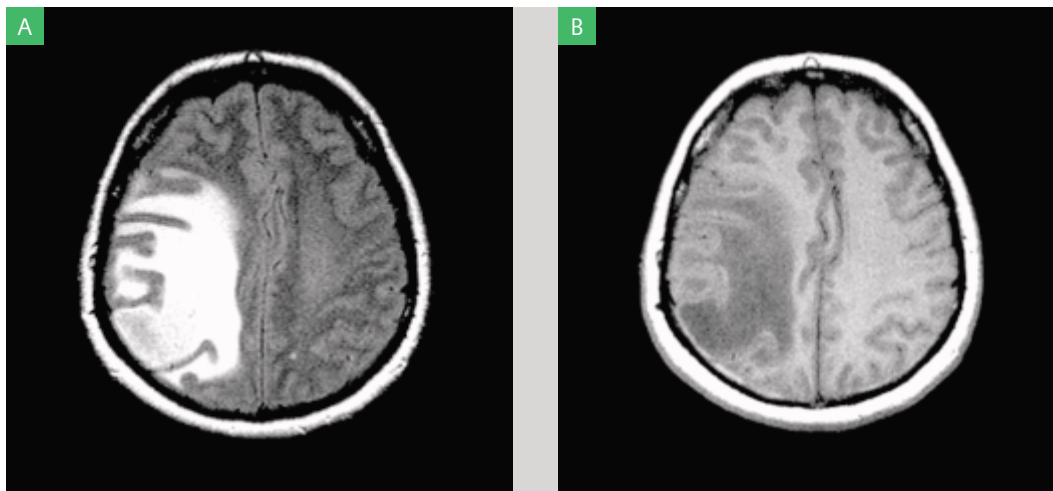


[Figure 3]
Images acquired with a FLAIR (A) and a T1-weighted spin-echo sequence (B) from a slice through the lesion of the examined patient.

In the MR image examination at 1.5T, a tumorous lesion was found right parietal with a large edema. In the T1-weighted image no differentiation was possible within the lesion, whereas in the FLAIR-image (TR 8,8 s TI 2,5 s, TE 118 ms) the lesion was slightly hyperintense in the posterior part. (Fig. 3). For further specification of the lesion, two CSI measurements at 3T were performed, which differed in the extent of the excited volume. To avoid an excitation of the extra cranial lipids in both measurements, the shape of the excited volume was nearly quadratic in first case and had the shape of a narrower rectangle in the second. The extension of both volumes and the position of the excited slice are shown in Fig. 4A and 4B. Results of both measurements were consistent in the spectral range of the main metabolites, but differences were observed in the frequency range of lipids (0.5–1.8 ppm). Examples of the similarity of spectra from the non affected brain hemisphere and from the lesion are shown in Fig. 4B–E. The signal variations within the frequency of lipids in Fig. 4C and 4D with partly negative peak amplitudes indicate, that these signals most probably represent erroneous contaminations from areas outside the field of view, which are excited in a different way in both measurements. The variable lipid signal also influenced the automatic phase correction and therefore the signal variation at the edge of the NAA peak can be seen. On the opposite side of the slice the lipid signals within the lesion (Fig. 4E,F) are much more intensive and largely consistent in both measurements. This suggests that the major part of the lipid signals within the lesion originated from the examined voxel.

As a consequence of these findings, the quantitative evaluation was limited to the spectral range of the main metabolites. All spectra within the excited volumes could be successfully evaluated with the automatic evaluation procedure and

for all voxels, the fitting of a sum of adjusted base spectra to the measured spectra was possible. Evaluated spectra from the unaffected hemisphere and from the lesion measured with and without outer volume suppression are shown together with the fitted spectrum and the residuum in Fig. 5. The quantitative evaluation of single metabolites in all voxels of the excited slice could be used for the calculation of parameter maps showing the relative concentration of selected metabolites as well as of the chosen metabolite ratios.

The metabolite maps of creatine and NAA as well as the ratios Creatine to NAA and Choline to Creatine are shown in Fig. 6. Within the lesion, they reveal a decreased NAA, a slightly decreased creatine and interestingly also a strong decrease of Choline. This pattern of metabolite changes leads the Choline to Creatine ratio to be seen as the most relevant parameter for the characterization of the lesion. Accordingly, a biopsy was planned under special consideration of the map of this ratio (Fig. 6D). A prominent peak of the Creatine to Choline ratio was found in the posterior part of the lesion, which seems to mark the central part of the lesion. This location was used as a guidance for the biopsy. The histological result of the biopsy was a low-grade glioma. This finding correlates with the large lipid signals within the lesion, but the decreased intensity of the Choline signal compared with the Creatine signal is an atypical pattern for this tumor type.

Discussion

The acquisition of proton spectra at a field strength of 3T offers the advantage of larger frequency range in the spectra enabling separation of metabolites such as glutamate and glutamine [11] and brings an increased sensitivity allowing an increase of the spatial resolution of CSI measurement.

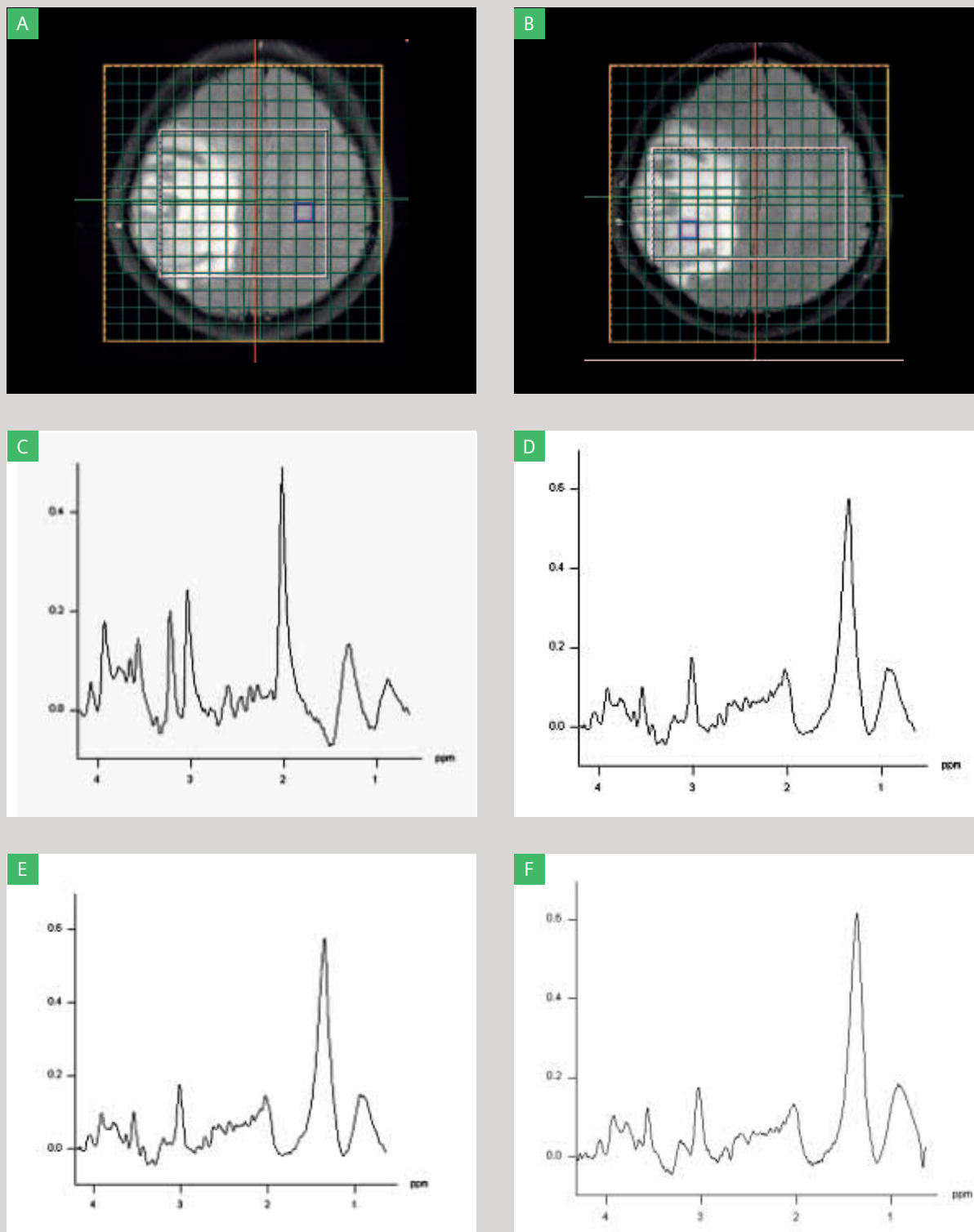


[Figure 4] Spectra and locations (blue quadrates) from voxels of the not affected hemisphere (A,C,E) and from the lesion (B,D,F), acquired with a more rectangular (C,E) and with a more quadratic (D,F) excitation volume (white rectangle). In A) the more rectangular, in B) the more quadratic volume is depicted.

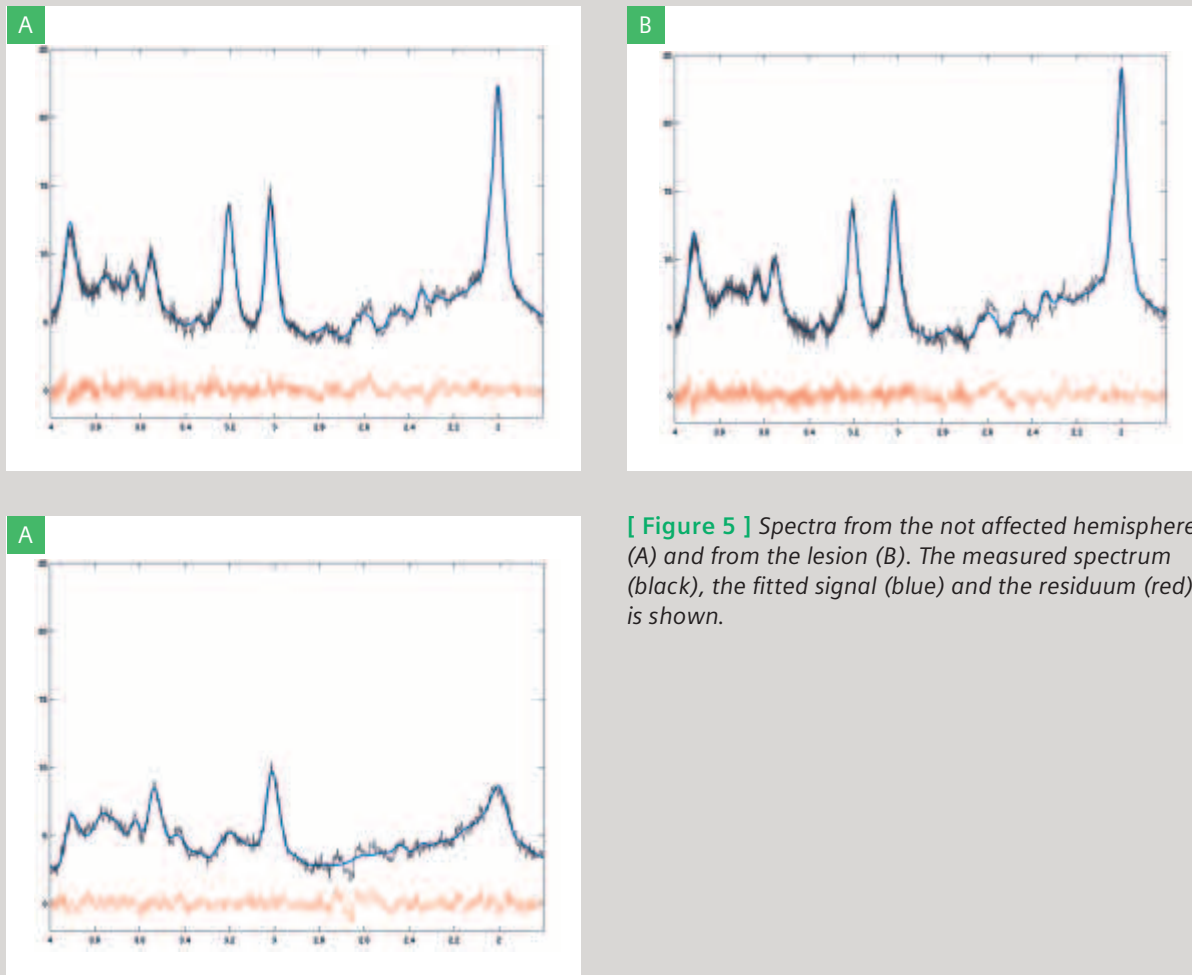


[Figure 5] Spectra from the not affected hemisphere (A) and from the lesion (B). The measured spectrum (black), the fitted signal (blue) and the residuum (red) is shown.

The signal-to-noise ratio can be further improved by the use of multi-channel coils. In this work it was shown that the combination of both technical improvements allows to perform CSI measurements with the high spatial resolution and good signal-to-noise ratio and to evaluate the results with a high level of reliability.

The quantitative evaluation of the CSI spectra was performed using the LC Model program. This technique is used for the calculation of absolute metabolite concentrations in single voxel spectroscopy. The absolute concentrations are calculated based on the known concentrations of the model solutions in the basis set. A prerequisite of this calculation is the identical measurement technique used both for the acquisition of spectra in the subject and in the model solutions.

For a correct fitting procedure of CSI spectra, CSI measurements of metabolite solutions with exactly the same spatial excitation as in the patient examination would be required.

The acquisition of such reference data would take extremely long measurement times, since generally the different size of the PRESS voxel is used in each examination. Therefore, reference spectra from single volume measurements were used in this study. Sequence type (PRESS), a repetition time and an echo time were the same as in the CSI measurement. Nevertheless, the differences between single voxel and CSI measurements can lead to errors of the fitting procedure. In single voxel measurements the whole excited volume including the edges of the voxel, where flip angle is lower than the nominal flip angle value, contribute to the measured signal, whereas in 2D-CSI measurements, the non-ideal excitation profiles of the rf pulses lead to variable flip angles among particular voxels. Due to this effect the spectra from the voxels in the CSI grid are not identical to the base spectra. This behavior is pronounced mainly in metabolites with coupled resonances. As a consequence, the evaluation tech-

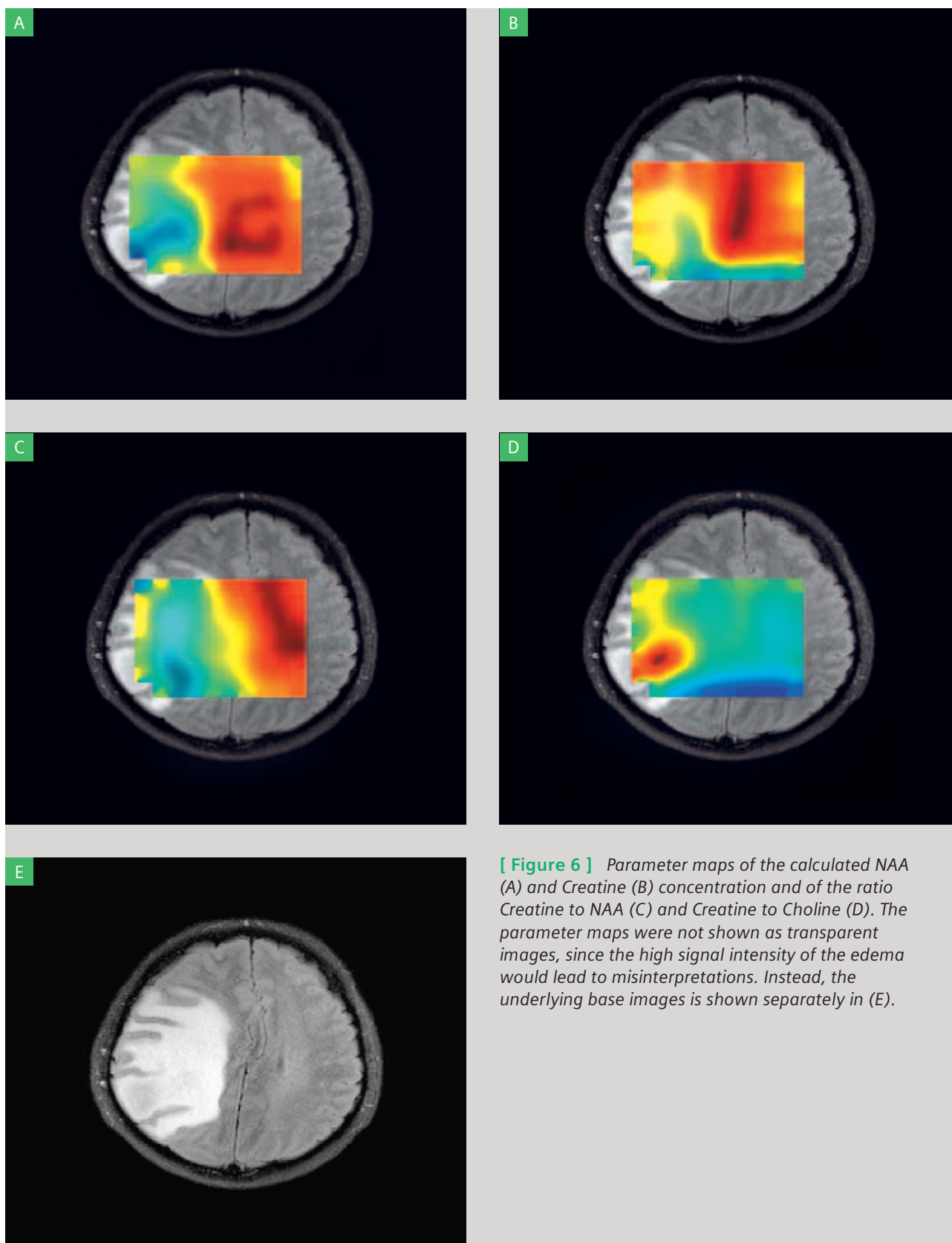


[Figure 6] Parameter maps of the calculated NAA (A) and Creatine (B) concentration and of the ratio Creatine to NAA (C) and Creatine to Choline (D). The parameter maps were not shown as transparent images, since the high signal intensity of the edema would lead to misinterpretations. Instead, the underlying base images is shown separately in (E).

nique cannot be used for the absolute quantification of metabolites. However, it allows the calculation of reliable relative concentrations of metabolites, which can be used to calculate metabolite and ratio maps. Despite these systematic obstacles, the fitting procedure leads to very good results within the selected frequency range, except for the region near the frequency corresponding to 2.7 ppm where minor systematic deviations were visible in the residuum. This can be ascribed to the mentioned deviations between acquired CSI data and the used single voxel reference data.

The quality of the short echo time CSI spectra can be hampered by the signal contamination from the extracranial fat tissue. A reduction of this artifact can be obtained by the use of the OVS technique [5]. However, the application of six saturation pulses in combination with a short echo time can lead to the interferences with the signal from the measured volume and in turn to inferior spectra quality, as was found in volunteer measurements. Therefore the patient examination was performed without OVS technique. To reduce the impact of the possible artifacts occurring in the lipid region on the remaining metabolites in the spectrum, the fitting was restricted to the frequency range 1.8 to 4.0 ppm. This procedure does not allow a quantification of lipid and lactate signals, but within the frequency range of the main metabolites, a very good fit with random residuals was obtained. The described measurement technique is not free from artifacts within the frequency range of lipid signal. These artifacts, however, have a limited amplitude and therefore the occurrence of increased lipid signals can be observed within the original spectra, if the amplitude of lipid signals e.g. in lesions is much higher than the amplitude of the contaminating signals as in Fig. 4C and D. The performed experiments show that high quality spectroscopic imaging measurements at the 3T scanner equipped with the multi channel head coil can be performed. This enables a reliable quantification of short echo time spectra, which is of high importance for clinical MR spectroscopy.

We used the CSI technique for the examination of a patient with low grade glioma. In general, Choline as a phospholipid and membrane marker is increased in all cerebral lesions with disintegration of cell membranes such as brain tumors [12, 13], inflammations [14] and also metastases [15]. In our case of a histologically-confirmed low grade glioma an atypical pattern was found. Whereas a strong decrease of NAA and slight decrease of Creatine is well known in case of glioma [12], a strong decrease of Choline has up to now only been described for radiation necrosis [16] and in Lhermitte-Duclos disease [17].

References

- [1] Roemer, P. B., Edelstein, W. A., Hayes, C. E., Souza, S. P., Mueller, O. M.: The NMR phased array. *Magn Reson Med* 16 (1990) 192–225.
- [2] Schaffter, T., Bornert, P., Leussler, C., Carlsen, I. C., Leibfritz, D.: Fast 1H spectroscopic imaging using a multi-element head-coil array. *Magn Reson Med* 40 (1998) 185–193.
- [3] Mlynarik, V., Gruber, S., Moser, E.: Proton T (1) and T (2) relaxation times of human brain metabolites at 3 Tesla. *NMR Biomed* 14 (2001) 325–331.
- [4] Barker, P. B., Hearshen, D. O., Boska, M. D.: Single-voxel proton MRS of the human brain at 1.5T and 3.0T. *Magn Reson Med* 45 (2001) 765–769.
- [5] Duyn, J. H., Gillen, J., Sobering, G., van Zijl, P. C., Moonen, C. T.: Multisection proton MR spectroscopic imaging of the brain. *Radiology* 188 (1993) 277–282.
- [6] Salibi, N., Roell, S.: MR spectroscopy with syngo MR 204 A/V: automation with flexibility SVS, 2D-CSI and 3D-CSI, with longa and short TE. *Magnetom Flash* 28 (2004) 8–12.
- [7] Wilman, A. H., Riederer, S. J., King, B. F., Debbins, J. P., Rossman, P. J., Ehman, R. L.: Fluoroscopically triggered contrast-enhanced three-dimensional MR angiography with elliptical centric view order: application to the renal arteries. *Radiology* 205 (1997) 137–146.
- [8] Jiru, F., Burian, M., Skoch, A., Hajek, M.: LCModel for spectroscopic imaging. *Magma* 15 (2002) S368.
- [9] Provencher, S. W.: Estimation of metabolite concentrations from localized in vivo proton NMR spectra. *Magn Reson Med* 30 (1993) 672–679.
- [10] Seeger, U., Klose, U., Mader, I., Grodd, W., Nägele, T.: Parameterized evaluation of macromolecules and lipids in proton MR spectroscopy of brain diseases. *Magn Reson Med* 49 (2003) 19–28.
- [11] Nägele, T., Seeger, U., Hass, H., Kueker, W., Heckl, S., Klose, U.: Localized proton spectroscopy in hepatic encephalopathy: advantage of 3T high field for discrimination of glutamine and glutamate. *Magnetom Flash* 28 (2004) 50–53.
- [12] Meyerand, M. E., Pipas, J. M., Mamourian, A., Tosteson, T. D., Dunn, J. F.: Classification of biopsy-confirmed brain tumors using single-voxel MR spectroscopy. *AJNR Am J Neuroradiol* 20 (1999) 117–123.
- [13] Negendank, W. G., Sauter, R., Brown, T. R., Evelhoch, J. L., Falini, A., Gotsis, E. D., Heerschap, A., Kamada, K., Lee, B. C., Mengeot, M. M., Moser, E., Padavic Shaller, K. A., Sanders, J. A., Spraggins, T. A., Stillman, A. E., Terwey, B., Vogl, T. J., Wicklow, K., Zimmerman, R. A.: Proton magnetic resonance spectroscopy in patients with glial tumors: a multicenter study. *J Neurosurg* 84 (1996) 449–458.
- [14] Rudkin, T. M., Arnold, D. L.: Proton magnetic resonance spectroscopy for the diagnosis and management of cerebral disorders. *Arch Neurol* 56 (1999) 919–926.
- [15] Harada, M., Tanouchi, M., Nishitani, H., Miyoshi, H., Bandou, K., Kannuki, S.: Non-invasive characterization of brain tumor by in-vivo proton magnetic resonance spectroscopy. *Jpn J Cancer Res* 86 (1995) 329–332.
- [16] Preul, M. C., Leblanc, R., Caramanos, Z., Kasrai, R., Narayanan, S., Arnold, D. L.: Magnetic resonance spectroscopy guided brain tumor resection: differentiation between recurrent glioma and radiation change in two diagnostically difficult cases. *Can J Neurol Sci* 25 (1998) 13–22.
- [17] Bueltmann, E., Ernemann, U., Schuele, R., Beschoner, R., Gharabaghi, A., Voigt, K., Nägele, T.: Diagnostische Wertigkeit der absolut quantifizierten, lokalisierten MR-Protonenspektroskopie beim dysplastischen zerebellären Gangliozytom (Lhermitte-Duclos). *Klinische Neuroradiologie* 15 (2005) 123–130.

MAGNETOM Trio with Tim

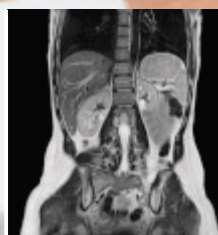
3T

that can leap from research
to clinical in a single exam.

We see a way to perform 3D abdominal imaging
with sub-millimeter resolution in 15 seconds.

Results may vary. Data on file.

www.siemens.com/medical



M-Z901-1-7600

Proven Outcomes with Clinical 3T MRI.

MAGNETOM® Trio with Tim™ (Total imaging matrix) doesn't just push the boundaries of clinical 3T MRI, it explodes them. Offering highest workflow. Highest speed. And highest resolution at 3T. With PAT factors of up to 16, advanced applications that were once the domain of research can now be translated into daily clinical routine.

For brilliant resolution of microscopic pathologies. And effortless tracking of the fastest physiological processes. MAGNETOM Trio with Tim. It's the ultimate dual-purpose machine. Truly, the best of all worlds.

Siemens **Medical Solutions** that help

SIEMENS
medical

Neuroimaging at MAGNETOM Trio, A Tim System

John Grinstead, Ph.D.

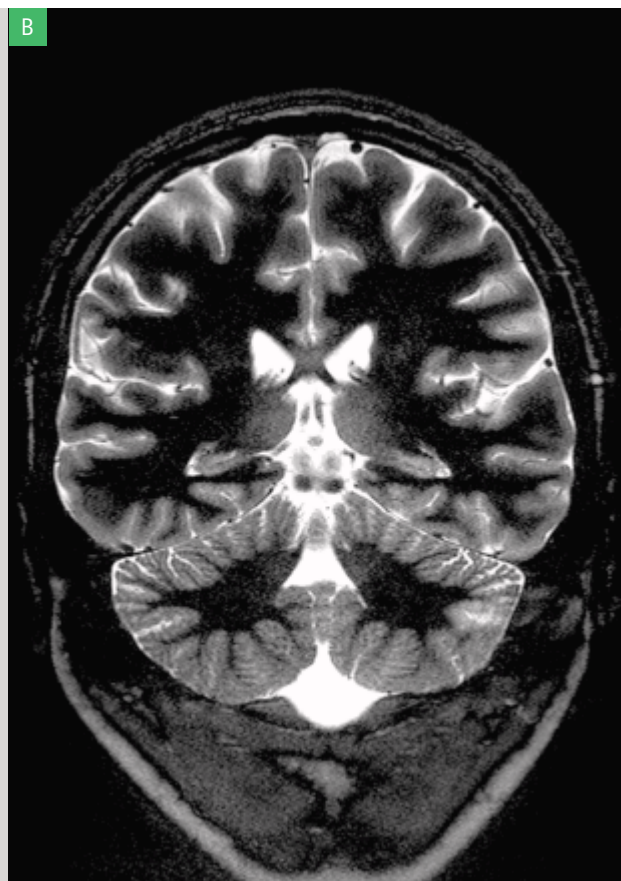
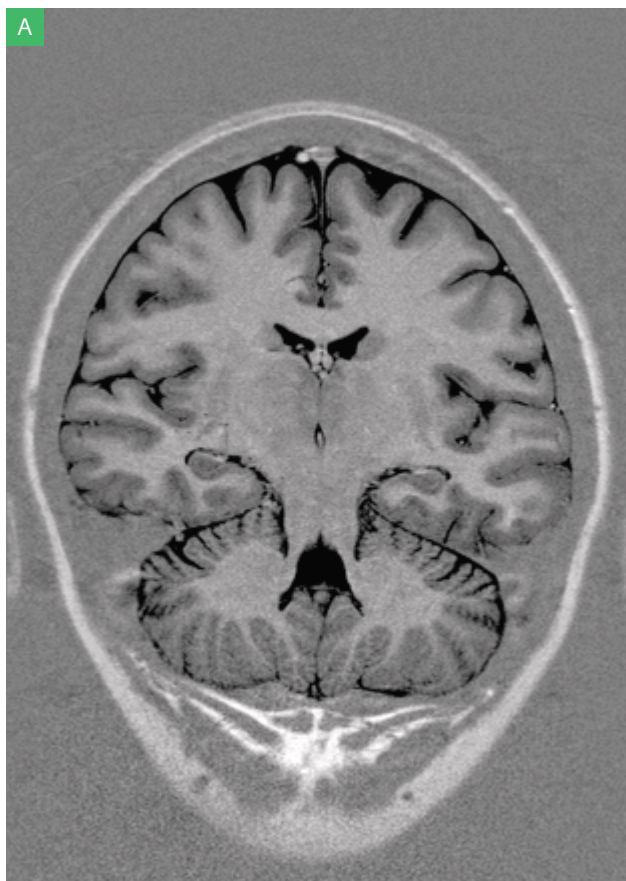
Staff Scientist, MR R&D Siemens Medical Solutions, Malvern, Pennsylvania, USA

Introduction

Siemens already has a proven track record as an industry leader in ultra-high field imaging at 3 Tesla with the MAGNETOM Allegra and MAGNETOM Trio, and at even higher field strengths with several 7 Tesla research systems already in the field. With the addition of the new MAGNETOM Trio, A Tim System, this leadership continues. Cutting-edge applications, with the proven reliability of the MAGNETOM Trio magnet (with zero spontaneous quenches), and now Tim (the leading RF and gradient system on the market) make for a powerful combination.

Ultra-High Field = Ultra-High Resolution

The most obvious benefit of 3 Tesla is the high signal-to-noise ratio (SNR), which allows excellent resolution within a clinically realistic scan time. This high SNR can also be used to reduce scan time for routine examinations to maximize patient throughput. However, one cannot simply take protocols that work great at lower field strengths and expect optimal results at 3 Tesla. A common example of this is T1 contrast, which is different at 3 Tesla because of the increase of the T1 relaxation time with the main magnetic field strength. Siemens has multiple solutions, including T1-weighted



FLASH, Inversion Recovery (IR), and MPAGE. Fig. 1 shows T1-IR, along with high resolution T2-IR and PD-TSE. The high performance gradient coil allows a maximum gradient strength of 45 mT/m (72 mT/m effective) and a slew rate of 200 T/m/s (346 T/m/s effective). This is useful in a variety of applications, from MRA (to reduce the TE which minimizes flow voids) to EPI (to reduce the echo train length and echo spacing which minimizes susceptibility artifacts). At the same time, the Tim gradient system reduces eddy currents, whilst acoustic noise levels drop by up to 90% with Audio-Comfort technology.

3T + Tim = Extreme Flexibility

The MAGNETOM Trio combined with Total Imaging Matrix (Tim) technology is the first completely integrated 3 Tesla system, with up to 102 individual coil elements that can be connected to 32 fully independent receiver channels. This RF system has the flexibility to allow the use only of the coils needed for a particular exam.

In a head-only study, one can use the 12-channel Head Matrix coil (standard with all 3 Tesla Tim configurations). The

receive coil elements are clustered in 4 groups of 3 coil elements per group. This unique design allows the Head Matrix to operate in three different modes that may be selected prior to acquisition: 4-channel CP Mode, 8-channel Dual Mode, and 12-channel Triple Mode. The CP Mode is preferred when not using parallel imaging to obtain the highest signal homogeneity over the image and the maximum signal-to-noise (SNR) at the center of the region of interest. The Dual and Triple modes act as 8 and 12 channel phased array coils, respectively, and can be used to improve the SNR in the periphery of the image and to enable higher iPAT factors (Integrated Parallel Acquisition Techniques). The new Prescan Normalize feature should be used, which improves homogeneity when using phased array coils.

The Head Matrix has also been designed with about 25% more headroom to facilitate larger subjects and to reduce claustrophobia. This also provides room for a wider range of fMRI stimulation equipment such as LCD goggles, which are often not compatible with more cramped coil designs.

In studies of the brain stem, cervical spine or neck soft-tissue, the 4-channel Neck Matrix (standard with all 3 Tesla Tim con-

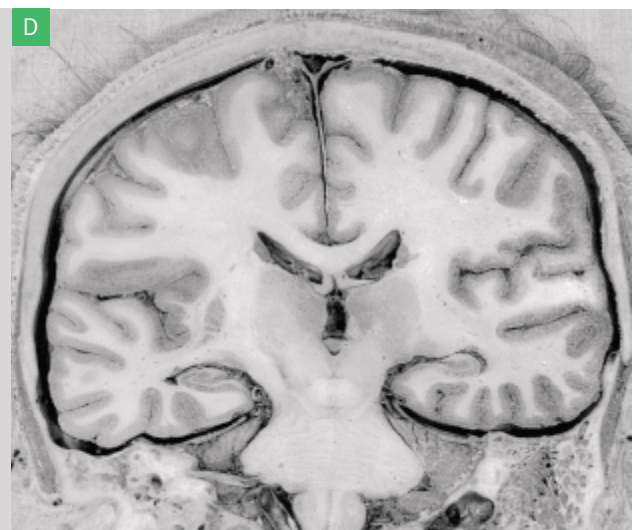
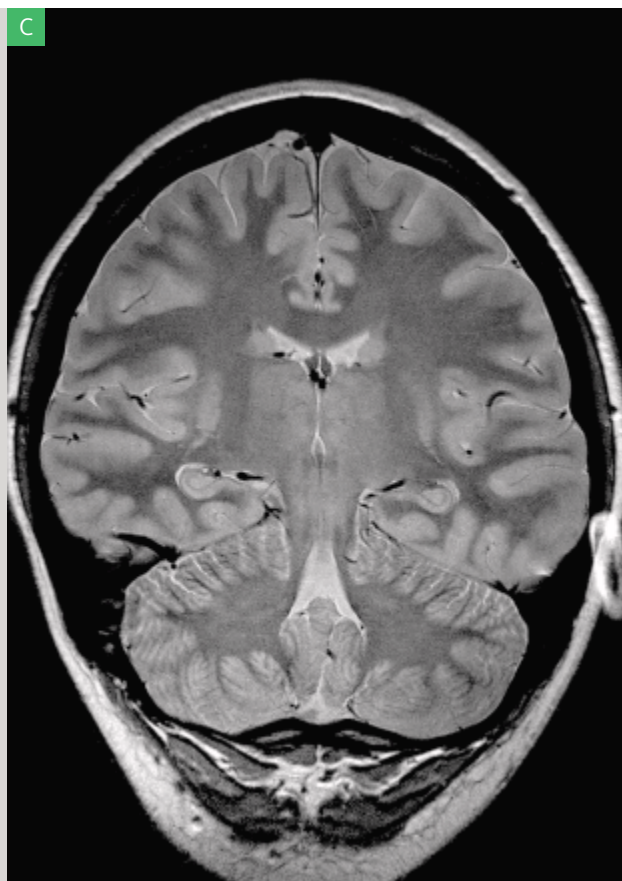


[Figure 1] High resolution imaging at 3 Tesla using the Tim Head Matrix coil: T1 Inversion Recovery (A), T2 Inversion Recovery (B), and proton density TSE (C). A photographic cross section is shown in (D) for comparison (Courtesy of N. Salamon et al., UCLA).

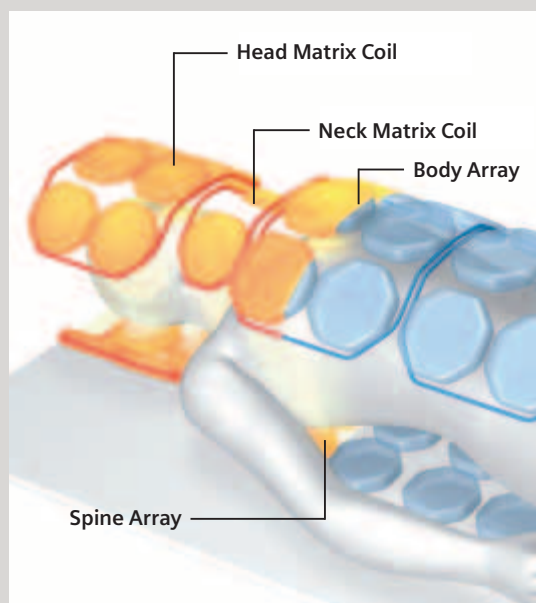


[Figure 2] Multiple coils can be used in combination depending on the application. The Head Matrix, Neck Matrix, Body Array and Spine Array can be used together as shown for neurovascular imaging from the upper chest to the brain.

figurations) can be used in combination with the 12-channel Head Matrix coil (Fig. 2). Even more coils can be used simultaneously to utilize the 32 independent RF receiver channels available for true 50 cm FOV imaging. This is particularly useful in angiographic applications, such as imaging bolus passage from the aorta to the brain (Fig. 3).

3T + Tim = Higher iPAT

Because of the 12 channel design of the Head Matrix coil, higher iPAT factors can be used more robustly than coils with fewer coil elements. This is useful for applications such as single-shot EPI, where iPAT can be used to minimize the echo train length to reduce susceptibility related image distortions, which can be essential at 3 Tesla especially at large matrix sizes and high resolution (Fig. 4). It can also be used to reduce the scan time of multiple-shot sequences.

The MAGNETOM Trio with Tim is already a true 32 channel RF system, and is readily extensible to receive custom built multi-element coils that allow even higher iPAT factors. Figure 5 shows the results of a prototype 32 channel head coil (work-in-progress G. Wiggins et al., MGH) used to acquire 3D FLASH images with 1 mm isotropic resolution in 1 min 20 s using an iPAT factor of 12.

3Tim fMRI

The basis of the fMRI signal is blood-oxygenation level dependent (BOLD) contrast, which generally increases quadratically with the magnetic field. This means the BOLD related signal change can be as much as 4 times as high at 3 Tesla compared to 1.5 Tesla, while at the same time the increased SNR reduces noise in the image. This translates to more robust functional activation statistics, and even the use of single trial paradigms. In addition, advanced application packages such as AutoAlign and 3D PACE help increase the data quality and reproducibility.

The AutoAlign package performs a quick 3D scan (under 1 minute) and matches the data to a brain atlas. It then adjusts the slice prescription to all subsequent scans to account for the subject's head position relative to the brain atlas. This means that multiple subjects in the same study will have nearly identical image orientations and also that the same slice orientations can be reproduced when rescanning a subject, reducing or eliminating the need to perform image registration.

3D PACE (Prospective Acquisition CorrEction) is used to reduce motion artifacts in BOLD imaging. It tracks head motion during an fMRI study, and calculates the complete 3D rotation and shift needed to dynamically update the slice prescription to effectively track the head throughout the study. This reduces spurious functional activation typically seen at the edge of the brain when motion is present.

The Neuro 3D software package (Fig. 6) allows 3D data display and evaluation. BOLD statistics can be calculated either during scanning to observe the experiment develop over time, or afterwards during customized post-processing. It can overlay the activation maps onto anatomical data and can also utilize a field map showing those regions which have a large amount of susceptibility-related image distortion where the data must be interpreted more carefully.

Standard BOLD processing in *syngo* uses a block design paradigm. However, for some research applications it is more desirable to use a different experimental design, namely a General Linear Model (GLM). This model (work-in-progress) gives a more valid description of the signal time-course. It can account for the hemodynamic response function of the brain to a stimulus, as well as slice timing differences. It also allows the modeling and removal of low-frequency signal drifts that may be present (such as physiologically related motion). The statistical maps generated by the GLM model are completely compatible with the standard BOLD processing already available, allowing all of the features of the Neuro 3D package to be used (Fig. 6). In addition to the applications mentioned already, the MAGNETOM Trio, A Tim System has



[Figure 3] Contrast enhanced MRA of the head and neck (courtesy of J.P. Finn and K. Nael, UCLA).

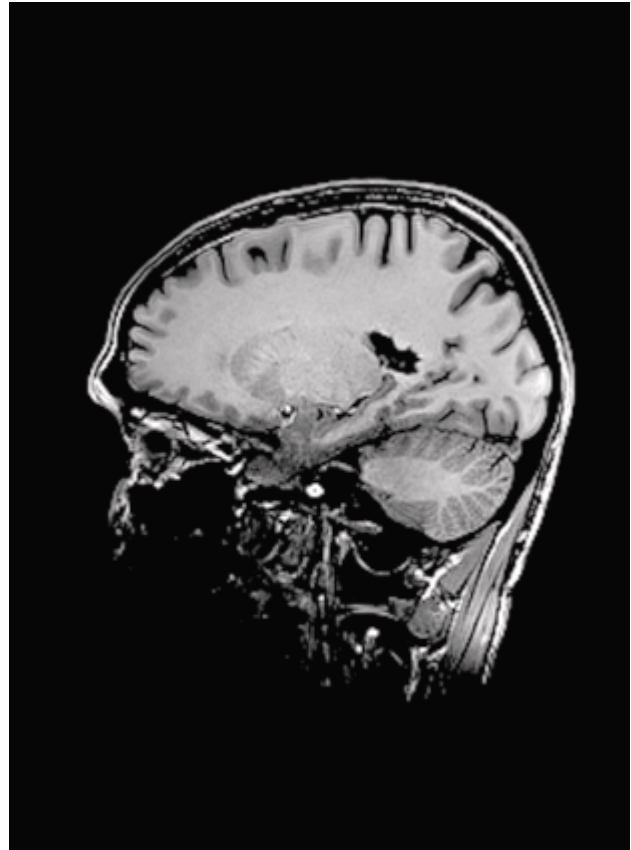


[Figure 5] 3D FLASH with 1 mm isotropic resolution acquired in 1:20 min with an iPAT factor of 12 using 32-channel array coil (work-in-progress, G. Wiggins et al., MGH)

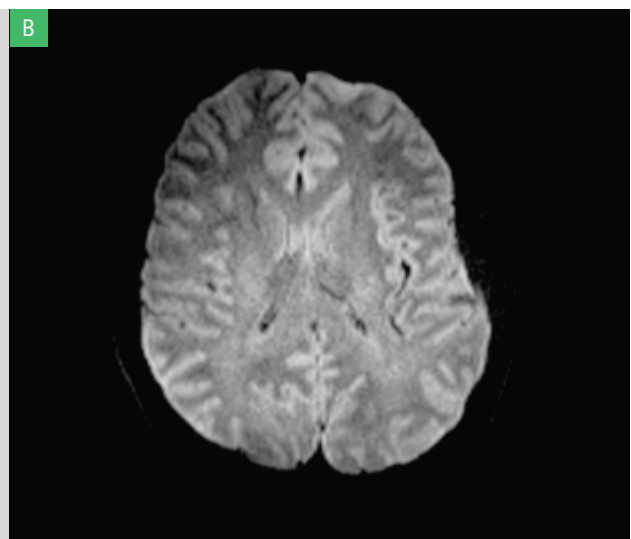
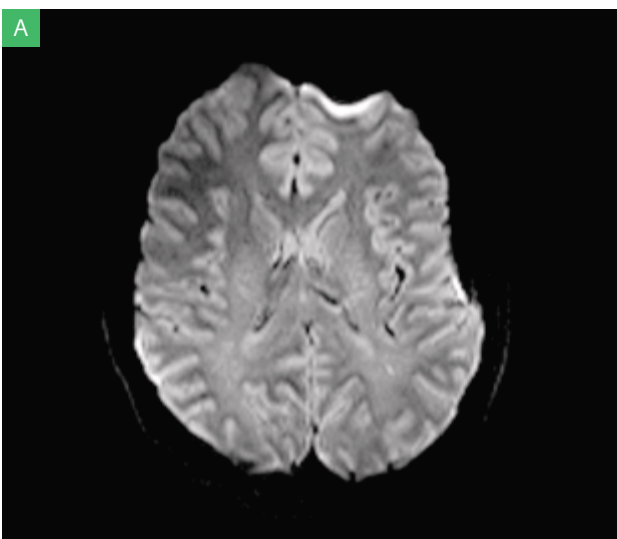


[Figure 4] Diffusion weighted EPI without iPAT demonstrating distortion artifacts (A). An iPAT factor of 3 greatly reduces the amount of distortion (B).

several other cutting-edge applications, such as SPACE (Sampling Perfection with Application Optimized Contrasts using different flip angle Evolutions), which allows 3D T2-weighted imaging at isotropic sub-millimeter resolution with reduced SAR. Also, BLADE is a technique based on a modified radial TSE sequence that is able to acquire images even in the presence of dramatic head motion, which is useful in uncooperative patients (Figure 7).

Conclusion


One of the reasons many institutions are making the move to 3 Tesla is for market differentiation. Workflow, flexibility, reliability and advanced applications are all key factors in a competitive imaging market where neuroimaging examinations are the predominant studies requested. The MAGNETOM Trio with Tim is a unique combination of these essential elements, as well as a powerful research instrument for a variety of applications.

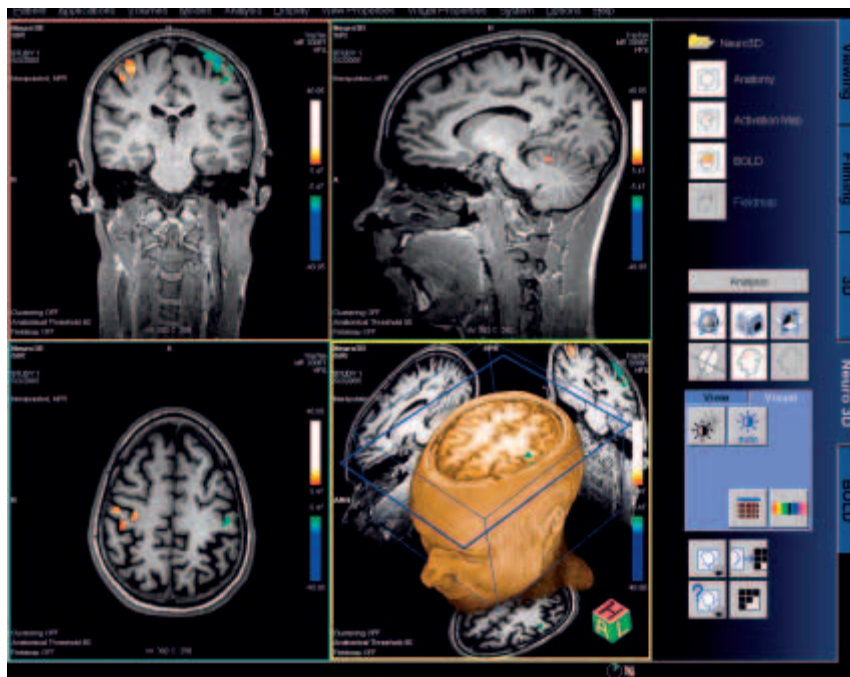


[Figure 6] The 3D Neuro taskcard showing functional activation using GLM (General Linear Model) statistical analysis. 3D PACE motion correction was also employed.

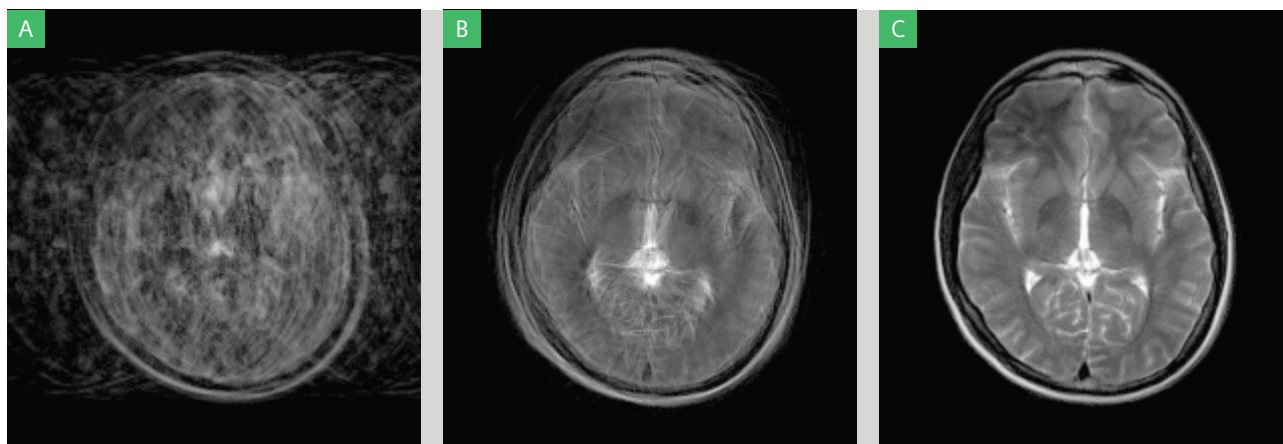


[Figure 7] Standard TSE images demonstrating severe artifacts in the presence of head motion (A). BLADE images acquired with motion correction turned off (B) and on (C), both from the same data set, showing the ability to image even in the presence of significant motion.



We see a way to do whole-body imaging with MR in as little as 6 minutes without any patient or coil repositioning

We see a way to seamlessly scan up to 181 cm with local coil quality

We see a way to do MR imaging with an increased signal-to-noise of up to 100%

Tim™ sees all.

www.siemens.com/medical

Results may vary. Data on file.

M-2835-1-7600

Proven Outcomes in MR.

Penetrating. Scrutinizing. Head to toe. Front to back. And side to side. Tim (Total imaging matrix) takes it all in. And in the process, opens up countless new possibilities. Tim brings together, for the first time ever, 102 matrix coil elements and up to 32 RF channels. All of which can be freely combined in any way. The highest

signal-to-noise ratio possible today, while still enabling seamless, whole-body imaging with a total FoV of 181 cm (6'). Tim is not just another round of enhancements. But a transforming technology that does so much more. So you can, too. See for yourself at www.Siemens.com/Tim.

Siemens **Medical Solutions** that help

SIEMENS
medical

SPACE Case Reports: Brain Imaging with MAGNETOM Trio

Dr. Andrea Bink, M.D.; Prof. Dr. Jochen Gaa, M.D.

Institute of Neuroradiology, Johann Wolfgang Goethe-University, Frankfurt/Main, Germany

Patient History

Patient 1:

30-year-old female patient with visual disturbances, swallowing difficulty, fine motor disturbances and paraesthesia of the right hand and of the abdominal skin. The diagnosis of multiple sclerosis (MS) was established in 1992.

Image Findings

The subcortical lesion which is detected on the Dark Fluid SPACE image (3D FLAIR) image can not be seen in the 2D FLAIR image (Figure 1 and 1A). Figure 2 and 2A illustrate that a subcortical lesion can be delineated much better on the SPACE (3D FLAIR) than on the 2D FLAIR sequence image. In Figure 3 and 3A one temporal lesion is not clearly visualized on the 2D FLAIR image, but on the SPACE (3D FLAIR) image it is identified as a lesion.

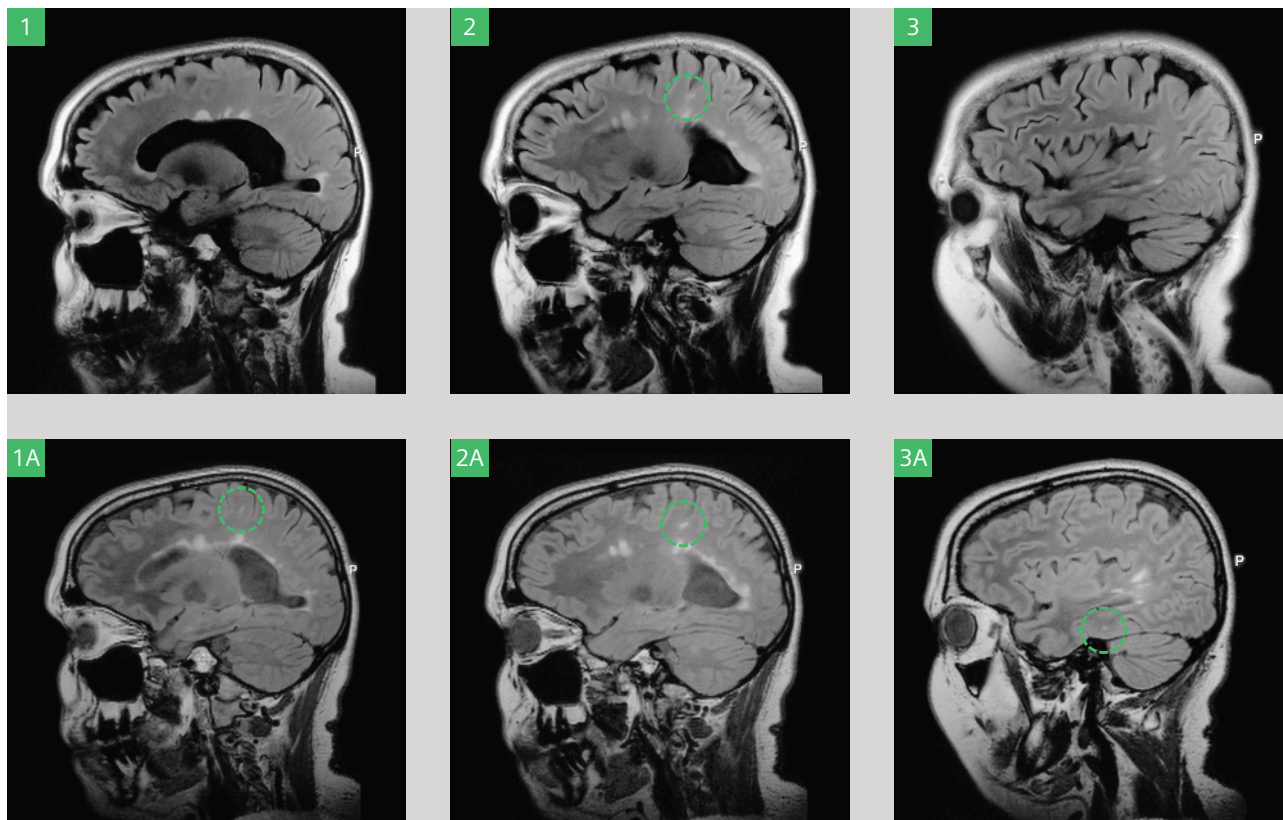


[Figure 1–3] 2D FLAIR, TR: 10,000 ms, TE: 97 ms, TI: 2,500 ms, slice thickness: 5 mm, FOV: 220.

[Figure 1A–3A] Dark Fluid SPACE (3D FLAIR), TR: 6000, TE: 353, TI: 2200, slice thickness: 1.1 mm, FoV 250.

Patient 2:

52-year-old female patient with visual disturbances. MS was diagnosed in 1970.

Image Findings

Many periventricular lesions are seen on the 2D FLAIR image (Figure 4). In the corresponding Dark Fluid SPACE (3D FLAIR) images not only are additional lesions found but the lesions are also much better delineated (Figure 4A and 4B).



[Figure 4] 2D FLAIR, TR: 10,000 ms, TE: 97 ms, TI: 2,500 ms, slice thickness: 5 mm, FOV: 220.

[Figure 4A and 4B] Dark Fluid SPACE (3D FLAIR), TR: 6000, TE: 353, TI: 2200, slice thickness: 1.1 mm, FOV 250.

Sequence Details

Parameter	2D FLAIR	Dark Fluid SPACE	Parameter	2D FLAIR	Dark Fluid SPACE
No. of slabs	n/a	1	Turbo Factor	15	221
No. of slices per slab	25	114	Base resolution	320	256
Slice thickness (mm)	5	1.1	Phase Resolution (%)	80	100
Repetition time (ms)	10,000	6,000	Field of view (mm)	220	250
Echo time (ms)	97	353	Field of view phase (%)	100	85.90
Inversion time (ms)	2,500	2,200	Pixel size (mm)	0.9 x 0.7	1.0 x 1.0



We see a way to reduce breath-hold times by more than 50%

We see a way to do Parallel Imaging in all three directions

We see a way to avoid sub-optimal image quality
by automatically recommending the optimal PAT factor

TimTM knows
no boundaries.

www.siemens.com/medical

Results may vary. Data on file.

M-Z836-1-7600

Proven Outcomes in MR.

Imagine what's possible. And then think of Tim (Total imaging matrix). Tim brings together, for the first time ever, 76 matrix coil elements and up to 32 RF channels. All of which can be freely combined in any way. You are no longer restricted by a limited Field of

View. Tim enables unlimited Parallel Imaging in all directions – throughout the entire FoV of 205 cm (6' 9"). All while exploiting the highest signal-to-noise ratio possible today. For the highest image contrast, even with the highest PAT factors. Meet Tim for yourself at www.Siemens.com/Tim.

Siemens **Medical Solutions** that help

SIEMENS
medical

Orthopedics

MAGNETOM Trio, A Tim System enables the visualization of microscopic pathologies in the extremities, previously unseen with MRI in such detail. Routine orthopaedic imaging in all joints can be performed in less than 1 minute. Imaging of all joints in 3D in just a few minutes with less than 0.7 mm isotropic resolution is now simply another standard protocol.



3T Cartilage Imaging in the Knee Joint

Tallal C. Mamisch, M.D.¹, Alexander Cavallaro, M.D.², Werner Bautz, M.D.², Gert Muhr, M.D.¹

¹University Hospital Bochum „Bergmannsheil“, Clinics Dept. of Trauma Surgery, Bochum, Germany

²University Hospital Erlangen, Dept. of Radiology, Erlangen, Germany

Introduction

The clinical use of MRI in diagnosis of cartilage lesions and monitoring of treatment is indicated in several studies. The use of cartilage thickness measurements as indication for the severity of the disease is described in the hip and the knee joint [1,2]. Studies comparing the cartilage lesion detection to arthroscopy show a high sensitivity and specificity for partial or total substance defects [3]. There is still a lack of MRI cartilage assessment for early osteoarthritic structural lesions [4]. The goal of our ongoing work is to fulfill the potential of 3T imaging for the detection of structural cartilage changes.

Examination and Analysis

Healthy volunteers and patients with severe osteoarthritis of the knee joint and indication for total knee replacement underwent in vivo 3T MRI (Siemens MAGNETOM Trio) with isotropic 3D DESS (TR = 15.6 ms, TE = 4.5 ms, resolution $0.6 \times 0.6 \times 0.6 \text{ mm}^3$), 3D MEDIC (TR = 31.0 ms, TE = 17.0 ms, resolution $0.5 \times 0.5 \times 0.5 \text{ mm}^3$) and 3D FLASH (TR = 12.2 ms, TE = 5.1 ms, resolution $0.5 \times 0.5 \times 0.5 \text{ mm}^3$) of the affected knee joint. The resected femoral condyle pieces in patients after total knee replacement were marked with 4 pins and imaged with the same MRI sequences but higher resolution (3D DESS $0.5 \times 0.5 \times 0.5 \text{ mm}$ and 3D FLASH and 3D MEDIC both $0.4 \times 0.4 \times 0.4 \text{ mm}$) on the day of resection. In the next step the resected femoral condyle was fixed and semi thick slices of 0.4 mm were made with toluidin blue staining. The histological data was staged according to the Mankin histopathological scale and registered to the MRI data of the pieces. The angle correction of the cutting planes during operation was used for the comparison with the preoperative MRI.

Findings

A variety of differences in the same cartilage regions for the three sequences were found relating to surface contour and signal intensity (Fig. 1–4). There were comparable results for grade 3 and 4 osteoarthritis for all three sequences with the histological data. For grade 2 lesions with loss of cartilage volume, 3D FLASH and 3D MEDIC were more comparable,

whilst for lesions without loss of cartilage thickness and therefore a mixture of structural changes, 3D DESS was more reliable (Fig. 5–8). For a grade 1 lesion with superficial loss of staining, 3D DESS was also most sensitive, but with false positive results. For grade 1 lesions with loss of cartilage structure and increase of chondrocytes all sequences were associated with false negative results.

Discussion

Based on these results it is possible to compare histological changes in cartilage by using in vivo 3T MRI. This also demonstrates the necessity of choosing the right sequence and of analyzing each sequence in a different way, due to limitations (3D FLASH) or to a range of signal intensity changes (3D DESS). We found overall fair results for moderate and severe stages of osteoarthritis. With the use of the 3T system it was possible to differentiate between loss of substance and loss of proteoglycans. However, these results still show a lack of diagnostic efficiency in detection of early osteoarthritic changes in MRI. They also reveal the limits of thickness measurement techniques, especially in detection of structural defects with intact surface.

References

- [1] Graichen H, von Eisenhart-Rothe R, Vogl T, Englmeier KH, Eckstein F. Quantitative assessment of cartilage status in osteoarthritis by quantitative magnetic resonance imaging: technical validation for use in analysis of cartilage volume and further morphologic parameters. *Arthritis Rheum.* 2004 Mar; 50(3): 811–6.
- [2] Nishii T, Sugano N, Sato Y, Tanaka H, Miki H, Yoshikawa H. Three-dimensional distribution of acetabular cartilage thickness in patients with hip dysplasia: a fully automated computational analysis of MRI imaging. *Osteoarthritis Cartilage* 2004 12, 650–657.
- [3] Mori R, Ochi M, Sakai Y, Adachi N, Uchio Y. Clinical significance of magnetic resonance imaging of osteoarthritis. *Rheum Dis Clin North Am* 1999; 25: 451–65.
- [4] Gahunia HK, Babyn P, Lemaire C, Kessler MJ, Pritzker KP. Osteoarthritis staging: comparison between magnetic resonance imaging, gross pathology and histopathology in the rhesus macaque.

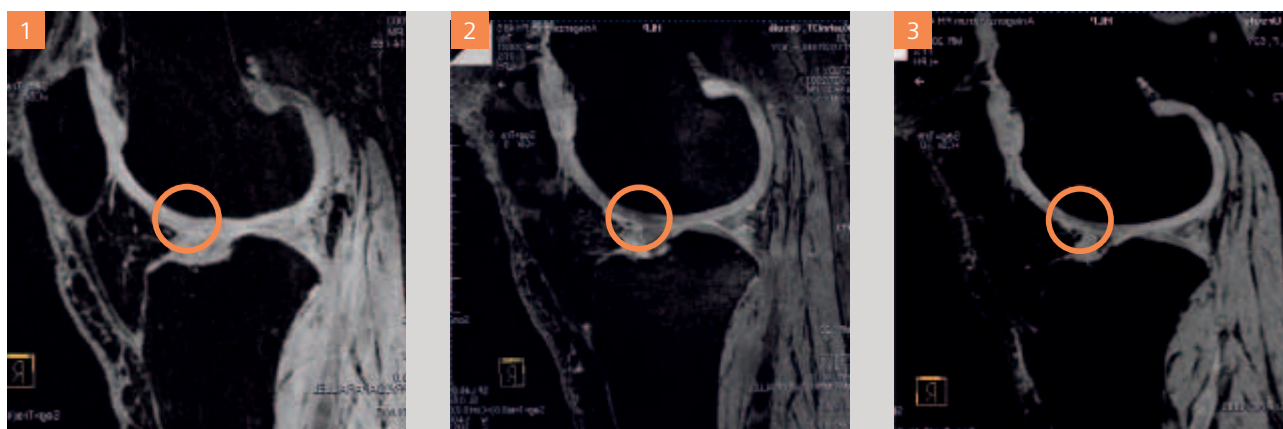


[Figure 1–4] Comparison of 3 cartilage sensitive sequences in an osteoarthritic knee joint. Changes in signal intensity and surface contour for the 3 sequences. Intraoperative comparison (green arrow) of this area with intraoperative findings for surface contour and resistance (red arrow).

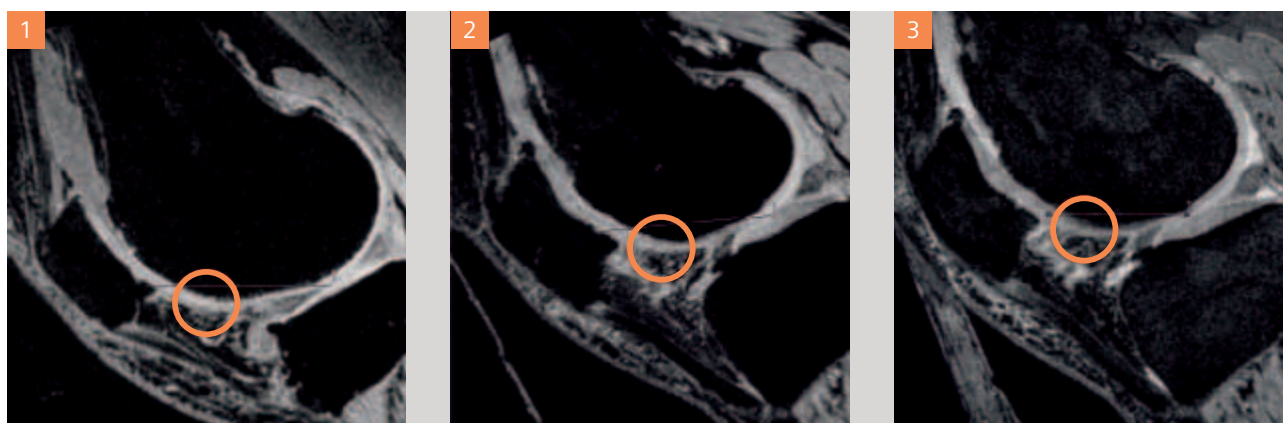


[Figure 5–8] Histological correlation for the three in vivo 3T MRI sequences showing a lack of information for the 3D Flash sequence in comparison to 3D MEDIC and 3D DESS.



3T Imaging in the Hip

Tallal C. Mamisch, M.D., Gert Muhr, M.D.

University Hospital Bochum, Bergmannsheil Clinics, Dept. of Trauma Surgery, Bochum, Germany

Introduction

The current practice of diagnosing osteoarthritis in the hip joint is based on typical clinical symptoms and x-ray findings – radiographic joint space narrowing and osteophytes [1]. This provides only a keyhole view of the disease process, and is limited in content validity as an assessment of disease development.

MRI-based detection of cartilage and acetabular labrum lesions has shown great potential in monitoring of osteoarthritis. In cases of hip dysplasia, MRI cartilage patterns are used to detect early degenerative changes prior to x-ray diagnosis [2]. Based on the current results for separation of acetabular and femoral cartilage, however, separation of the acetabular labrum and the corresponding cartilage and cartilage structure grading is not yet satisfactory.

The recent introduction of clinical use for 3T in the hip has been the subject of an ongoing study to compare diagnostic efficiency for the above parameters for 3T and 1.5T

Examination and Analysis

Healthy volunteers and patients with x-ray signs of moderate osteoarthritis underwent MRI examination by a 1.5 T MAGNETOM Symphony and 3T MAGNETOM Trio system. The 1.5 T system imaged both hips separately (3D MEDIC, TR = 31.0 ms, TE = 17.0 ms, resolution 0.84 x 0.84 x 0.84 cm), whilst the 3T system imaged both hips in one slab (3D MEDIC, 0.64 x 0.64 x 0.64 cm) with a body flex coil of the same geometric design. Radial images based on the center of rotation in the axis of the femoral neck, each of 30 degrees, were reconstructed and used for the analysis of separation of femoral and acetabular cartilage, and the assessment of cartilage structure. The detection of cartilage structure was compared by using a classification of visibility of changes and a cartilage grading according to Outerbridge criteria.

Perpendicular reconstructions in the acetabular opening were used to determine the ability of separation and quality analysis of the acetabular labrum in terms of monitoring for osteoarthritis.

Findings

There is a significant improvement in the separation of acetabular and femoral cartilage for the images obtained at the 3T system (Image 1 and 2), especially in the lateral portions of the hip joint.

However, there is also an increased separation assessed in the 1.5T at the radial reconstructions in the acetabular opening compared to the standard reconstructions.

The interobserver correlation is significantly higher for cartilage thickness measurements at the 3T system.

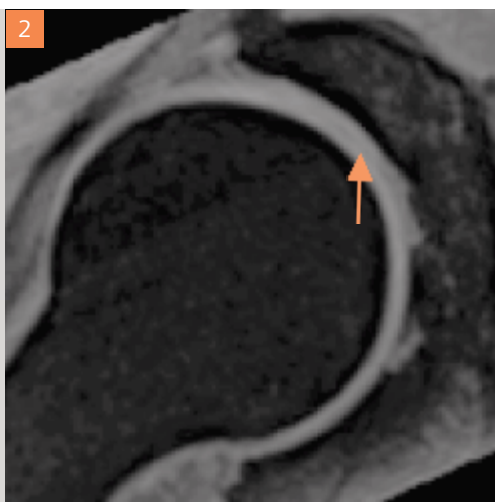
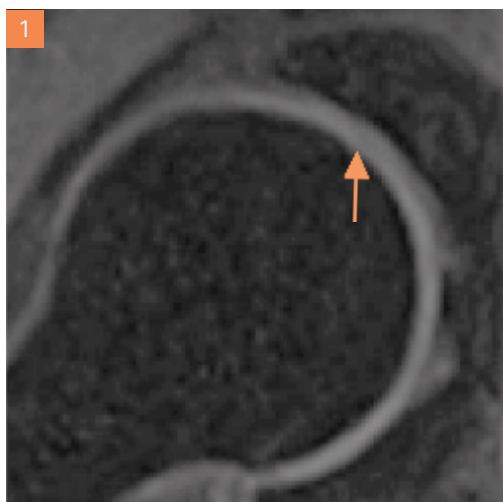
Cartilage loss was graded as "less than %50" and "more than %50" to simplify the assessment (Images 5 and 6). There was a significant improvement for separation of the acetabular labrum and the corresponding cartilage (Image 3 and 4). Therefore the cartilage quality analysis in this area was significantly improved.

Discussion

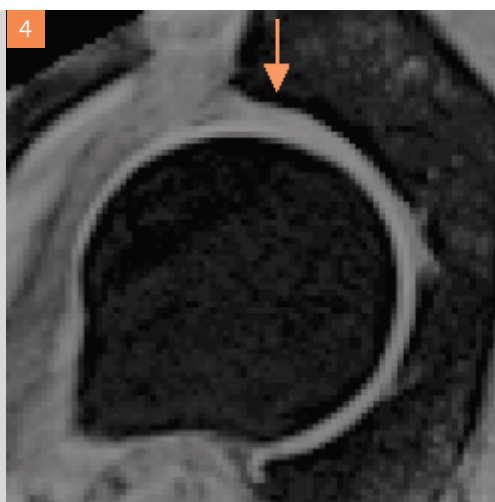
Images using a 3T system in comparison to the images obtained at the 1.5T system showed an improvement for all diagnostic criteria of early osteoarthritis. There is an indication for the clinical use of 3T based on these results, which overcomes the current limitation of hip imaging without contrast agent by detection of acetabular morphology and assessment of the geometric curvature of the femoral and acetabular cartilage. This is mainly important in cases of early prevention of osteoarthritic changes of the hip in cases of impingement [3] and before performing reorientation osteotomy.

References:

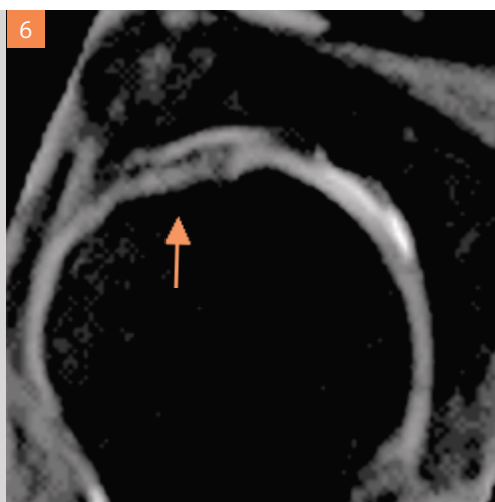
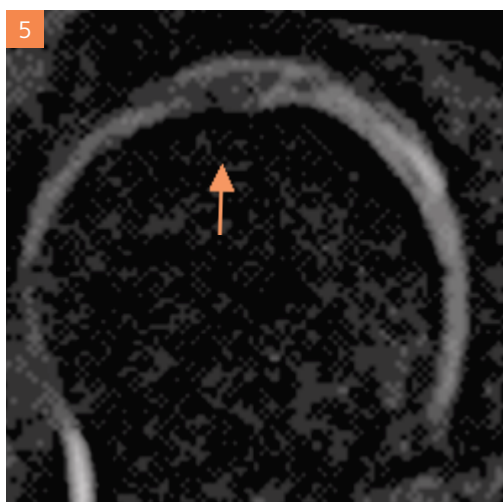
- [1] Kellgren J, Lawrence J. Radiological assessment of osteoarthritis. *Ann Rheum Dis* 1957; 16: 494–501.
- [2] Nishii T, Sugano N, Sato Y, Tanaka H, Miki H, Yoshikawa H. Three-dimensional distribution of acetabular cartilage thickness in patients with hip dysplasia: a fully automated computational analysis of MRI imaging. *Osteoarthritis Cartilage* 2004 12, 650–657.
- [3] Wagner, Siebenrock et al, Early osteoarthritic changes of human femoral head cartilage subsequent to femoroacetabular impingement. *Osteoarthritis and Cartilage* (2003).11; 508–518.



Comparison of separation for femoral and acetabular cartilage (1.5T left side 3T right side).



Comparison of separation for acetabular labrum and corresponding cartilage (1.5T left side 3T right side).



Comparison of cartilage grading (1.5T left side 3T right side).

3T MRI in Orthopedics

David Purdy Ph.D.

Siemens Medical Solutions, MR R&D, Research and Collaborations, USA

SNR Advantage:

Orthopedic imaging is greatly enhanced by improvements in resolution. However, this reduction in voxel size is ultimately limited by the signal-to-noise ratio (SNR) of the images. The development of 3T systems affords a significant increase in SNR, compared to widely-used 1.5T imagers. The improved SNR gives images of better quality; alternatively, the SNR currency may be spent to obtain higher resolution or shorter imaging times.

Sites that routinely acquire high-resolution scans in two or three planes at 1.5T may want to save time by using a single 3-D isotropic voxel protocol at 3T, displaying the other two planes by reformatting.

Even using a single acquisition, the imaging time for scans with large matrix sizes (e.g. 1024) can be prohibitive at 1.5T, and parallel imaging techniques (iPAT) result in a loss of SNR. At 3T, the additional SNR permits both small voxels and the use of parallel imaging techniques to make these studies feasible. Doubling the field strength to 3T doubles the initial magnetization of the nuclear spins. This can lead the unwary to think that the SNR of every protocol will be doubled. In fact, great care must be exercised to take full benefit of the higher field strength, and even this does not ensure that every examination is significantly improved at 3T.

More Spatial Shift between the Fat and Water Components of the Image

In nearly all MR scans, the fat and water components of the image are not in perfect registration. Orthopedic images often contain fatty bone marrow or fat pads in close proximity to important structures such as cartilage. A poorly-chosen protocol may cause the bright, shifted fat signal to obscure these structures. Many orthopedic protocols suppress the fat signal to avoid this problem.

During the data acquisition (readout) period, the fat spins precess (and the signal oscillates) slightly slower than the water spins. If, during this period, the fat spins precess two cycles less than the water spins, the image reconstruction will shift the position of the fat by two pixels. Even though the precessional frequencies of the water, the fat, and the difference between them all depend on the magnetic field, the strength of the readout gradient has almost no effect on this frequency difference. If a gradient increases the field of a voxel by 1 mT, it changes the precessional frequencies by about 42,600 Hz, but changes the frequency difference between fat and water by a miniscule 0.15 Hz. The shift between the fat and water components of the image is essentially unaffected by the readout gradient strength. What will change the spatial shift between these compo-

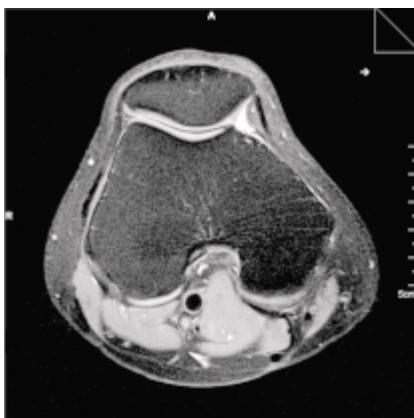


[Figure 1] Proton density turbo spin echo with fat-sat. Matrix 512, 0.3x0.3x0.3 mm.

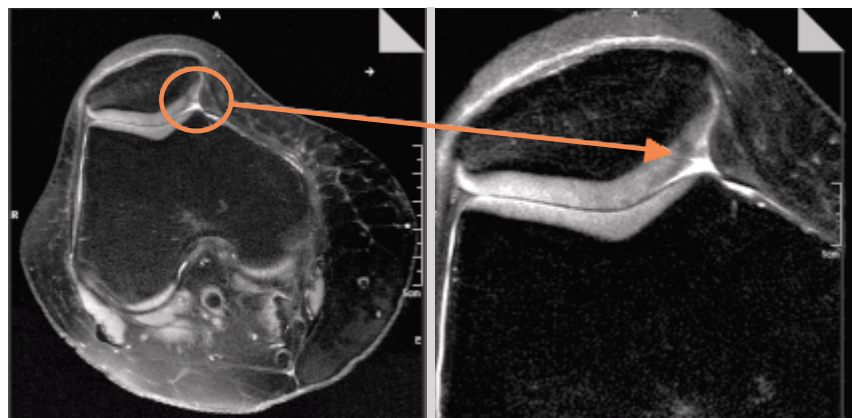


[Figure 2] High resolution knee imaging with 8 channel tx/rx knee coil. 0.3x0.3x0.3 mm, PATx2.

nents is shortening the duration of the readout: if the duration in this example is halved, the fat and water spins now dephase by only one cycle, and the fat-water shift following reconstruction is reduced from two pixels to one pixel.

This is referred to as “doubling the receiver bandwidth”, but this phrase is shorthand for four changes: the readout period is halved (this is what we care about), the readout gradient is doubled (this maintains resolution), the voltage is sampled twice as often (the “sampling bandwidth” is doubled) so that the same number of points are acquired, and the bandwidth of the analog or digital filtration of the signal is made wider (reducing the SNR by 30%),

If the orthopedic protocol uses fat suppression, a low receiver bandwidth can be used, and it may be possible to realize the full SNR enhancement of the 3T scanner. If fat suppression cannot be used, the receiver bandwidth should be approximately doubled relative to the 1.5T protocol. The theoretical 3T SNR gain of a factor of two will be reduced to 1.4-fold gain. A receiver bandwidth of 220 Hz/pixel gives a fat-water shift of one pixel at 1.5T; a bandwidth of 440 Hz/pixel gives the same shift at 3T.

This shift of the fat and water image components does not occur in the phase encoding direction. The phase changes caused by the incrementation of the phase encoding gradient affect the fat and water spins almost equally. It should be noted that the dark border that completely surrounds some organs in the abdomen when gradient echo images are acquired with an “opposed phase” echo time (the “India ink effect”) can ordinarily be attributed more to partial volume effects rather than to the fat-water spatial shift.

Better Fat Suppression

The increased separation of the fat and water resonant frequencies at 3T makes it easier to saturate the fat without affecting the water signal. It also permits the use of a shorter FATSAT radiofrequency (RF) pulse. Similarly, the waiting time between the components of water excitation pulses may be halved. Fat suppression is simply easier at 3T than at 1.5T.

Longer T₁

The T₁ of many tissues of orthopedic interest increases about 20% as the field doubles to 3T [1]. This has little effect on proton density- or T₂-weighted scans, but will ordinarily require some increase in TR for T₁-weighted scans. Whether this leads to a less time-efficient scan will depend on the protocol. If the corresponding 1.5T protocol had less than the desired number of slices, or if the slices were thicker than desired to reduce their number, then a 20% increase in TR could lead to a more desirable result at 3T. If the 1.5T proto-



[Figure 3] High resolution shoulder imaging. Proton density turbo spin echo with fat-sat. 0.4x0.4x2mm PATx2.

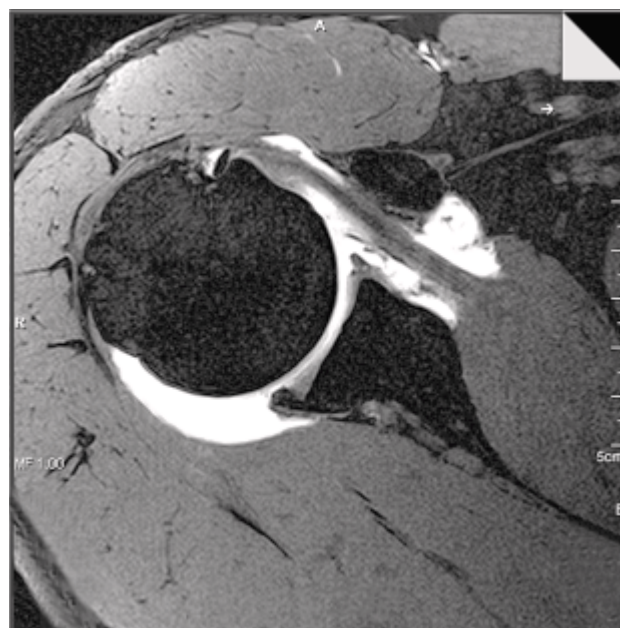


[Figure 4] VIBE arthrography. 0.5x0.5x1mm.

col had multiple averages, then fewer averages could be used, trading some of the SNR advantage of 3T for a faster scan. Similarly, if the 1.5T scan were a single acquisition, parallel acquisition techniques (iPAT) could result in a faster scan. A side effect of the elongation of T₁ is somewhat better



[Figure 5] Isotropic 3D wrist imaging. VIBE, 0.4x0.4x0.4 mm.

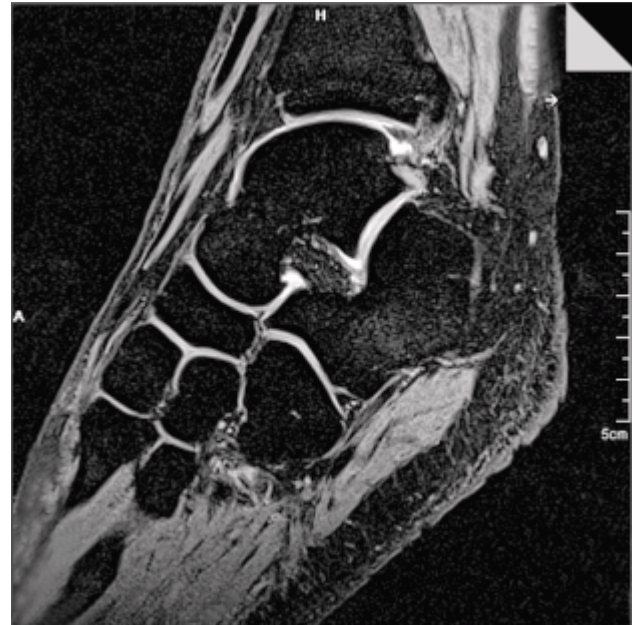


[Figure 6] 3D isotropic ankle imaging. DESS, 0.4 x 0.4 x 0.4 mm. Courtesy: Prof. Fukatsu, University of Nagoya, Japan

saturation of blood. This may improve the effectiveness of saturation bands used to reduce the pulsatility artifact of arteries such as the popliteal.

iPAT

There is a natural fit between 3T orthopedic imaging and parallel imaging techniques (iPAT). High resolution joint imaging with matrices of 512 and greater is desirable, but this is limited by both SNR and acquisition time. The extra SNR at 3T maintains the image quality, while iPAT keeps the imaging time within reason.

Shorter T₂

Doubling the field strength to 3T shortens the T₂ of various tissue by 10-37% [1], suggesting that excessive echo train lengths for turbo spin echo pulse sequences should be avoided to prevent blurring. It does not appear that the changes in T₂ will produce significant changes in tissue contrast for most protocols.

Increased Specific Absorption Rate (SAR)

For RF pulses of the same duration, tip angle and shape, a doubling of the main magnetic field leads to approximately four times the SAR. Fortunately, many orthopedic exams employ smaller transmit/receive coils that use much less power than the body coil, and most protocols can be run without alteration. T₁-weighted spin echo sequences with

many slices and turbo spin echo sequences with many 180° refocusing pulses are the most likely to be troublesome. When SAR must be reduced, low SAR RF pulses can be selected, the number of slices can be reduced, or alternative sequences may be employed. These alternatives may be as commonplace as low angle FLASH or FISP sequences, or new techniques such as hyperechoes. Sites that are willing to accept these changes in contrast relationships relative to their 1.5 T protocols will adjust quickly to imaging at 3T.

Increased Artifact from Orthopedic “Hardware”

Nonferromagnetic orthopedic implants have a magnetic susceptibility that differs from tissue, and can distort the local magnetic field. This distortion increases linearly with the main magnetic field, and can be considered an unwanted, misshapen gradient. Since the slice selection process and the readout depend directly on the linearity of the gradients, these field errors cause artifacts. By contrast, phase encoding uses the changes that occur as the phase gradient is incremented, and is less affected by constant local field errors. The solution, then, is to ensure that the applied slice and read gradients overwhelm the gradients created by the implant. As the main magnetic field is doubled to 3T, it is desirable to double the slice and read gradients for implant imaging. The readout gradient and associated pulses along the same axis can be doubled by doubling the receiver band-

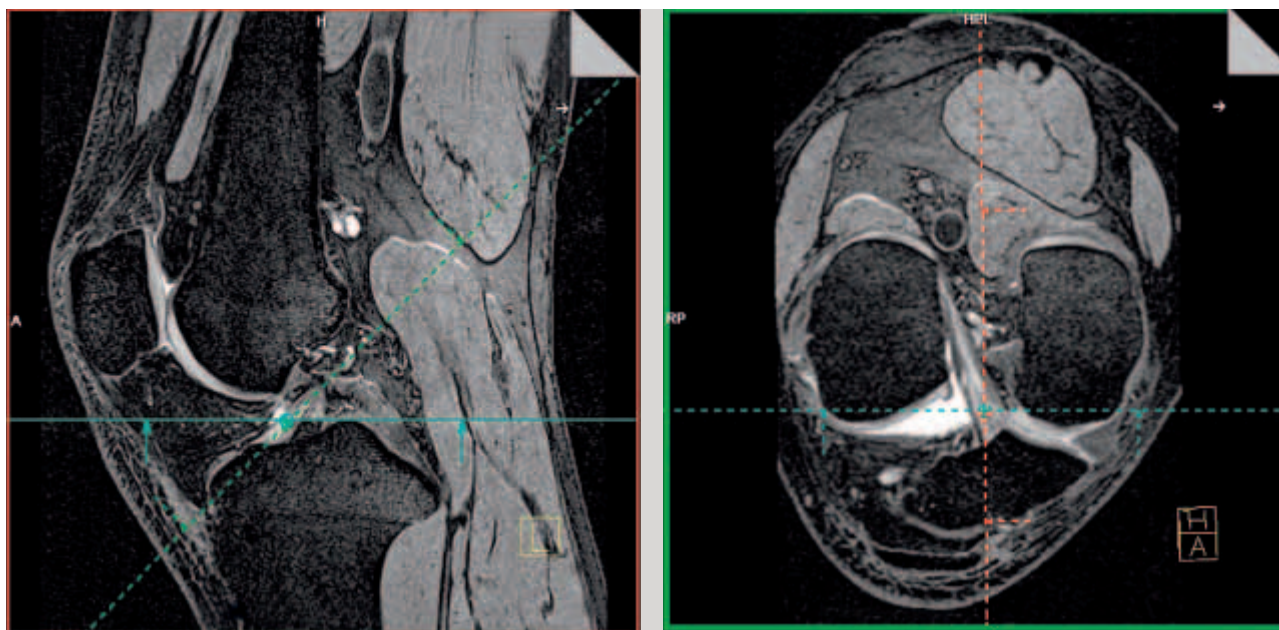


[Figure 7] Visualization of anterior cruciate ligament with isotropic 3D DESS dataset.

Courtesy: Prof. Fukatsu, University of Nagoya, Japan

width on the Sequence card of the protocol. This reduces the SNR by 30%. Some of this SNR loss may be recovered by averaging multiple high bandwidth echoes, as in the MEDIC pulse sequence. The slice selection gradient can be increased by selecting the “fast RF mode” on the Sequence card. This will increase the SAR and may increase the minimum slice thickness.

Additional artifacts are caused by RF current flow that is induced in a metallic implant. The appearance of these artifacts is complex [2], but is not dramatically worse at 3 T compared to 1.5T. However, the change in this artifact may cause implants to have a different appearance at different field strengths.

RF Artifacts

At 3T, the dielectric properties of the body reduce the wavelength of the RF such that it is comparable to body dimensions, leading to the formation of standing waves and degrading the RF homogeneity. In addition, signal inhomogeneities caused by tissue conductivity are more noticeable at 3T than at 1.5T. These effects are minimal for small joint imaging, but may become significant for hip protocols.

Conclusions

The improved signal-to-noise performance at 3T relative to 1.5T makes this the preferred field strength for the majority of orthopedic exams. At the same time, one must resist the

temptation to consider increased field strength as a simple amplifier of image quality. Those users who recognize the unique aspects of 3T imaging, and adjust their protocols accordingly, will be rewarded with superior results. In general, fat suppressed protocols used for patients without metallic hardware will give results greatly superior to 1.5T. When the receiver bandwidth must be increased to reduce the chemical shift artifact or to reduce metal artifacts, the SNR will still be better than a 1.5T exam, and this improvement may be traded for higher resolution. With careful selection of parameters, only a few examinations will have results that show no improvement compared to 1.5T.

References

- [1] Garry E. Gold, Eric Han, Jeff Stainsby, Graham Wright, Jean Brittain, and Christopher Beaulieu, “Musculoskeletal MRI at 3.0 T: Relaxation Times and Image Contrast,” *AJR* 183 (2004) 343.
- [2] Ulrike A. Lauer, Hansjorg Graf, Alexander Berger, Claus D. Claussen, and Fritz Schick, “Radio frequency versus susceptibility effects of small conductive implants – a systematic MRI study on aneurysm clips at 1.5 and 3 T,” *Magnetic Resonance Imaging* 23 (2005) 563.
- [3] Garry E. Gold, Brian Suh, Anne Sawyer-Glover, and Christopher Beaulieu, “Musculoskeletal MRI at 3.0 T: Initial Clinical Experience,” *AJR* 183 (2004) 1479.

Case Report:

Comparison of Acetabular Labrum Lesion and Corresponding Cartilage

Tallal C. Mamisch, M.D.¹, Götz Welsch, M.D.², Gert Muhr, M.D.¹

¹University Hospital Bochum, „Bergmannsheil“ Clinics, Dept. of Trauma Surgery, Bochum, Germany

²University Hospital Erlangen, Dept. of Trauma Surgery, Erlangen, Germany

Introduction

Acetabular labrum morphology changes have been indicated in several studies as a potential reason for hip pain. In cases of femoro-acetabular impingement the changed geometry of the femoral neck causes damage to the acetabular labrum, a possible reason for development of early osteoarthritic changes of the acetabular cartilage.

MR Arthrography of the hip is used for diagnosis and indication for therapy in cases of acetabular lesions, but still has a lack of cartilage quality diagnosis. The aim of the ongoing study is therefore to assess the cartilage quality in comparison to the morphology of the acetabular labrum and correlate it with the portion of the labrum based on MRI.

Patient History

A 27-year-old female patient presented with a history of hip pain for the last two years, especially during internal rotations. Clinical examination revealed symptoms of impingement.

Examination

For the MRI examination we used a 3D DESS sequence (isotropic resolution 0.7 x 0.7 x 0.7 mm, Siemens MAGNETOM Trio 3T) and a radially sectioned PD-TSE sequence (resolution 0.4 x 0.4 x 5.0 mm) perpendicular to the acetabular labrum was performed. For planning of the radial sections the plane of the acetabular opening was assessed double oblique using the isotropic cartilage sequence. The acetabular labrum morphology was analyzed based on shape, grading and the signal intensity in MRI. The results were compared to the corresponding femoral and acetabular cartilage quality based on modified Outerbridge criteria.

Findings

We assessed a solid cartilage damage in the anterior part of the femoral head based on the 3D DESS sequence with correlation to the femoral neck geometry. By additional analysis of the PD-TSE sequence in the same orientation we found a mycoid

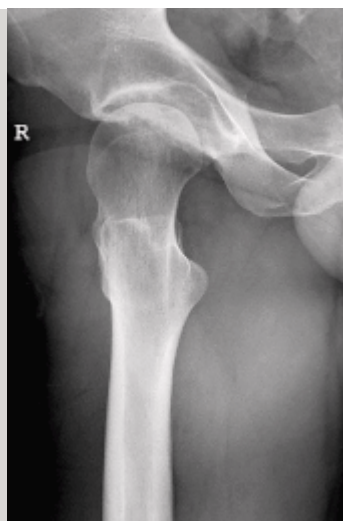


[Figure 1] X-ray with no signs of osteoarthritic changes and reduced acetabular coverage.

degeneration of the acetabular labrum, based on the mechanical conflict of the femoral head and the acetabular rim. This is an indication for labrum surgery due to the solid cartilage defect and the correlated changes of labrum morphology.

Discussion

It was possible to compare cartilage morphology to acetabular abnormalities by using an isotropic cartilage sequence for

positioning of the acetabular opening. An affection of the labrum and corresponding cartilage was found in the patient which correlated to femoral bone remodelling. This seems to be a possible cause of osteoarthritic changes in patients with SCFE (Slipped Capital Femoral Epiphysis) and is an indication for joint preserving surgery.

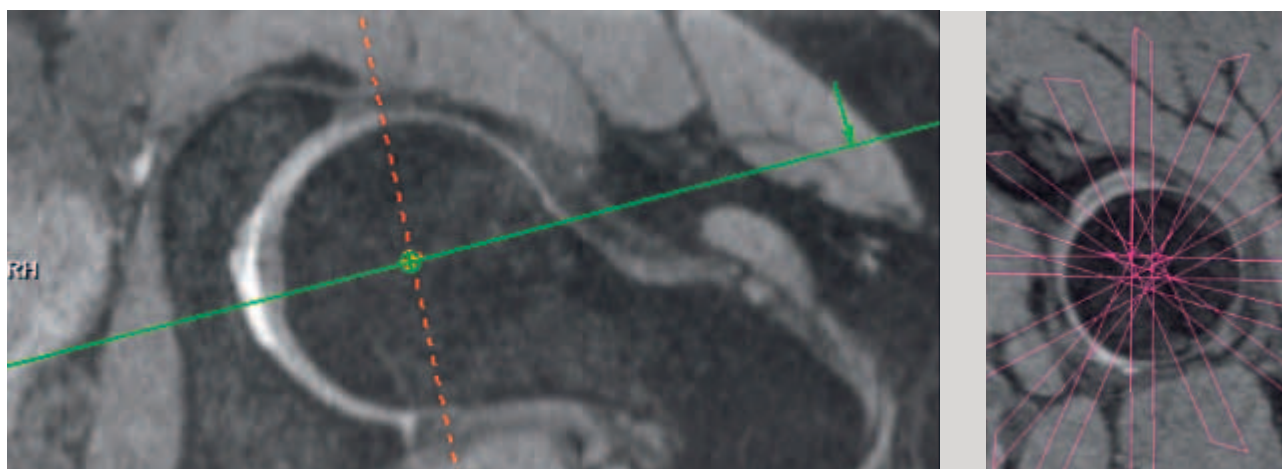


[Figure 2] Determination of the acetabular opening (left) for radial planing of the PD-TSE sequence (right).

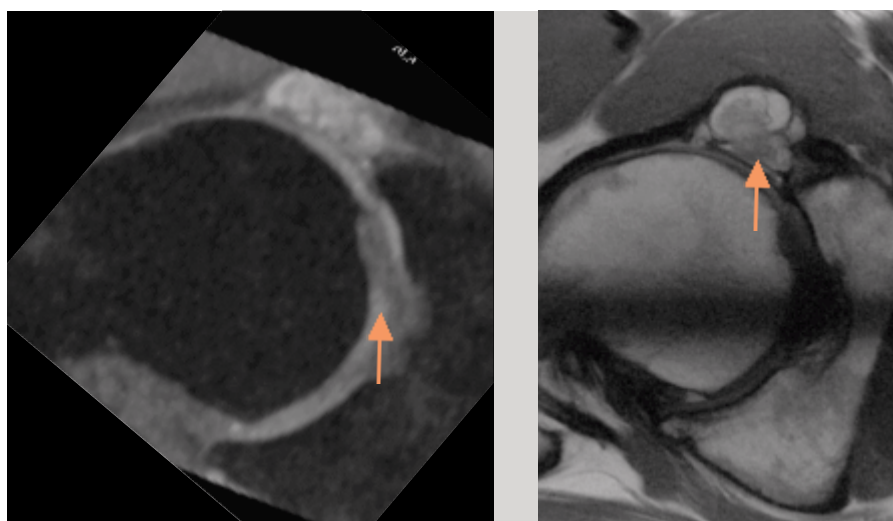


[Figure 3] Comparison of cartilage quality and acetabular lesion.

3T Neuropediatric Imaging, Initial Experience at the Children's Hospital of Philadelphia

Robert A. Zimmerman, M.D.¹, Heiko Meyer, Ph.D.²

¹Children's Hospital of Philadelphia

²Research Collaborations, Siemens Medical Solutions, USA

Introduction

Six months ago a new 3T MAGNETOM Trio was installed at Children's Hospital of Philadelphia. After three months operating from 8am to 4pm mostly on out-patients, the system was then utilized from 8am to 10pm in line with our standard clinical hours of operation. The initial three months were used to focus on protocol development and comparisons to the 1.5T systems MAGNETOM Avanto and MAGNETOM Sonata also set up in our hospital. In the meantime we have scanned over 800 patients, more than 500 of them being sedated.

On the one hand, since the relaxation time T1 increases, while T2 decreases, when moving from 1.5T to 3T, we anticipated that some protocol optimizations would be needed to maintain a certain contrast. On the other hand, 3T offered the opportunity to use the higher signal-to-noise ratio (SNR), the longer T1 times, and the greater contrast medium (Gadolinium) conspicuity to improve the diagnostic quality. The question was, however, whether routine studies on the MAGNETOM Trio could be done with sufficient diagnostic accuracy and satisfactory throughput to substitute for another 1.5T system. To address this question, we put the same load on the MAGNETOM Trio as on the other clinical scanners, working on a one-hour time slot per patient basis. Then we developed protocols to use the additional SNR for protocols with higher resolution and shorter scan times.

Results

The ability to use iPAT in numerous protocols proved to be vital to achieve the acquisition of more data in the same or a shorter period of time. A 3D T2-weighted non-iPAT scan covering the whole brain takes 9:25 min with a matrix size of 256x192, while the scan time for an isotropic matrix of 320x320 can be reduced to 4:30 min with an iPAT factor of 2. The results can be seen in Fig. 1.

Although T1-weighted scans are in general faster, the application of iPAT allowed us to shorten a whole head 3D acquisition

with a 256x244 matrix from 7:05 min to 3:56 min. The grey-white matter contrast using the 3D MPRAGE sequence is excellent, providing the ability to reconstruct images with sub-millimeter resolution. Fig. 2 shows an example of an 11-year-old male who underwent surgery for DNET tumor resection. The images clearly show residual tumor in the cavity, which was not enhancing and remained elusive on 12 previous follow up MRI studies on a 1.5T system over a period of 3½ years. The ability to demonstrate the tumor unequivocally depended on the 3T higher field strength and signal-to-noise that allowed excellent quality thin section resolution of the surgical cavity margins, not achievable at 1.5 Tesla.

3D techniques to acquire isotropic voxels allow reformatting

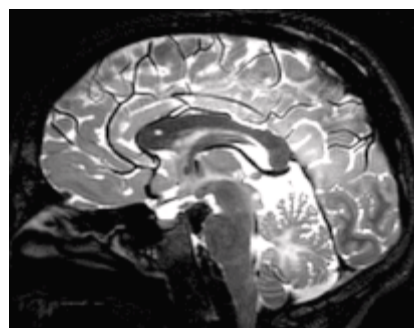


[Figure 1]
8-year-old male
with Neuro-
fibromatosis,
1 mm isotropic
3D TSE T2.

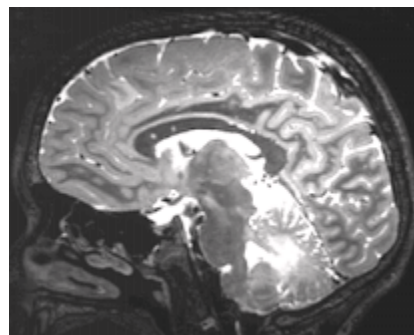


[Figure 2]
3D MPRAGE of
an 11-year-old
male post oper-
ative tumor
resection of an
dysembryoplas-
tic neuroepithe-
lial tumor with
residual tumor.



[Figure 3] 1.5T MRA (left) and 3T MRA (right) of a 4-year-old male with absent left internal carotid artery.

the images in any given plane, as well as with different slice thicknesses, which we use to obtain transverse and coronal views. This way we avoid scanning one or two additional planes, which helps to save valuable time.

Time-of-Flight Magnetic Resonance Angiographies (TOF-MRAs) also benefit from the higher SNR, as well as from the longer T1 relaxation times, which allow the imaging of smaller and deeper vessels. Where on a 1.5T system the acquisition times are in the range of 9 to 10 minutes, the use of iPAT allowed the acquisition of the same 512x224 matrix in 4:16 min. Smaller and deeper vessels can be depicted as can be seen in Fig. 3.

Another application, for which the longer T1 times at 3T are beneficial, is Arterial Spin Labeling (ASL). This technique utilizes the blood as an intrinsic contrast agent by labeling the inflowing blood and using it to measure perfusion. The longer the T1, the deeper inside the brain perfusion can be measured. Since the signal difference between unlabeled tissue and labeled blood is less than 10 percent, SNR is also a crucial point. We imaged the above mentioned 4-year-old with a home-built ASL at 3T, which shows that both hemispheres are perfused despite the absent left internal carotid artery (see Fig. 4). Compared to contrast enhanced perfusion imaging, ASL has the advantage that measurements can be easily repeated if, for example, there is patient motion degrading the diagnostic quality.

When looking at acute infarction, diffusion weighted imaging is one of the key techniques to assess the tissue at risk at an early stage. Fig. 5 shows a diffusion weighted image with a b-value of 1000 s/mm² using a 192x192 matrix, which reveals the infarction area.

Alongside the advantages of 3T, we were aware that a higher field strength would increase the local radio-frequency power deposition (SAR) and the risk potential for medical devices

and surgical implants. Therefore we only admitted patients with implants to the 3T scanner, which were explicitly compatible with a field strength of 3T. To counteract the higher SAR, especially for T2-weighted sequences, we routinely run the SPACE (Sampling Perfection with Application optimized Contrast using different flip angle Evolutions) sequence which can reduce the SAR by up to 80%.

SPACE is using a Turbo Spin Echo type of acquisition scheme, but instead of sampling 15–25 echoes, as it is usually done for T2-weighted imaging, 200–400 echoes are acquired in each echo train. To compensate for the strong signal decay that would normally occur with this HASTE-type of acquisition, the flip angle of each refocusing radio-frequency pulse is specifically calculated and modified. This maximizes the contrast between different tissue types, e.g. gray and white matter and CSF and it also avoids the blurring due to T2 decay, which occurs in HASTE-type of scans with such a long



[Figure 4] 3T Arterial Spin Labeling image of a 4-year-old male with absent left internal carotid artery.

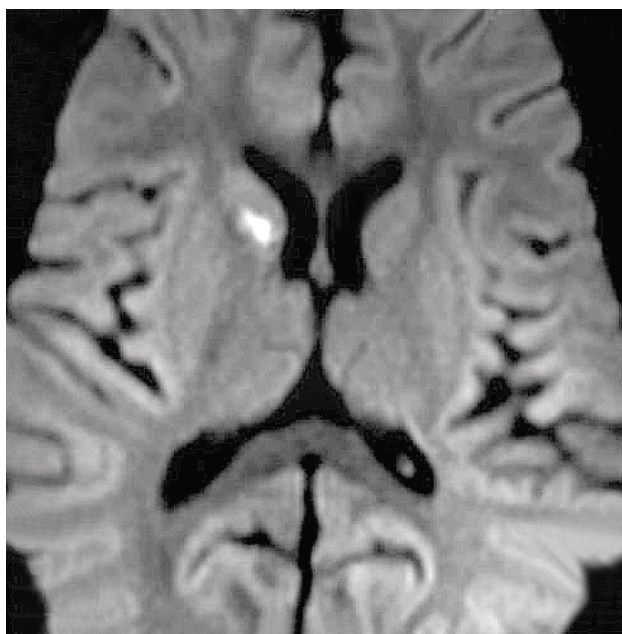


[Figure 5] Diffusion-weighted image with $b = 1000 \text{ s/mm}^2$ of a 14-month-old male with sickle cell disease after acute infarction.

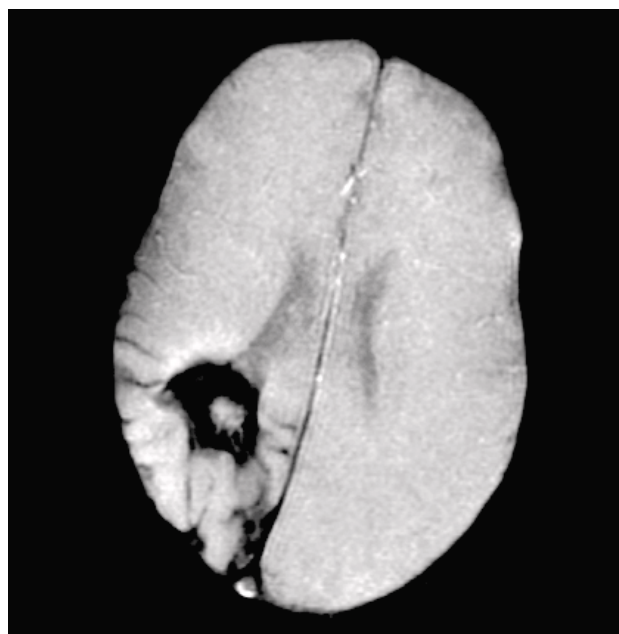


[Figure 6] Susceptibility-weighted scan of a 1.5-months-old infant.

echo train. The long echo train made it feasible to cut down the scan time for an isotropic whole brain scan to 4–6 minutes, while providing a high degree of details in all planes. Although an in-plane resolution of $\sim 1 \times 1 \text{ mm}^2$ was standard at our institution, we typically acquired 3–5 mm thick sections, making it necessary to run separate scans for different orientations. Using the SPACE technique we now scan in one orientation and reconstruct the other planes maintaining the high resolution. The higher sensitivity to susceptibility differences in the tissue at 3T is helpful when looking at intracranial hemorrhages (see Fig. 6), but it also degrades the image quality in the presence of e.g. braces. However, sequences with higher bandwidth and shorter echo spacing, as well as the use of iPAT can reduce this effect.

Conclusion

In conclusion, we found that the MAGNETOM Trio is able to handle the full clinical load, providing in some cases superior diagnostic information compared to 1.5T imaging. Further improvements will involve protocol optimizations to reduce susceptibility-induced artifacts and setting up standards for metallic implants. Due to the extended use of high-resolution 3D imaging techniques, new strategies need to be developed for reading the substantially increased amount of images.

We are planning a Tim upgrade this fall which should increase the performance of the system even further and give us the same technology as on the MAGNETOM Avanto. One of the reasons to upgrade is the ability to then use iPAT in any direction in any region of the body. The 12-channel Head Matrix coil will allow iPAT factors of 4–6 for standard applications whereas the Tim concept of using as many coil elements as necessary for a specific examination will improve patient throughput and diagnostic quality even more. In a pediatric environment, the size and the weight of the coils are always of concern and we see a clear advantage of the Tim technology which features adequately sized coils, while providing high SNR in conjunction with lightweight coils. Not having to change the coils for combined head and whole spine examinations, for example, will be beneficial given the already long sedation time for this kind of study and the danger of the child waking up during repositioning. All this has a positive effect on the safety of the patient and efficiency of the scan. After all upgrades are done we will have five state-of-the-art MR systems to provide exceptional patient care as well as a platform for research studies – reflecting our commitment to remaining one of the leading pediatric hospitals worldwide.

SPACE (Clinical Practice)

Georges B. Leroux, M.D.¹, Luaba Tshibanda, M.D.², Mahmoud Baghaie, M.D.², Roger J. Demeure, Ph.D.³

¹Clinique André Renard, Herstal, Belgium

²Centre Hospitalier Universitaire de Liège, Belgium

³MR Application Specialist, Siemens Medical Solutions, Belgium

Introduction

Our MRI unit combines 3 hospital institutions of different sizes within one university center, making it possible to create a completely specialized service. The unit currently owns 3 MR systems (MAGNETOM Harmony, Symphony, Trio). We perform an average of between 50 and 60 examinations per day, aiming to fulfill through team work the wishes of the clinicians and patients.

The presence on the same site of the 3 MR machines allows the gathering of the various techniques and medical competences that guarantee to each patient and each examination indication an optimal quality. In addition, the radiologists carrying out the examinations also have a diagnostic radiology activity (CT, US, angiography...) in the medical imaging services of the partner institutions.

We recently acquired a 3T MAGNETOM Trio, A Tim System for processing functional and spectroscopy imaging. But our continuing heavy clinical load means that we have to perform routine MRI examinations in this MR system.

So it was necessary to develop regular T1, T2, and FLAIR weighted imaging sequences in this particular field strength. It quickly became apparent that conventional spin echo and TSE sequences cannot be transferred from 1.5 T to 3T because we face T1 tissues lengthening, T2 shortening and strong magnetic susceptibility and chemical artifacts.

Our challenge, therefore, was how to achieve the high definition imaging that the 3T increase in signal-to-noise ratio promises.

Methods

Image contrast with T2-weighting is impossible to circumvent for routine MR examinations. Up to now, these images have only been acquired by using 2D-SE or 2D-TSE pulse sequences which could be classified into 2 categories : (i) bright fluid T2 and (ii) dark fluid T2 (with optionally Fat Saturation).

Although there exist 3D-Gradient Echo (GRE) pulse sequences providing T2(*)-weighted images (i.e. DESS, MEDIC), there is a lack of 3D pulse sequences generating optimal image contrast with T2-weighting. This necessary demand requires

3D techniques based on SE or TSE pulse sequences.

The arrival of SPACE (Sampling Perfection with Application optimized Contrast using different angle Evolutions), combined with 3T magnetic field and iPAT (Integrated Parallel Acquisition Technique), fills the gap.

SPACE satisfies the following requirements of routine clinical examinations :

1. Contrast : T2-TSE contrast with an imaging time comparable to 2D protocols.

2. Spatial Resolution – 3D post-processing : The combined power of iPAT (and Tim technology) with 3T offers the best of all worlds. Now high-resolution 3D true isotropic imaging with sub-millimeter resolution is possible for all body regions and that with the shortest ever acquisition times. Having regard to the increasing role of 3D reformatting and post-processing in multi-detector CT exams, the Multi-Planar Reconstruction (MPR) of such 3D data makes possible free slice prescription after the scan, bringing CT-like post processing practices to MRI.

3. Acquisition Time: SPACE must indeed not only provide high spatial resolution but also offer this with measuring time acceptable for routine examinations. It must be comparable to the current T2-weighted 2D TSE pulse sequences. Compared to a conventional T2-weighted 3D TSE pulse sequence, the acquisition time reduction is more than 85%. In addition, thanks to multiple array coils, iPAT leads to at least 15% further reduction in acquisition time.

4. Flexibility to provide contrast optimization for different applications like dark fluid, MRCP, orthopedic, ... reflecting the T1- and T2-times of the tissues involved.

5. Lower RF power deposition (lower SAR) which is fundamental when working with higher magnetic fields (3T).

With SPACE, therefore, we are able, as with multi-slice CT, to realize retrospective reconstruction in any image plane. This is an additional decisive advantage when dealing with complex relationship between anatomical structures and pathological changes.

Clinical Cases

Case 1

Bright Fluid – Metastatic lesion

This patient suffers from a hemorrhagic renal cell brain metastasis (Fig. 1). Only one sagittal 3D-acquisition with almost isotropic resolution ($1.5 \times 1.1 \times 0.9$ mm³), was performed (Fig. 1: upper left image). Two orthogonal slices series (coronal, transversal; Fig. 1: lower left and upper right images) were reformatted using MPR post-processing. Three series of high spatial resolution images are available so as to inspect the pathology with precision. The data set was acquired in less than 5 minutes and avoids the need to acquire additional T2-weighted evaluation planes, as with 2D techniques.

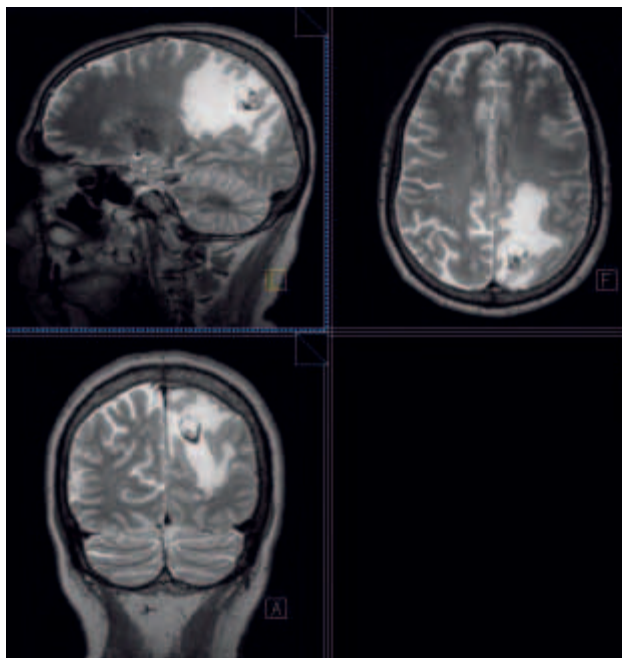


[Figure 1] The MR parameters of this bright fluid SPACE pulse sequence that nicely depicts this metastatic lesion are: TR/TE/ETL=3200ms/455ms/139, slice thickness = 1.5 mm and voxel size = $1.5 \times 1.1 \times 0.9$ mm³

Case 2

Dark Fluid – Brain Screening (Fig. 2)

In this MS patient, an isotropic 3D dark fluid SPACE data set was acquired. Note the procedure chosen to examine the hypophysis; as for cerebellar peduncle, the acquisition of thin slices using a dark fluid pulse sequence was used instead of a classical pure T2- TSE pulse sequence. The images were realized in the sagittal orientation and cover the whole brain. The high spatial resolution permits extension of the survey to the sella. This allows the discovery of a small, old, hemorrhagic Rathke's Cleft cyst (Fig. 2: arrow HEM RCC). The Fig. 3 shows a series of sagittal source images selected in the 82 images of the 3D-SPACE slab. The high spatial resolution (mainly the millimetric slice thickness) allows the precise travel through the sella and the hypophysis nicely depicting the lesion structures.

The sella region is known as being a specific target for systemic pathologies. Dark fluid images are also of great interest for the subarachnoid region in hemorrhage or metastasis. Consequently high spatial resolution SPACE T2-weighted images are very helpful for brain screening. In addition, the 3D approach makes possible a retrospective, time delayed, deeper analysis.



[Figure 2] The MR parameters of this dark fluid SPACE pulse sequence that very well depicts this hemorrhagic Rathke's Cleft's cyst (arrow: HEM RCC) are: TR/TE/ TI/ ETL = 5000 ms/ 353 ms/ 1800ms /221, slice thickness = 1 mm and voxel size = $1.0 \times 1.1 \times 0.9$ mm³

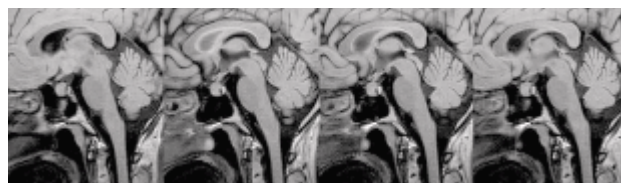


[Figure 3] The fine structure of the lesion in the hypophysis is very well depicted thanks to the millimetric slice thickness.

Case 3A**Dark Fluid – MS patient**

For this MS patient, 3 mm slice thickness SPACE dark fluid axial set of slices was performed in an acquisition time of five minutes. Due to the higher spatial resolution and the slice contiguity (3D acquisition), the MS plaques (Fig. 4: red circles) are nicely resolved and delineated. Compared to a routine 5 mm slice thickness 2D-dark fluid tse sequence, the partial volume averaging effect is greatly reduced when using the dark fluid SPACE pulse sequence (Fig. 5). Consequently, the dark fluid SPACE pulse sequence offers a sharper and more accurate depiction of individual lesions.



[Figure 4] Red circles indicate very well delineated MS plaques thanks to the 3D features of the dark fluid SPACE pulse sequence. The sequence parameters were: TR/TE/TI/ETL = 6000 ms/366 ms/2100 ms/115 to provide a voxel size of: $3 \times 0.9 \times 0.9 \text{ mm}^3$.

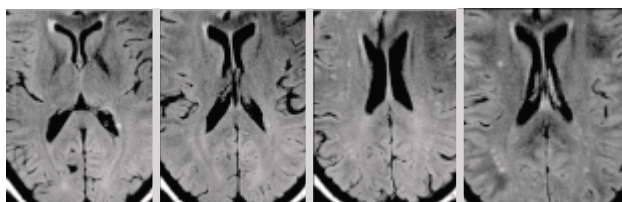


[Figure 5] The 3 images on the left show transversal slices acquired with the classical dark fluid 2D TSE pulse sequence (tir2d1rs9, 5 mm slice thickness and distance factor = 30%).

The second image from the left is almost the same slice position as the slice on the right which was acquired with the dark fluid SPACE pulse sequence (3 mm slice thickness and contiguous slices). The great advantage of SPACE becomes obvious as the classical dark fluid TSE pulse sequence does not clearly delineate (blurring) MS plaques or could miss some of them. Therefore, dark fluid SPACE appears as being of huge interest for MS plaques identification and counting among others for therapy follow-up.

Case 3B**Dark Fluid – MS patient**

In this young lady a single pending diagnosis: pseudotumoral MS, based on cerebrospinal fluid tests, is well visualized in the cerebellar peduncle (Fig. 6). The isotropic (voxel size = 1 mm^3) of the 3D SPACE acquisition allows easy travel through the 3D volume. The image reformatting (MPR post-processing) permits a better delineation of the lesion.

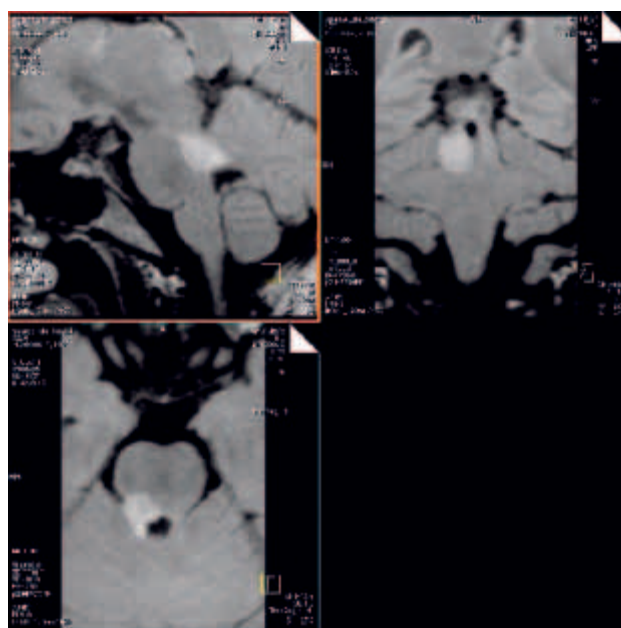


[Figure 6] The MR acquisition parameters of this sagittal non slab-selective excitation dark fluid SPACE pulse sequence are: TR/TE/TI/ETL = 6000 ms/400 ms/2100 ms/123, slice thickness = 1mm and voxel size = 1.0 mm^3 . The measuring time was 5 min to acquire one 3D-slab containing 144 contiguous slices.

Case 4**Bright Fluid – IAC investigation:**

A high-resolution CISS sequence is a generally recognized procedure for the inner ear and auditory canal. The SPACE technique (Fig. 7) can even go down to 0.3 mm thick contiguous axial slices set. In addition, image quality is improved thanks to the lower sensitivity to flow and magnetic susceptibility artifacts. In this antro-attical cholesteatoma, referred to MR for evaluation of intracranial extension, we can also see that the integrity of the external semicircular canal is well preserved with its bright fluid-like signal. The diagnosis correlated well with the CT examination. Both modalities present a similar spatial resolution, however image contrast is better with SPACE-MRI than with CT.

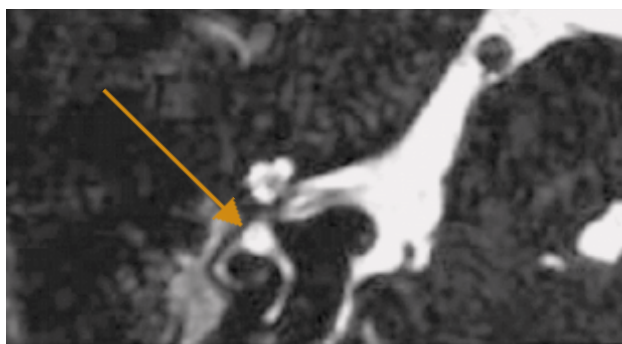


[Figure 7] The acquisition MR parameters of this transversal fat-saturation bright fluid SPACE pulse sequence are: TR/TE/ETL = 1300 ms/246 ms/160, slice thickness = 0.4 mm. For an isotropic voxel size of $(0.4 \times 0.4 \times 0.4) \text{ mm}^3$, the measuring time was 7 min to acquire one 3D-slab containing 52 sub-millimetric contiguous slices through the inner ear.

*The information about this product is preliminary. The product is under development and is not commercially available in the U.S. and its future availability cannot be assured.

Case 5**Bright Signal: MRCP with SPACE coupled with PACE (free breathing):**

1. Due to the better signal-to-noise ratio provided by MAGNETOM Trio, the 8 channel phased array body coil and the SPACE (3D) procedure, we get a higher spatial resolution better tuned to the anatomical requirements of the organ under investigation. This hugely improves the quality of the exams realized with the traditional RARE* and HASTE pulse sequences. At 3T with SPACE, iPAT is used to reduce the acquisition time to less than 4 minutes without any compromise in the image quality. Last but not least, this exam is performed in free breathing thanks to PACE, (echo navigator) leading to images without any motion artifacts, which is very useful for uncooperative patients.
2. As discussed previously but maybe more relevant for MRCP, 3D acquisition offers a different procedure for reviewing the examination of the biliary and pancreatic system. Indeed, the source images, the MPR and the MIP, are both very helpful because they provide complementary morphologic information. We aim for a better depiction (detection) of small or complex anomalies of ducts, i.e. intrahepatic bile ducts stenosis in, for instance, "Sclerosing Cholangitis", small intraductal stones, rupture of the Wirsung and post-surgical bile leakage/stenosis.



[Figure 8] The MR parameters of this coronal bright fluid SPACE acquisition are: TR/TE/TI/ ETL= 3983 ms/ 740 ms/ 2100 ms/203, slice thickness=1.5 mm and voxel size= $(1.5 \text{ m} \times 1.0 \times 0.7) \text{ mm}^3$. The examination was performed in free breathing thank to the PACE technique and lasts 4 min to acquire one 3D-slab containing 52 contiguous slices.

Case 6

MR Sialography

As a result of the higher signal-to-noise ratio obtained thanks to MAGNETOM Trio and the 8 channel phased array (PA) head coil, we can get the very high spatial resolution requested for the investigation of the salivary gland ducts. Fig. 9 presents one of the 72 images of the examination of the parotid salivary gland in a suspected pleomorphic adenoma (arrow). The data were acquired using a strongly T₂ weighted SPACE pulse sequence. The acquisition parameters are roughly based on those of the SPACE-MRCP but with a spatial resolution pushed to an isotropic voxel size of 0.21 mm³. The use of the 8 channel head coil, and consequently iPAT, allows the acquisition of data in a timeframe acceptable for clinical examinations. High SNR provides excellent resolution and detailed information in the case of a tumor and shows that there is no contact between the tumor and the main salivary duct (Fig. 10).

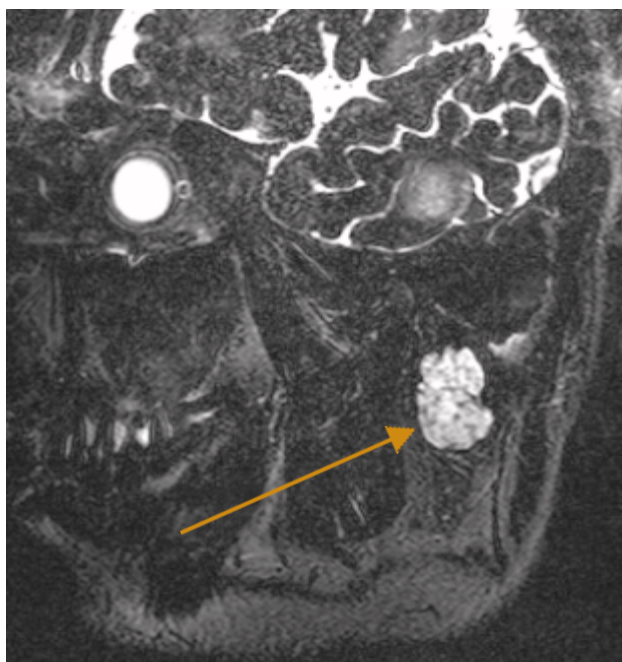


[Figure 9] To investigate the salivary glands a sagittal bright fluid SPACE acquisition was used. The acquisition parameters are : TR/TE/ETL= 1300 ms/313 ms/140. The slice thickness and the voxel size are respectively 0.5 mm and (0.5 x 0.7 x 0.6) mm³. The examination time was 5:26 min to produce one 3D-slab composed with 72 sub-millimetric contiguous slices.

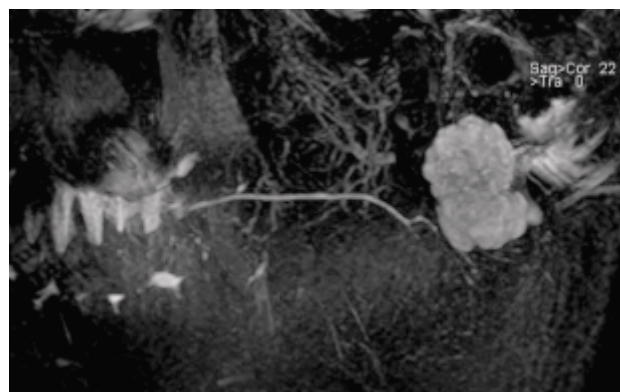


[Figure 10] As for MRCP, MIP reformatting allows perfect visualization of the salivary ducts and evaluate its possible connection with the lesion.

Multinuclear MR Spectroscopy at 3 Tesla

Nouha Salibi, Ph.D.¹, Uwe Boettcher, Ph.D.²

¹Siemens Medical Solutions, R&D Collaborations, Malvern, PA, USA

²Siemens Medical Solutions, MREA, Erlangen, Germany

Introduction

Proton MR spectroscopy (^1H MRS) is commonly used for detection and monitoring of metabolites in the brain and prostate; There is also a growing interest in clinical applications to other parts of the body such as characterizing lesions in breast, ovaries and liver, and understanding lipid metabolism in muscle and liver. Although metabolic information obtained with ^1H MRS is invaluable, it represents a fraction of the wealth of information that is available from in vivo MR spectroscopy in general, which can also be performed with other nuclei including phosphorus (^{31}P), carbon (^{13}C), and fluorine (^{19}F), referred to as x-nuclei. Compared to ^1H these nuclei have lower sensitivity especially so for ^{31}P and ^{13}C ; X-nuclei spectra with adequate signal to noise ratio (SNR) require much longer measurement times and/or lower spatial resolution. The SNR gain from higher field systems helps in reducing scan times and improving spatial resolution. Another benefit for multinuclear MRS at higher field strength is the improved spectral resolution, which helps simplify the typically complex spectra.

Multinuclear MR Spectroscopy

While ^1H MRS is performed on standard MR scanners with standard RF coils, x-nuclei MRS requires additional transmis-

sion and detection hardware that operates at the resonant frequency of the nucleus of interest. Typical spectra from x-nuclei are complex; they have a wide chemical shift range, and they include signals that are split into multiple peaks (multiplets). The splitting is due to coupling of the x-nuclei with neighboring protons, and can often be removed using decoupling techniques, which have the added benefit of improving sensitivity. Decoupling techniques consist of applying rf power to saturate protons that are coupled to the x-nucleus during detection of its signal. The rf power can be applied in a variety of schemes including low power continuous wave (CW), and schemes of composite rf pulses such as the WALTZ decoupling technique or wideband alternating-phase low-power technique for zero residual splitting. Signal enhancement may also be achieved with the nuclear Overhauser enhancement (NOE) effect by saturating the coupled protons prior to excitation of the x-nucleus and detection of its signal. CW decoupling, Waltz decoupling and NOE can be incorporated in x-nuclei MRS measurements on the MAGNETOM Trio*. Figure 1 illustrates the effect of ^1H decoupling on a ^{13}C spectrum from an ethylene glycol phantom. Here decoupling causes the triplet from the methylene groups (Figure 1A) to collapse into a single higher peak (Figure 1B).

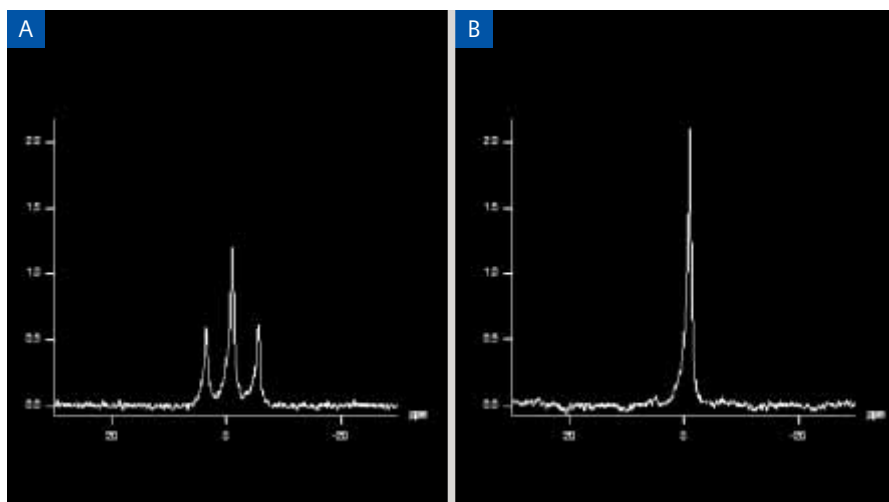


[Figure 1] ^{13}C spectra from a phantom of ethylene glycol acquired on the MAGNETOM Trio without decoupling (A) and with WALTZ ^1H decoupling (B). The ^{13}C methylene signal is represented by a triplet in (A), which collapses into a higher single peak in (B). The spectra were acquired with a free induction decay (FID) sequence, 32 averages, a TR = 5000 ms and an acquisition time of 2 min 10 s.

In vivo multinuclear spectra: ^{31}P in vivo MRS

Phosphorus MRS has been used in the evaluation of tumors, liver function, and the energetic state of tissues such as muscle, brain and heart. Examples of MAGNETOM Trio ^{31}P spectra from brain and muscle are shown in Figures 2–5. Figures 2 and 3 represent spectra from the brain of a healthy volunteer acquired with a double resonant flex coil (Advanced Imaging Research, Inc, Cleveland, Ohio, USA). The non-local-

ized spectrum in Figure 2 is from a free induction decay (FID) measurement and the localized spectrum in Figure 3 is from a csi-fid sequence, a FID based chemical shift imaging (CSI) sequence. The major peaks are seen between -20 ppm and 10 ppm including alpha, beta and gamma adenosine triphosphate (ATP), phosphocreatine (PCr), phosphodiester (PDE) compounds, inorganic phosphate (Pi) and phosphomonoester compounds (PME).

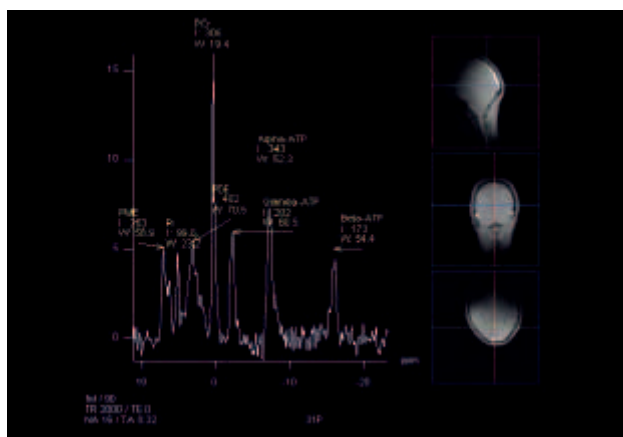


[Figure 2] A non localized ^{31}P brain spectrum from the MAGNETOM Trio using a double resonant flex coil.*

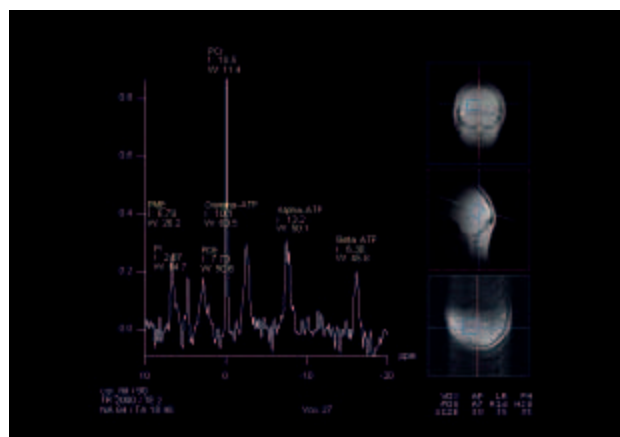


[Figure 3] A localized ^{31}P brain spectrum from the indicated (30x35x35)mm³ voxel of a csi_fid measurement using a double resonant flex coil*, TR = 2000s, 64 averages, 8x8 matrix with weighted k space sampling and a measurement time of 18 min 48 s.

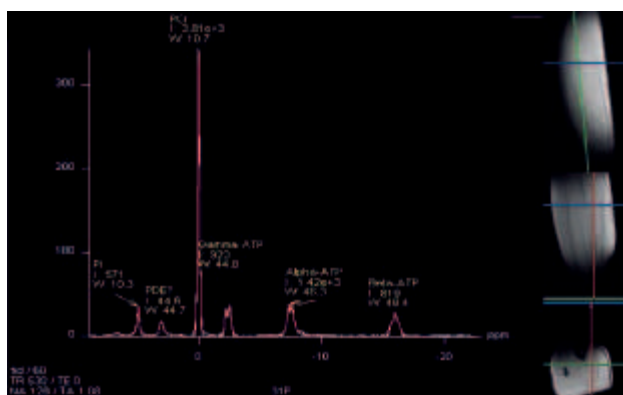


[Figure 4] Non-localized ^{31}P spectrum from calf muscle of a healthy volunteer acquired on the MAGNETOM Trio with a 14 cm double resonant loop coil*, a csi_FID sequence with NOE, a TR = 530 ms, 128 averages in 1 min 8 s.

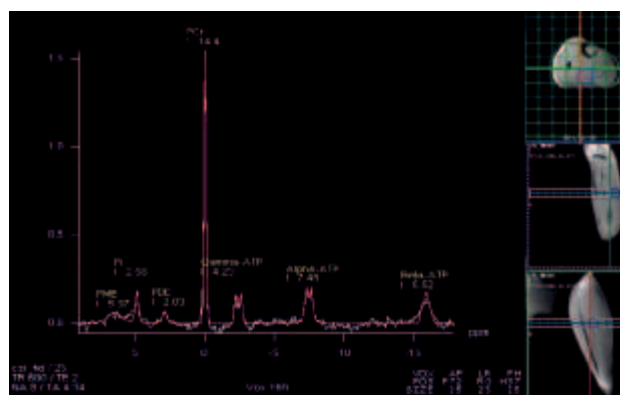


[Figure 5] Localized ^{31}P spectrum from calf muscle of a healthy volunteer acquired on the MAGNETOM Trio with a 14 cm double resonant loop coil*, a csi_FID sequence, a TR of 600 ms, 8 averages in 4 min 34 s. The spatial resolution is 15.6 cm³ (25 mm x 25 mm x 25 mm).

Figures 4 and 5 are ^{31}P spectra from healthy calf muscle at rest acquired with a double resonant 14 cm loop coil (Advanced Imaging Research, Cleveland, Ohio, USA.). The spectrum in Figure 4 is from a non-localized FID measurement, and the spectrum in Figure 5 is from a localized csi_fid measurement. In these spectra the dominant peak is phosphocreatine (PCr), which serves as a high energy phosphate storage compound.

* Advanced Imaging Research, Inc, Cleveland, Ohio, USA.

¹³C in vivo MRS

Use of higher field strength in human studies opens up new opportunities for observing extremely low sensitive nuclei such as ¹³C, which has a very low natural abundance along with a low gyromagnetic ratio. As illustrated in Figure 6, MRS with naturally abundant ¹³C can be used for evaluating in vivo glycogen storage diseases. The spectrum* was acquired on a MAGNETOM Trio from calf muscle of a two-year-old child with Pompe's disease, which is characterized by an increased glycogen concentration due to a deficiency in the enzyme needed for breaking down excessive glycogen. The ability to detect non-invasively elevated levels of glycogen makes ¹³C MRS an attractive and potential alternative to biopsy.

The low sensitivity of naturally occurring ¹³C made it possible to study metabolic pathways with MRS using ¹³C enriched molecules such as ¹³C-labeled glucose and ¹³C-labeled acetate. Figure 5 illustrates a ¹³C spectrum following administration of ¹³C-labeled glucose. Through metabolic processes, the ¹³C label is transferred to molecules that can be observed and monitored in vivo with MRS such as the ones indicated in Figure 7: glutamines, glutamates, aspartates, GABA and lactate. The information from these spectra is a powerful complement to metabolic information obtained from ¹H MRS spectra.

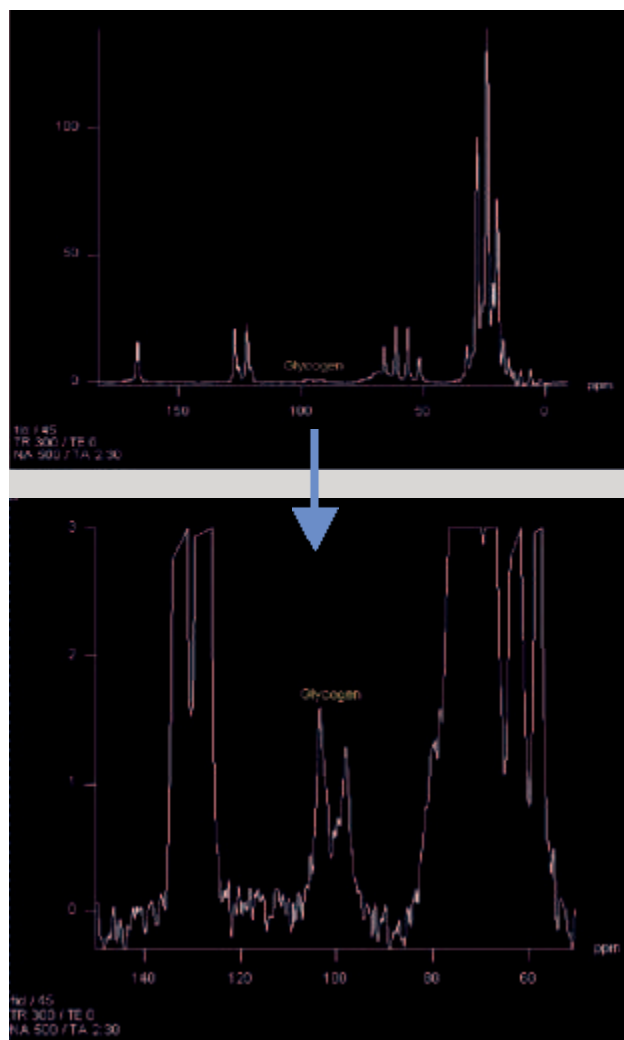


[Figure 6] Natural ¹³C spectrum from calf muscle of a two-year-old child with Pompe's disease. The C1 signal of glucose in glycogen is clearly visible* especially as displayed on the expanded vertical scale in the lower spectrum.

The spectrum was acquired with a FID sequence, TR = 300 ms, 500 averages and 2 min 30 s in ¹³C birdcage coil**.

* Courtesy of H.C. Charles, Duke University, Durham, North Carolina., USA.

** R. Hashoian, Clinical MR Solutions, Brookfield, WI, USA

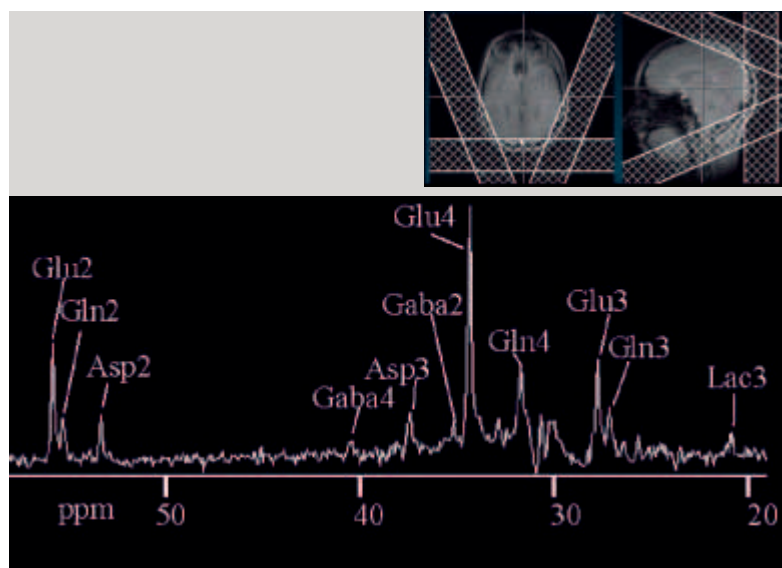


[Figure 7] A ^{13}C spectrum* of the human healthy brain following Euglycemic infusion of 30% ^{13}C -labelled glucose. The spectrum was acquired on the MAGNETOM Trio using a double resonant $^{13}\text{C}/^1\text{H}$ coil**, a FID sequence with WALTZ ^1H decoupling and a measurement time of 30 minutes.

Well separated peaks are seen from Glutamate-2 (Glu2), Glutamate-3 (Glu3), Glutamate-4 (Glu4), Glutamine-2 (Gln2), Glutamine-3 (Gln3), Glutamine-4 (Gln4), Aspartate-2 (Asp2), Aspartate-3 (Asp3), Gaba-2, Gaba-4, Lactate-3 (Lac3).

^{19}F in vivo MRS

The absence of interfering detectable ^{19}F metabolites in living tissue has been successfully exploited in the application of ^{19}F MRS to monitoring the uptake of therapeutic agents such as 5-fluorouracil (5-FU) and its conversion to intermediate metabolites for predicting tumor response to treatment. The spectrum* in Figure 8 is obtained on the MAGNETOM Trio

from a liver tumor after administration of 5-Fu. It shows well separated peaks of fluoro-betaalanine (FBAL) and alpha-fluoro-beta-ureido-propionic acid (FUPA). FBAL is the major and final catabolite of the 5-FU metabolism and FUPA is its precursor in the catabolic pathway. These two peaks are typically not so well resolved on 1.5T spectra.

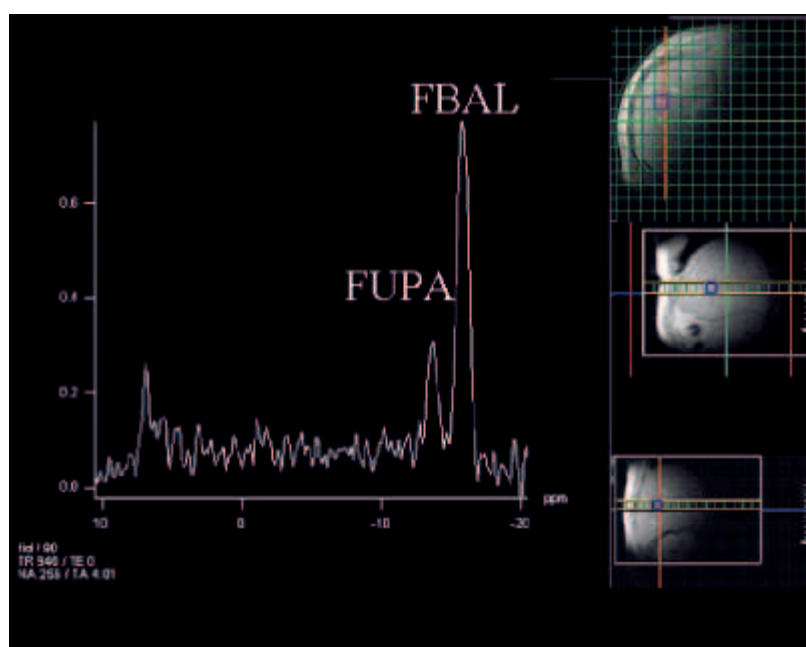


[Figure 8] Monitoring of the metabolism of the chemotherapeutic drug 5-Fluorouracil (5-FU) in human liver tumors. A ^{19}F spectrum acquired on the MAGNETOM Trio using a single tuned ^{19}F coil, a FID sequence, TR = 940 ms, 256 averages and a 4 min 1 s measurement time. The spectrum shows well separated peaks from fluoro-beta-alanine (FBAL) and fluoro-ureido-propionic acid (FUPA).

* Courtesy of D. Klomp, A. Heerschap, University Medical Center Nijmegen, Nijmegen, The Netherlands.

** Coil designed and built by D. Klomp, University Medical Center Nijmegen, Nijmegen, The Netherlands.

University of Utah uses Siemens MAGNETOM Open Architecture for Applications from Carotid Wall Imaging to Image Guided Thermal Therapy

Authors: Dennis L. Parker, Glen Morrell, Robert B. Roemer

Contributors: Eugene Kholmovski, J. Rock Hadley, Eun-Kee Jeong, Seong-Eun Kim, Dhiraj Arora, Andrew Richardson, Jeff Moellmer, Dan Cooley, Junyu Guo.

MRI History at Utah

Faculty and students at the University of Utah have been carrying out MRI research since the installation of the first MRI scanners in about 1984. During the subsequent 20 years, a variety of MRI research programs have been initiated and several have flourished because of the excellent academic and clinical environment.

Magnetic resonance angiography became an early focus of research with the development of multiple overlapping thin

slab acquisition (MOTSA) in about 1989.¹ This time-of-flight (TOF) or inflow enhancement technique has been applied throughout the body, but was found to be of primary utility for intracranial and cervical carotid applications.²⁻⁴

Studies of the cervical carotid artery led to the development of specialized RF coils⁵ for the neck area as well as the development of pulse sequences designed to image the carotid artery wall.⁶⁻⁹

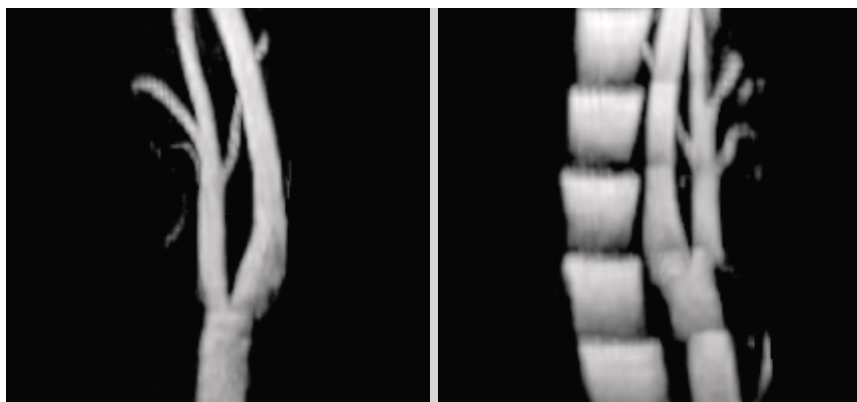


[Figure 1] Maximum intensity projection (MIP) images from MOTSA studies of the cervical carotid artery. With proper setup the divisions of the slabs are not visible (left). With improper setup slab divisions are easily seen (right).



[Figure 2] Left, (top) cervical carotid T1-weighted images obtained using the bilateral carotid coil arrays (2 paddles x 2 elements/paddle) shown above. (bottom) Image obtained with an anterior neck coil using identical pulse sequence

Transition to Siemens

Our experience with Siemens technology began around the beginning of July 2003 with the installation of the Siemens MAGNETOM Trio 3.0T MRI scanner. There was substantial concern on the part of the researchers about how flexible the new technology would be, how rapidly we would be able to transition experiments from 1.5T to 3.0T, how long it would take to adapt to the new coil interface and coils, and what strengths and limitations there would be in pulse sequence development.

Introduction to the new world of Siemens began with a course describing IDEA, the Siemens pulse programming language, which provided nearly all of the faculty and students with a detailed overview of the capabilities of the system, and the methods for pulse sequence development. The layered C++ approach was taught in some detail. The course also provided training in the capabilities of the image reconstruction environment (ICE). Of great importance to our group was the description of the real-time interactive capabilities of the image acquisition environment. The system has been designed to allow communication between the reconstruction process and the data acquisition process. Thus, in principle, it is possible for the pulse sequence to make decisions about acquisition procedure based upon feedback received from data already acquired.

High resolution Intracranial MRA

Arterial MRA: Our migration of research to the Siemens MAGNETOM Trio began with the implementation of our high-resolution intracranial MRA techniques. We began with 0.6 mm isotropic resolution, to match our original work at 1.5T. We saw very quickly that there was substantially more SNR available in the system than we anticipated, and we modified to a higher resolution acquisition at $0.3 \times 0.45 \times 0.6 \text{ mm}^3$ resolution, with zero-filled interpolation to $0.15 \times 0.15 \times 0.3 \text{ mm}^3$ spacing. As shown in Figure 3, the image quality has been spectacular.

Intracranial Venography

The Siemens MAGNETOM Trio has also allowed us to implement very high resolution, high quality venography protocols as shown in Figure 4.

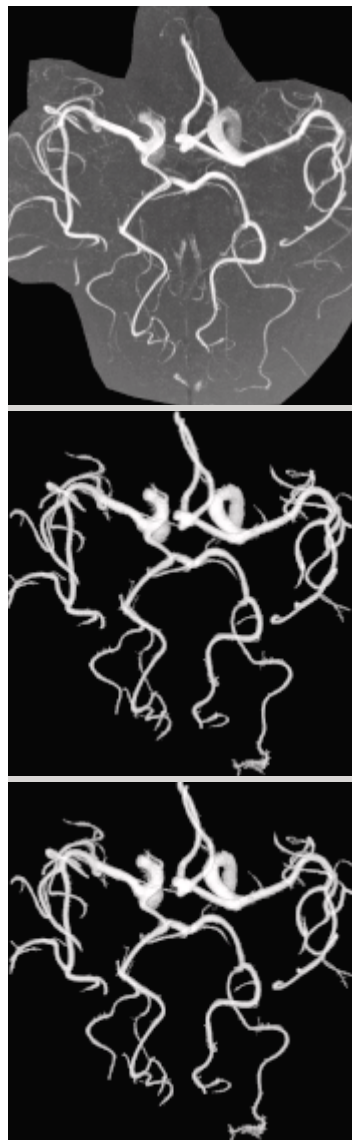


[Figure 3] Example images from 3D high-resolution intracranial study. $TR/TE/flip = 30 \text{ ms}/4.4 \text{ ms}/17^\circ$, $rbw = 100 \text{ Hz/pixel}$, voxel dimensions: $0.3 \times 0.45 \times 0.6 \text{ mm}^3$ acquisition, interpolated to $0.15 \times 0.15 \times 0.3 \text{ mm}^3$ for display. Partial Fourier in all 3 directions, $0.625 \times 7/8 \times 7/8$ (read, phase, slice). Total scan time was 9 minutes 30 seconds. On top is the MIP image of the original 3D image data. Below are cross-eyed stereo pair displays of the ZBS segmentation of the same image data¹⁰. Note the multi-lobular appearance of the ACOM aneurysm.

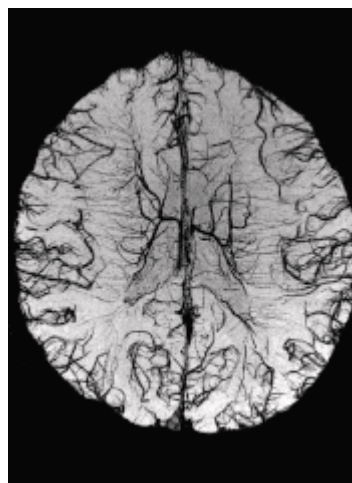


[Figure 4] Venography 3D volume acquired with susceptibility weighting technique and special post processing.

Cervical Carotid MRA

High-resolution intracranial imaging such as that shown in Fig. 3 was performed with product pulse sequences and custom post-processing on the 3.0T system. Imaging of the extra-cranial carotid arteries has required the use of custom pulse sequences and coils, which we had originally designed for 1.5T systems. Use of these techniques required translation of custom pulse sequences to the Siemens environment and redesign of dedicated carotid imaging coils.

Pulse sequences: Our research in high resolution carotid imaging requires the use of Turbo Spin Echo sequences combined with various methods of magnetization preparation.⁸ We found that our customized Turbo Spin Echo sequences designed for use at 1.5T resulted in excessive power deposition (SAR) when used at 3.0T, requiring increases in TR or modification of other fundamental sequence parameters to avoid violation of FDA SAR guidelines. Changes to sequence

parameters needed to reduce SAR resulted in increased scan times or alteration of image timing and T1 and T2 contrast. To overcome this problem, we implemented variable bandwidth pulses with the VERSE technique (Conolly et al, J Magn Reson 1988; 78:440-458) in a multislice Turbo Spin Echo sequence to reduce the SAR of the Turbo Spin Echo refocusing pulse train. Use of the VERSE pulses shown in Figure 5 resulted in reduction of SAR in the refocusing pulse train by 50% without any change in pulse duration, slice profile, flip angle, T1- and T2-weighting, or other imaging parameters. Images obtained using VERSE pulses are subjectively identical to those obtained with the conventional pulses. Use of VERSE pulses has reduced SAR sufficiently to allow the use of imaging protocols developed for 1.5T without modification at 3.0T. Incorporation of VERSE pulses and custom magnetization preparation into the Siemens product multi-slice Turbo

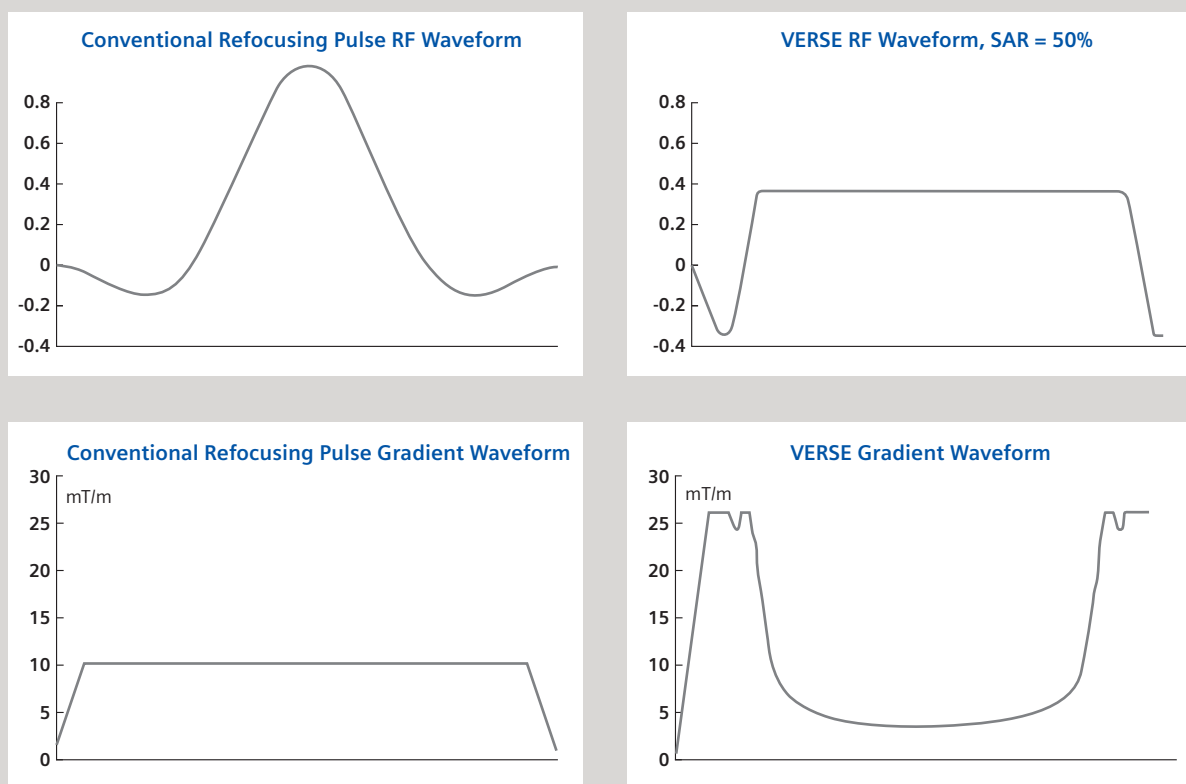


[Figure 5] VERSE pulse design for SAR reduction in turbo spin-echo imaging. Conventional RF and gradient waveforms are shown on the left for a 180-degree refocusing pulse used in the Siemens product Turbo Spin Echo sequence. VERSE equivalent RF and gradient waveforms are shown on the right which have been incorporated into the product sequence to achieve SAR reduction of 50% in the refocusing pulse train without any effect on image contrast, timing, or other sequence parameters.

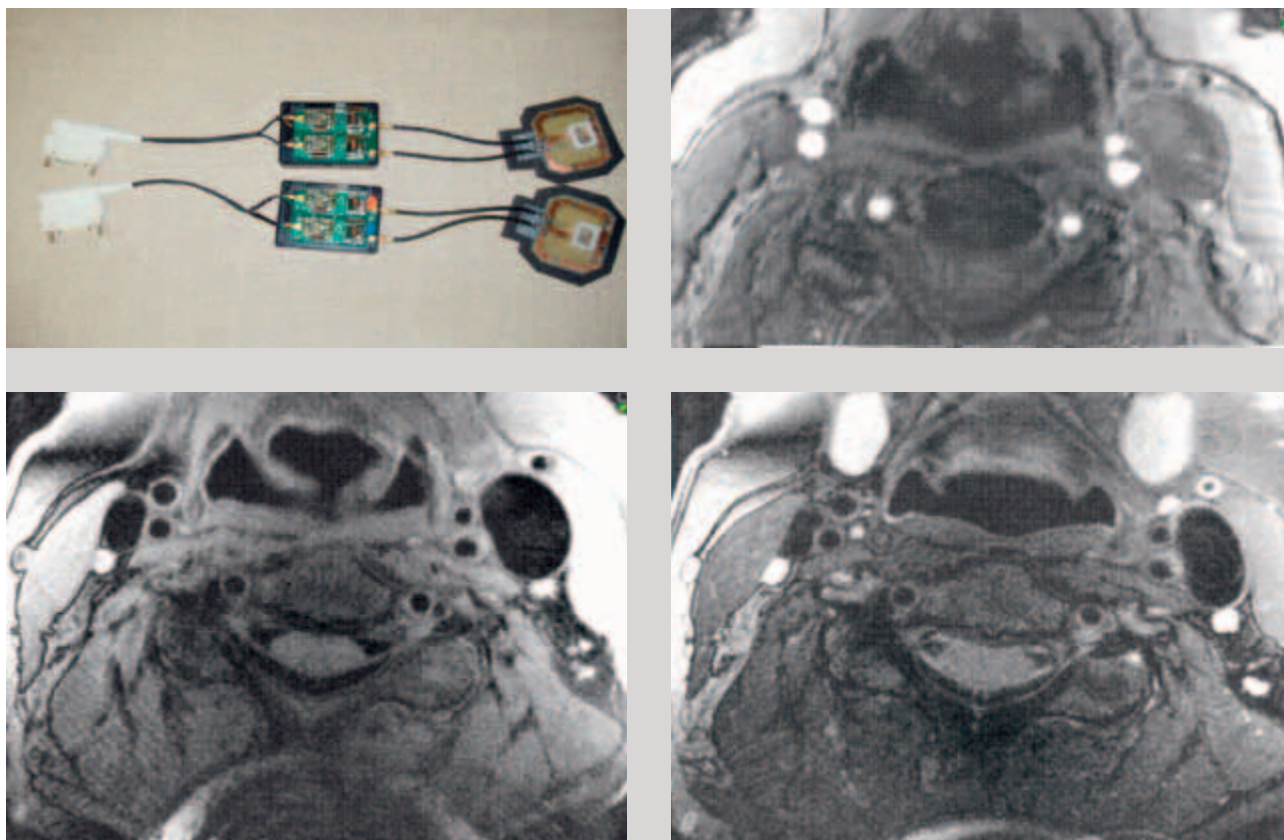


[Figure 6] Bilateral carotid phased array coils (upper left) and example 3T carotid images obtained using TOF, T1- and T2-weighting.

Spin Echo sequence for fast carotid imaging was made possible by open access to Siemens pulse sequence source code provided under our master research agreement and by the use of the IDEA pulse programming environment. The excellent pulse sequence simulator provided with the IDEA environment enables much of the pulse sequence development to occur on a stand-alone desktop PC rather than consuming valuable scanner time for sequence debugging. An active IDEA users' group electronic bulletin board is also a valuable resource in the development of custom pulse sequences for Siemens systems.

RF Coils: Despite our considerable experience designing and building RF coils for 1.5T systems, the implementation of coils at 3.0T has presented some unique challenges. We have found that the Siemens MAGNETOM Trio system pro-

vides great flexibility in the placement of preamplifiers relative to coil elements, allowing easy design of coil geometry. A flexible port design allows coils to be attached at many different possible locations. Siemens connectors and other coil interface hardware have proven to be sturdy and reliable. Coil configuration files aid in ensuring that coils will not inadvertently be used in unintended configurations. We have found Siemens technical assistance to be excellent, and there are several users external to Siemens who have experience building and interfacing coils who have been very helpful to those of us who are still learning. In a short period of time, we have successfully designed and constructed several custom coils for the 3.0T MAGNETOM Trio system which have performed well, including a dedicated two-element carotid imaging coil and head positioning system.

MRI temperature feedback control for high intensity focused ultrasound (HIFU) therapy.

As mentioned earlier, the Siemens software environment allows communication between the reconstruction process, the acquisition process, as well as communication with the outside world. It was this flexibility that enticed us to implement our most complicated research project on the MAGNETOM Trio platform:

Thermal tumor ablation therapy has been widely used in clinical practice with heating methods including percutaneously placed RF probes and high intensity focused ultrasound. Ablation therapy has previously been performed without the ability to accurately monitor tissue temperature throughout the tumor volume and in surrounding normal tissue. As a result, ablation therapy has not been applied with great precision; the extent of tissue ablation often does not encompass the full extent of the tumor, and surrounding normal tissue is often destroyed.

Real time MR temperature mapping during thermal ablation therapy has recently been introduced. This technique promises to revolutionize thermal ablation therapy. For the first time, temperature and thermal dose can be directly imaged during ablation. Power input and location of application can be adjusted during treatment to optimize the extent of tumor destruction while preserving nearby normal tissue.

Groundbreaking work has been done in our lab in conjunction with researchers in the Mechanical Engineering Department over the past several years in the design and construction of a high intensity ultrasound thermal ablation system incorporating MR temperature mapping and automated control.¹¹⁻¹⁵ Our initial work in this project was to verify that stable phase maps could be obtained. Because temperature changes cause small changes in the proton resonant frequency, it is possible to use phase change images to create

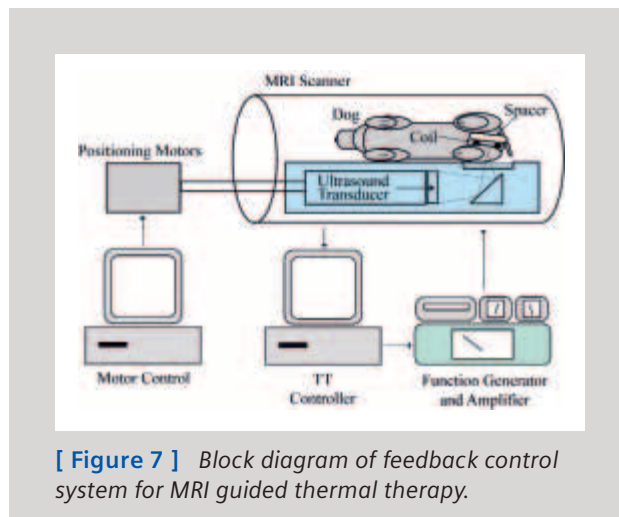


[Figure 7] Block diagram of feedback control system for MRI guided thermal therapy.

temperature change images. We have found it straightforward to implement such temperature change imaging techniques on the Siemens MAGNETOM Trio and have found the measurements to be quite stable and repeatable.

One of the most exciting aspects of fast and accurate MR temperature measurement is its use in real time feedback control systems to shape the applied power deposition fields during treatment in order to reach the desired treatment goals. Such advanced control systems coupled with advanced MR temperature imaging will be an "enabling technology" that will allow the effective use of advanced thermal therapy heating modalities such as large ultrasonic phased arrays where the many degrees of freedom of the applicator must be optimally applied and automatically controlled. Our approach to this problem involves using a sophisticated control system to regulate ultrasound power input and location of the ultrasound beam to insure both treatment efficacy and safety with the shortest possible

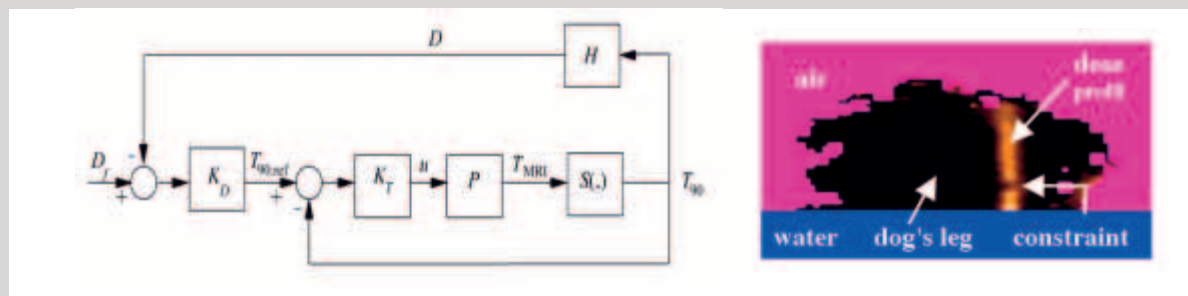


[Figure 8] Left: Thermal dose controller: K_D = Dose controller; K_T = Temperature controller; P = Patient; $S(.)$ = T_{90} selector; H = Dose Estimator; Right: Sagittal image of dose delivered during in vivo heating of dog's leg.

treatment times.^{14,15} The treatment efficacy is ensured as the controller delivers the specified thermal dose to the treatment volume, while safety is ensured as the controller continually monitors temperature at clinician-specified constraint points to ensure that no unsafe thermal dose is delivered to surrounding normal tissue. The controller block diagram for an animal experiment is shown in Figure 7.

The feedback control schematic and the results from an in vivo ultrasound heating procedure inside our Siemens 3T MAGNETOM Trio using our controller and real time temperature images for feedback are shown in Figure 8.

The progression of the treatment in terms of reaching the specified thermal dose in the treatment volume and avoiding thermal dose at the constraint points in adjacent normal tissue are shown in Figure 9. The power control is shown in the top plot. The temperatures in the treated region and the control region are shown in the middle plot, and the thermal dose in equivalent minutes is shown in the lower plot. The figure is a demonstration that MRI guidance can be used to achieve thermal control of dose delivery to specific tumor locations while controlling the maximum temperature experienced in surrounding, normal tissues.

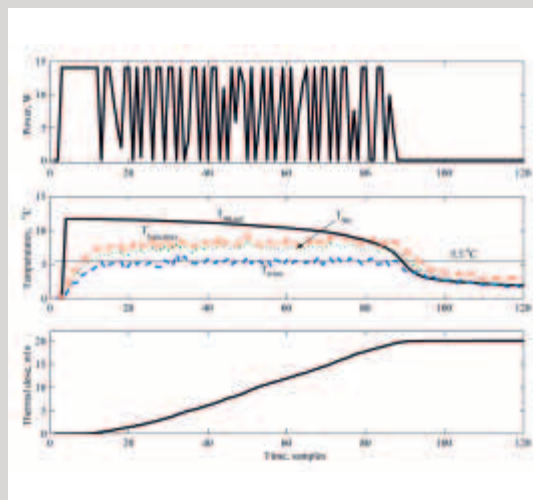


[Figure 9] Thermal dose control in in-vivo canine muscle with $u_{max} = 14W$. The desired dose (described as CEM43° T90) was set to 20 min. The maximum allowable temperature increase in the specified location inside the normal tissue was 5.5°C. The results were obtained with the moving treatment horizon $\Delta t = 4$, prediction horizon $p = 4$, and the control horizon $m = 1$. (a) Control input. (b) Increase in T90, T90; ref, Tcons and Ttum, max. (c) Tumor thermal dose.

Summary

The flexibility and generality of the Siemens development environment has been a pleasant surprise. Not only have we been able to implement most of our research pulse sequences on the MAGNETOM Trio MRI scanner, but we have been able to develop the first of what we hope will be many imaging techniques where dynamic image information is used to control other processes and make decisions in real time during MRI scanning. We are currently investigating real-time phase measurement and control during multi-shot diffusion tensor imaging (DTI) sequences. The flexibility of the system will allow us and others to explore many other interesting and important applications.

References

- [1] Parker DL, Yuan C, Blatter DD. MR angiography by multiple thin slab 3D acquisition. *Magn Reson Med*. Feb. 1991;17(2): 434–451.
- [2] Blatter DD, Bahr AL, Parker DL, et al. Cervical carotid MR angiography with multiple overlapping thin-slab acquisition: comparison with conventional angiography. *AJR Am J Roentgenol*. Dec. 1993; 161(6): 1269–1277.
- [3] Blatter DD, Parker DL, Ahn SS, et al. Cerebral MR angiography with multiple overlapping thin slab acquisition. Part II. Early clinical experience. *Radiology*. May 1992; 183(2): 379–389.
- [4] Blatter DD, Parker DL, Robison RO. Cerebral MR angiography with multiple overlapping thin slab acquisition. Part I. Quantitative analysis of vessel visibility. *Radiology*. Jun 1991; 179(3): 805–811.
- [5] Hadley JR, J.A. Roberts, K.C. Goodrich, H.R. Buswell and Dennis L. Parker. Relative RF Coil Performance in Cervical Carotid Imaging. Paper presented at: ISMRM Tenth Scientific Meeting; 18–24 May, 2002; Honolulu, Hawaii, USA.
- [6] Kim SE, Kholmovski EG, Goodrich KC, et al. Time Efficient Triple Contrast Acquisition in Double Inversion Fast Spin Echo. *Proc. ISMRM 2004*, Kyoto, Japan. 15–21 May 2004 2004: p 698.
- [7] Kim SE, Kholmovski EG, Jeong EK, et al. Triple contrast technique for black blood imaging with double inversion preparation. *Magn Reson Med*. Dec. 2004; 52(6): 1379–1387.
- [8] Kim S-E, Jeong E-K, Hadley JR, et al. Implementation of Time Efficient Double Inversion FSE technique on a 3.0T system. *ISMRM 2005*, Miami, Florida. 7–13 May 2005 2005.
- [9] Parker DL, Goodrich KC, Masiker M, et al. Improved efficiency in double-inversion fast spin-echo imaging. *Magn Reson Med*. May 2002; 47(5): 1017–1021.
- [10] Parker DL, Chapman BE, Roberts JA, et al. Enhanced image detail using continuity in the MIP Z-buffer: applications to magnetic resonance angiography. *J Magn Reson Imaging*. Apr 2000;11(4):378–388.
- [11] Arora D, Cooley D, Perry T, et al. Direct thermal dose control of constrained focused ultrasound treatments: phantom and in vivo evaluation. *Phys Med Biol*. Apr. 21 2005; 50(8): 1919–1935.
- [12] Arora D, Skliar M, Roemer RB. Model-predictive control of hyperthermia treatments. *IEEE Trans Biomed Eng*. Jul. 2002; 49(7): 629–639.
- [13] Arora D, Skliar M, Roemer RB. Minimum-time thermal dose control of thermal therapies. *IEEE Trans Biomed Eng*. Feb. 2005;52(2): 191–200.
- [14] Arora D, Cooley D, Perry T, et al. In-Vivo Evaluation of a MR Thermometry Based Thermal Dose Controller for Focused Ultrasound Treatment. *Magn. Reson. Med*. 2005; In Press.
- [15] Arora D, Perry T, Cooley D, et al., eds. Constrained model-predictive thermal dose control for MRI-guided ultrasound thermal treatments. Bellingham, WA, 2005: SPIE, Bellingham, WA, 2005; 2005. Thomas P. Ryan, ed. *Proceedings of SPIE*; No. 5698.

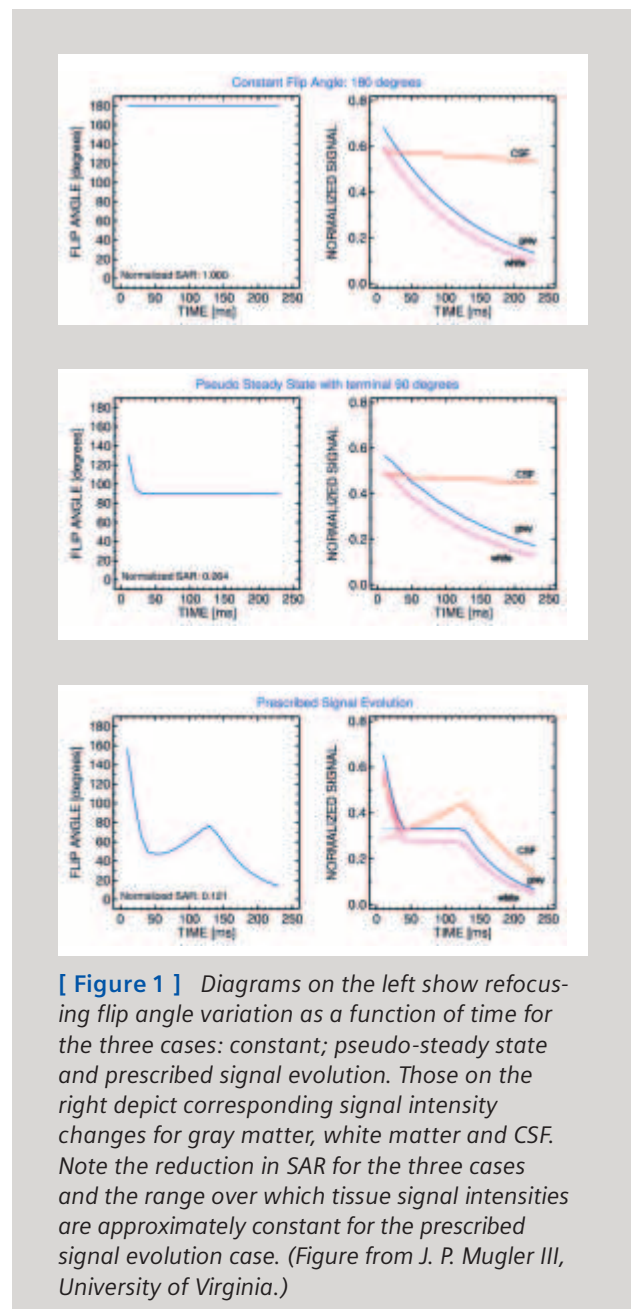
SPACE: An Innovative Solution to Rapid, Low SAR, T2-Weighted Contrast in 3D Spin Echo Imaging

Katherine T. Scott, Ph.D. & Stuart H. Schmeets, BSRT (MR), Siemens Medical Solutions, USA

The contrast properties and inherent insensitivity of spin echo based sequences to RF and magnetic field inhomogeneities make them a particularly desirable addition to a clinical high field protocol, where susceptibility effects can be quite pronounced. Fast imaging methods, such as Turbo Spin Echo (TSE), use a train of refocusing pulses (the Turbo factor or Echo Train Length (ETL)) to enable multiple phase encoding steps to be carried out after each excitation pulse. The increased RF power deposition can, however, severely limit the coverage possible in multi-slice applications at high field, since power deposition or Specific Absorption Rate (SAR) increases as the square of field strength as well as the square of the flip angle. Additionally, increased saturation and magnetization transfer effects reduce contrast and signal-to-noise ratios (CNR and SNR). High resolution 3D acquisitions enable precise characterization and localization of anatomy and pathology, but acquisition times are prohibitively long and T2-weighted sequences are usually only a viable option in 2D mode. Acquisition speed increases are limited by the length of the echo train (T2 decay restraints) and very long echo trains are generally not possible due to loss of contrast and blurring. To enable high field and 3D imaging with these sequences at 3T and above, appropriate measures to address these issues need to be implemented.

Method

Reduced flip angle refocusing approaches¹ lengthen the usable echo train length, since the complex combination of spin and stimulated echoes introduces a T1 dependence to the signal evolution. Significantly reduced SAR at comparable SNR can be obtained by replacing a constant low flip angle refocusing train by a variable flip angle pulse train designed to produce a constant echo amplitude^{2,3} – see Fig. 1. Starting the pulse train with higher amplitude pulses and slowly decreasing to approach a constant (“asymptotic”) value, enables acquisition of images with SNR values close to those acquired with 180 degree refocusing pulses, for asymptotic flip angles as low as 60 degrees³. This “pseudo steady state” of signal intensities decays slowly due to T1 and



T2 effects. It is possible to obtain both an increase in signal intensity and an almost constant signal from the tissue of interest (e.g. gray matter) for the bulk of the signal acquisition, by using prescribed signal evolutions which include relaxation effects in the calculation of refocusing flip angles⁴. Flip angles need to be optimized for only one tissue of interest (e.g. gray matter in the brain) as the prescribed signal evolutions depend only weakly on the T1 and T2 relaxation times and are therefore similar for many other tissues. Using an initial exponential decay, a constant and then another exponential decay for the prescribed signal evolution pro-

duces images in which the contrast is similar to those obtained using conventional T2-weighted Spin Echo sequences. This approach allows very long echo trains and 3D imaging, since the effective T2 of the echo train is longer than the tissue T2 for tissues with long T1s ($\geq 10 T_2$) and acquisition times can be commensurately reduced or resolution increased. "T2-weighted" 3D TSE whole brain images with SAR values well below FDA limits have been acquired at both 1.5 and 3T^{4,5} and with echo train lengths of up to 250 echoes, enabling 3D datasets of the whole brain to be acquired in 3.5 minutes⁶.

Applications

This prescribed signal evolution approach has been adapted and implemented in the software of all current Siemens 1.5T and 3T systems as the SPACE sequence and provides high quality 3D Turbo Spin Echo images in which the contrast is similar to those of conventional T2-weighted Spin Echo sequences for head and knee applications. Some examples are shown here:

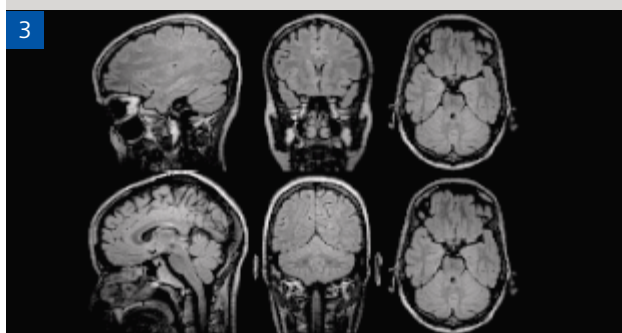
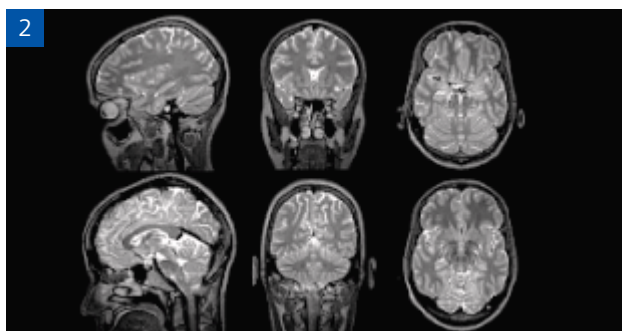


[Figure 2] T2-weighted sagittal, coronal and axial brain images reconstructed from a 4.4 min. single-slab 3D-TSE acquisition with isotropic 0.9 mm spatial resolution.

[Figure 3] FLAIR sagittal, coronal and axial brain images reconstructed from a 7.1 min. single-slab 3D-TSE acquisition with isotropic 0.9 mm spatial resolution.

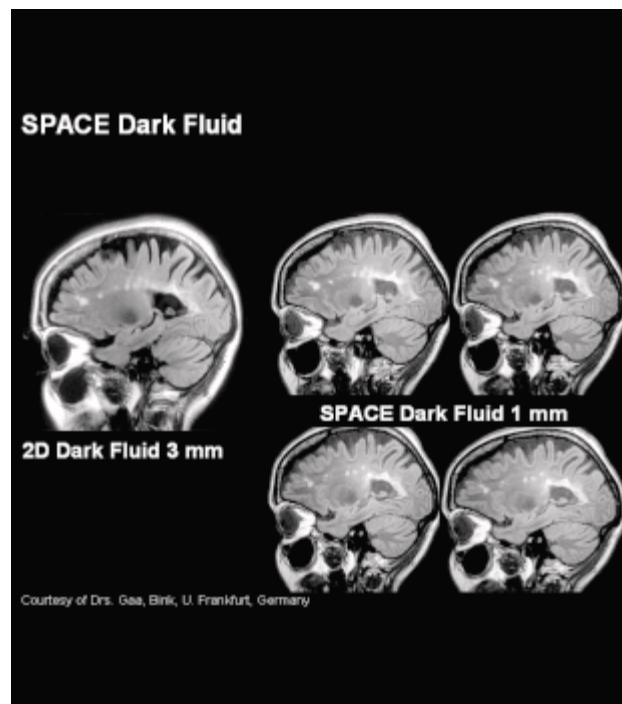
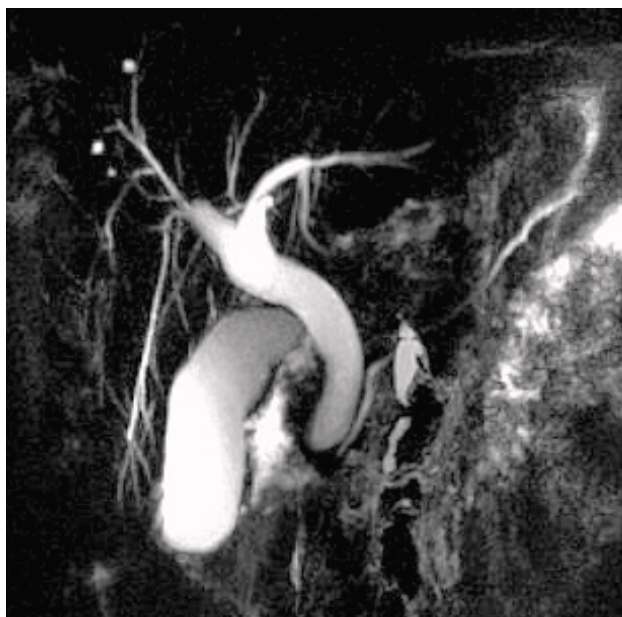


[Figure 4] Thinner partitions and the flexibility to reformat in any orientation enables better definition of multiple sclerosis lesions in images obtained using the SPACE sequence than in those acquired with the corresponding 2D TSE sequence. One 3 mm slice from a 2D Dark Fluid contrast acquisition is shown on the left, while the same anatomy is covered with four 1 mm partitions from the SPACE 3D acquisition on the right.

More recently, spatially (slice) selective single slab 3D TSE imaging has been developed and demonstrated⁷, extending the range of clinical applications to examinations previously precluded due to aliasing concerns. Prescribed signal evolutions of over 1,000 echoes per excitation have been shown to be possible and by making use of long echo trains to acquire multiple k-space planes after each excitation – rather than the usual single plane – further increases in acquisition speed have been achieved⁸. Combining this approach with

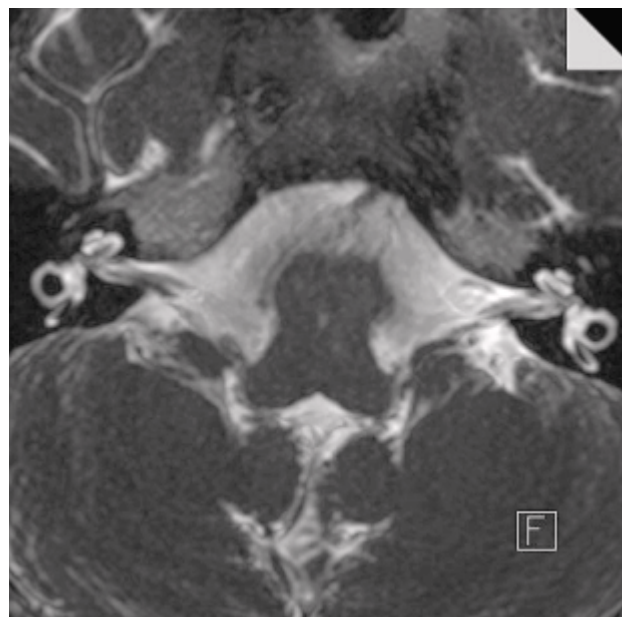
parallel imaging techniques (iPAT), has enabled the acquisition of whole-brain 3D TSE data sets with isotropic 0.9 mm spatial resolution at 3T in 4.5 minutes (T2 contrast) and 7 minutes (Dark Fluid) respectively, with reduced susceptibility and chemical shift artefacts⁹.

The latest Siemens version of the SPACE sequence incorporates all of these advances and now includes protocols with a range of contrasts for head, inner ear, spine, MRCP (Magnetic Resonance Cholangio-Pancreatography) and pelvic examinations.



Axial reformat for pancreatic duct evaluation

[Figure 5] Previous MRCP techniques required rapid single shot slabs or breath hold acquisitions that were limited in spatial resolution and anatomic detail. The SPACE MRCP technique incorporates PACE free breathing techniques for a 3D volumetric evaluation of the entire cholangio-pancreatic ductal system in a heavily T2-weighted acquisition. The volumetric data can also be loaded into 3D evaluation software for partitioning in additional orientations.



Sagittal Reformat



Coronal Reformat

[Figure 6] Isotropic (0.4 mm) 3D acquisitions of the inner ear clearly delineate the nerve pathways in some cases reducing or eliminating the need for IV contrasts. MAGNETOM Trio, A Tim System images below.

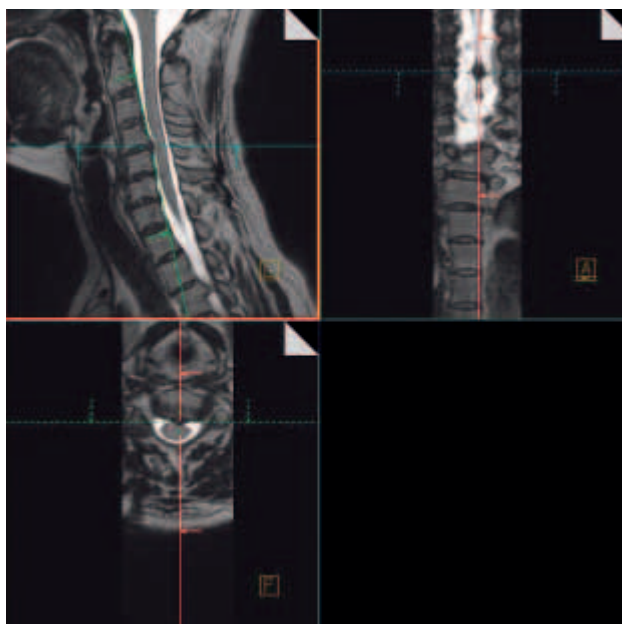


[Figure 7] Multi-planar reconstructions (MPR) of isotropic 3D acquisitions of the spine provide an interactive approach to evaluating pathology in multiple orientations and angles without the need for additional acquisitions. This isotropic (0.9 mm) sagittal acquisition demonstrates a bulging disc at the level of C4-C5 evaluated axially and coronally without additional measurements.



[Figure 8] SPACE acquisitions of the spine in conjunction with the large field of view capable on the MAGNETOM Trio provide a more complete evaluation of spinal anatomy than ever before. The example below demonstrates an 0.9 mm 3D isotropic evaluation of the spine from the mid-brain to L5 without patient repositioning.

Summary

The SPACE sequence enables acquisition of high resolution 3D datasets with contrasts similar to those obtained from 2D T2-weighted and dark fluid protocols at 1.5T and 3T within a clinically acceptable timeframe and without SAR limitations. This allows the data to be viewed in multiple orientations and retrospectively reformatted to better view features of interest, as well as to generate views that correspond to slices acquired with other sequences, if desired. Current developments focus on applications requiring reduced fields of view in one or more dimensions such as the spine and internal auditory canal. Applying iPAT and the large field of view functionality provided by the Tim technology enables 3D data sets of the complete CNS to be acquired in as little as 10 minutes without patient repositioning.

References

- [1] Henning J., Multiecho imaging sequences with low refocusing flip angles, J. Magn. Reson., 1988; 78: 397–407.
- [2] Le Roux P, Hinks RS. Stabilization of echo amplitudes in FSE sequences. Magn Reson Med. 1993; 30: 183–90
- [3] Alsop DC. The Sensitivity of Low Flip Angle RARE imaging. Magn Reson Med.1997; 37:176–84.
- [4] Mugler JP, Kiefer B, Brookeman JR. Proc ISMRM 8 (2000); 687.
- [5] Mugler JP, Wald LL, Brookeman JR. Proc ISMRM 9 (2001); 438.
- [6] Mugler JP, Brookeman JR. Proc ISMRM 11 (2003); 970.
- [7] Mugler JP, Brookeman JR. Proc ISMRM 12 (2004); 695.
- [8] Mugler JP, Brookeman JR. Proc ISMRM 12 (2004); 2106.
- [9] Mugler JP, Menzel MI, Horger W, Krueger G, Kiefer B. Proc ISMRM 13 (2005); 1238.

Acknowledgements

Thanks to Marion I. Menzel, Ph.D. for many helpful discussions.

Tim at 3T: Highlights

Arne Reykowski, Ph.D.

Siemens AG, Medical Solutions, Magnetic Resonance Division, Coil Development, Erlangen, Germany

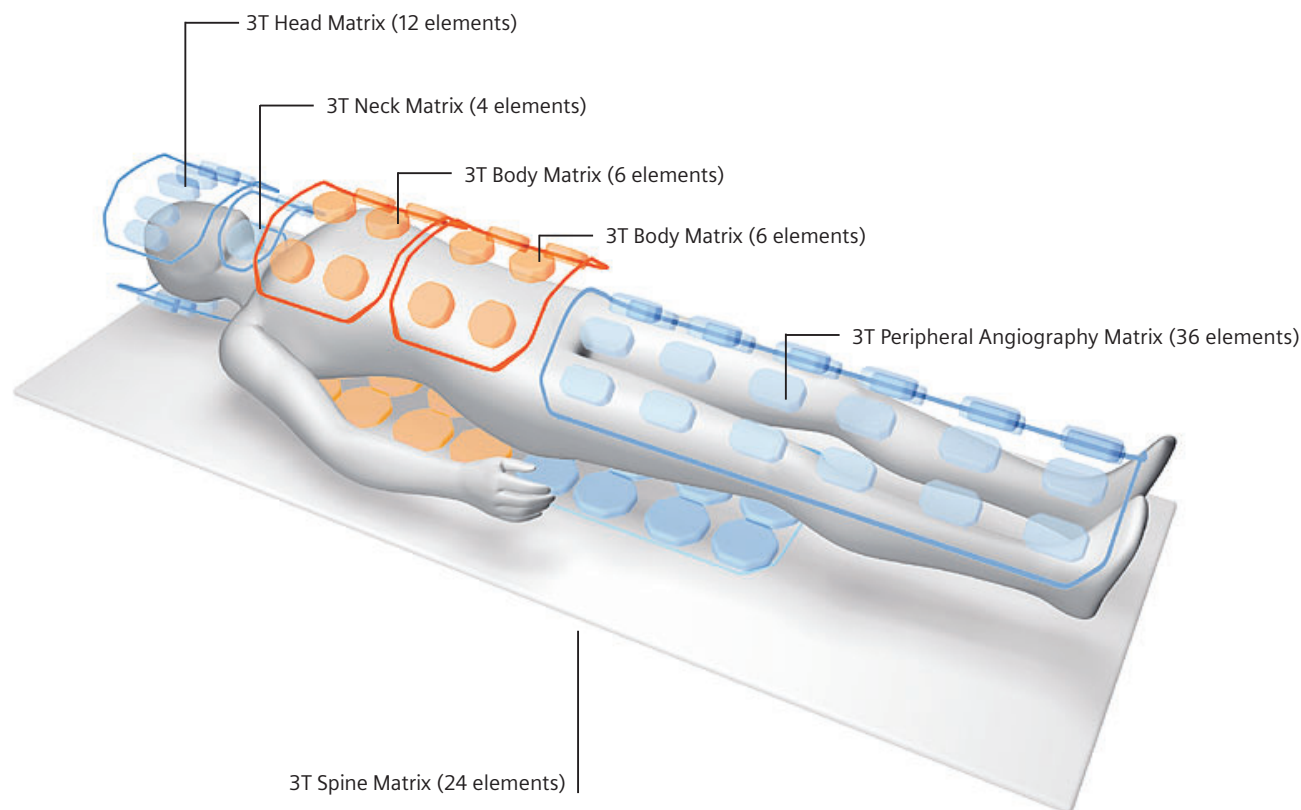


[Figure 1] Matrix coils for MAGNETOM Trio, A Tim System.

1. Total of 102 Coil Elements

The new MAGNETOM Trio, A Tim System comes in three versions: 102x8, 102x18 and 102x32 (Fig. 2). This means that a total number of 102 seamlessly integrated coil elements can be connected to a system with 8, 18 or 32 RF channels at the same time. In comparison, the MAGNETOM Avanto permitted a maximum of 76 coil elements to be used during a single exam without patient repositioning. The main reason for this increase of 26 coil elements (from 76 to 102) is a completely new designed 3T PA Matrix with integrated coil channel switch.

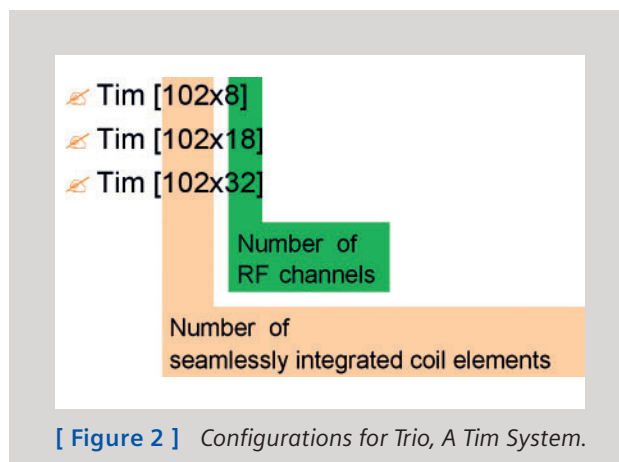
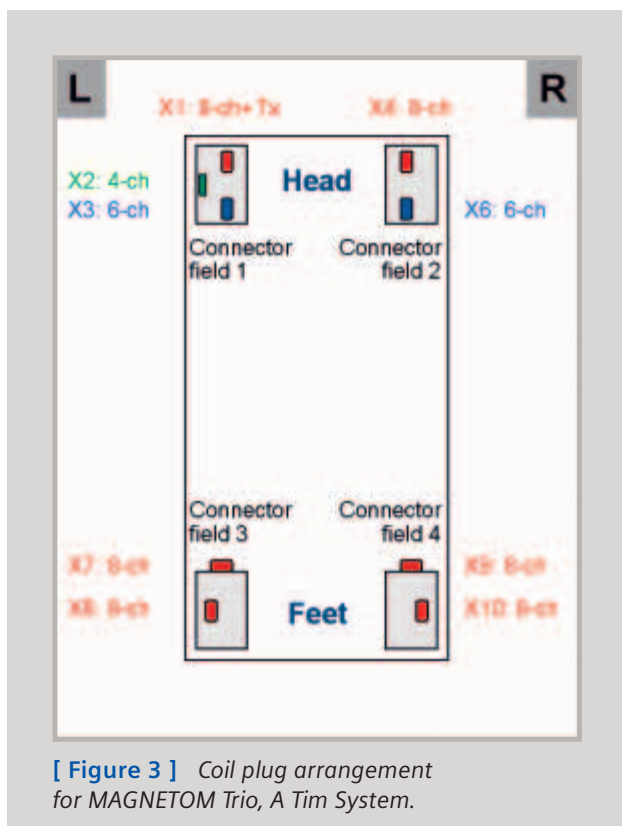


[Figure 2] Configurations for Trio, A Tim System.



2. Coil Plug Arrangement

The MAGNETOM Trio, A Tim system has a slightly different coil plug arrangement than the MAGNETOM Avanto (Fig. 3). Both Avanto and Trio Tim systems have the identical number of 64 RF channel connectors. 12 additional coil elements are made available to the system via an internal RF channel switching matrix inside the Spine Matrix. Another 26 coil elements are made available with a second RF channel switching matrix inside the completely new designed 3T PA Matrix. Adding all these channels leads to the total number of $64 + 12 + 26 = 102$ coil elements.

3. New Head Matrix Design

The 3T Head Matrix is a completely new design that addresses the demand for highest PAT factors with left/right and anterior/posterior phase-encoding (PE) direction (Fig. 4).

All 12 coil elements of the Head Matrix are arranged in a single ring around the Head. The elements are grouped in 4 clusters with 3 elements each. Depending on the Matrix Mode chosen (CP, Dual, or Triple), each cluster behaves like a single channel CP coil, a dual channel CP array, or a triple channel array respectively.

In the same manner, the entire Head Matrix behaves like a 4, 8 or 12 channel array, as a function of the Matrix Mode (Fig. 5).

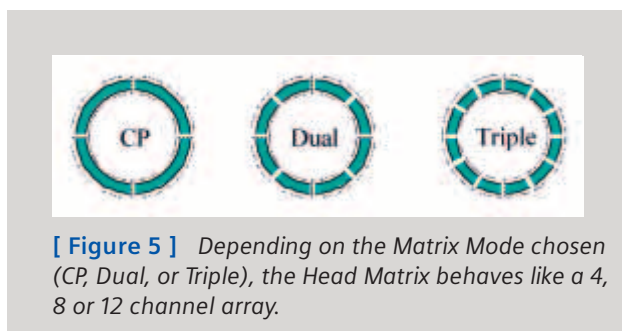


[Figure 4] The new 3T Head Matrix design.

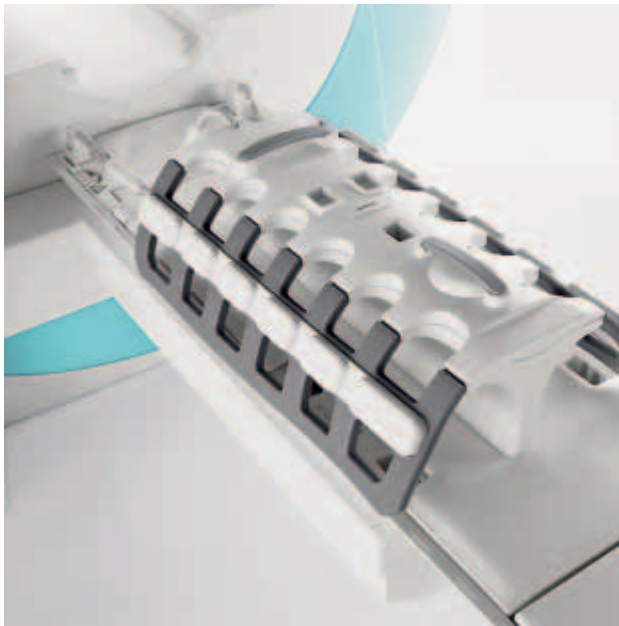


[Figure 6] The new 3T PA Matrix.

4. New PA Matrix Design (to be released February 2006)

The new 3T PA Matrix has a total of 36 coil elements. The elements are organized in 6 levels along the patient axis (z-direction). Each level consists of two clusters, one for each leg. Each cluster consists of 3 coil elements (Fig. 7a).

A total of 24 PA Matrix coil elements, or a total of 4 levels in z, are sufficient to cover a FoV of 50 cm (Fig. 7b).

An additional 3T Body Matrix can be connected to the PA Matrix by using a plug that is integrated into the housing of the PA Matrix (Fig. 8a).

The combination of PA Matrix and Body Matrix creates a combined Matrix coil with 8 levels in z direction and a total of 42 coil elements (Fig. 8b). The combined array is connected to the MRI system via two 8 channel plugs. A channel switch which resides inside the PA Matrix can select 4 out of these 8 levels from the combined array.

The Spine Matrix can be used together with the PA Matrix in feet-first applications, creating a combined Matrix coil with 9 coil elements for each level (Fig. 9).

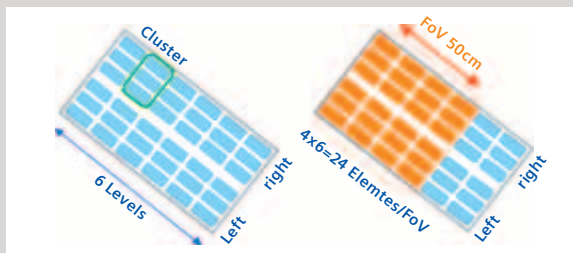


[Figure 7]

- a) The PA Matrix consists of 36 elements, organized in 6 levels with 2 clusters per level.
- b) A total of 24 PA Matrix coil elements, or a total of 4 levels in z, are sufficient to cover a FoV of 50 cm.

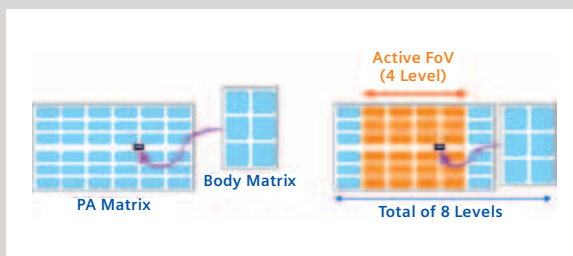


[Figure 8]

- a) An additional 3T Body Matrix can be connected to the PA Matrix.
- b) The combination of PA Matrix and Body Matrix results in an array with 8 levels in z direction.

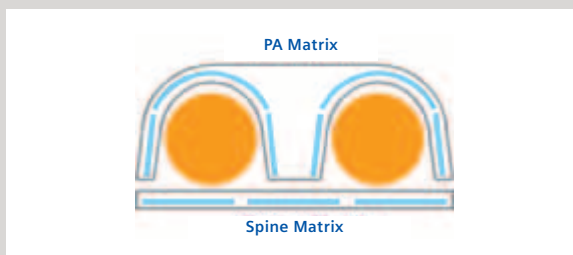


[Figure 9]

Combination of Spine Matrix and PA Matrix leads to a high density array with 9 coil elements per level.

Sometimes it's difficult to see the details.



Especially when it comes to MRIs.

MAGNETOM Trio with Tim

reveals exceptional details – so you can differentiate between what might be hazardous from what is benign. This system provides visualization of microscopic data that can help accelerate early diagnosis and treatment. With everyday ease and reliability. All in one powerful 3T system.

SIEMENS
medical

Initial Results from MAGNETOM Trio, A Tim System in Asia Pacific Hong Kong Sanatorium and Hospital

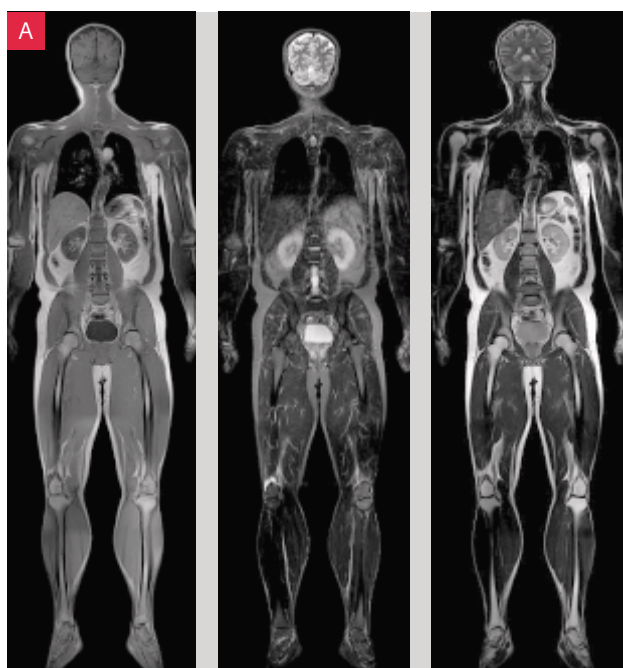
Wyncent Wong, MRI Applications Specialist, MSc, BAppSc, DCR (R), Dip

Siemens Medical Solutions, Asia Pacific Headquarters, Singapore

Hong Kong Sanatorium and Hospital Ltd (HKSH) is no stranger to the MAGNETOM 3T MRI community. The Department of Diagnostic Radiology believes that early detection allows prompt treatment and cures. It therefore continually strives to stay at the forefront of medical imaging technologies in order to provide patients with a fast, accurate and reliable diagnosis. In line with this philosophy, and in recognition by Siemens of its excellent work in, and commitment to, 3T MRI, HKSH once again leads the world by upgrading its existing Trio system with Total imaging matrix (Tim) technology, Tim [102x32]. This configuration enables the connection of up to 102 coil elements simultaneously and the reading of the signal by up to 32 independent RF receiver channels. This is truly the state-of-the-art top-range MRI scanner, offering the highest density of coil elements and highest number of truly independent RF channels in the entire MR market.

Thanks to Tim's revolutionary technology, certain processes have become a thing of the past. The radiographer no longer needs to consider coil changing but may instead simply select the required exam: the automatic table movement control means that most parts of the body can be scanned easily. This not only makes the exam more tolerable to the patient but also improves workflow and increases productivity. According to Dr. Gladys Lo, Honorary Consultant and Radiologist-in-charge, "The main motivation for the upgrade to Tim technology is due to the increase in requests for metastatic work-up in patients with known malignancy and an increased demand for whole body screening amongst the population at large.

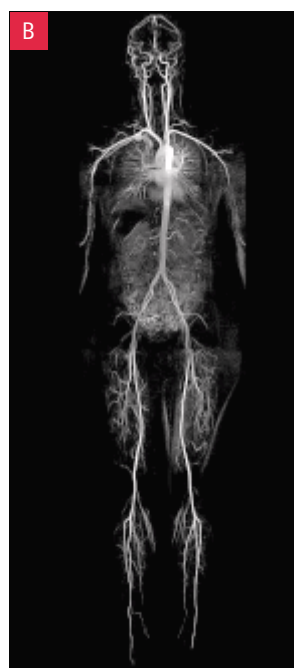
For example, at present the department offers MRI brain and MRI whole body bone scans to complement PET-CT examinations. With the integrated Trio and Tim technology, MRI



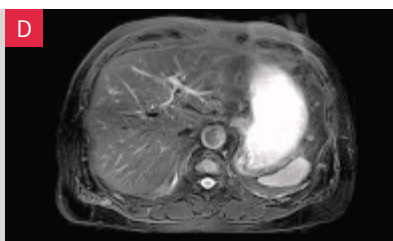
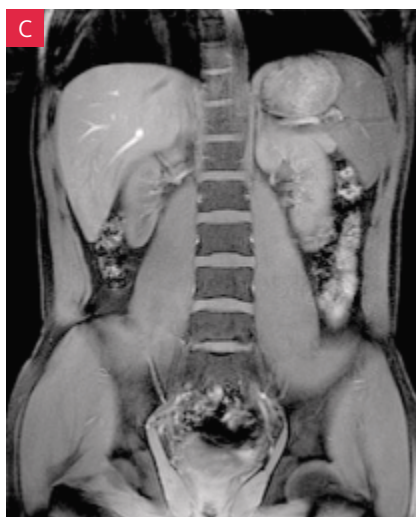
T1 f12d Coronal

T1 TIRM Coronal

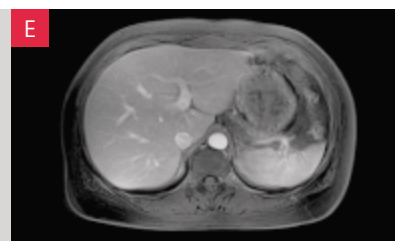
T2 TSE Coronal



[B] Whole body MRA in 48 s with iPAT x 3. With faster gradients, improved signal to noise and iPAT, contrast enhanced MRA is now routinely performed at 512 resolution at a mere 12 seconds scan time using iPAT factor 3. Whole body MRA with such high resolution was not possible before this. Contrast dosage required for the example above is just 30 cc.

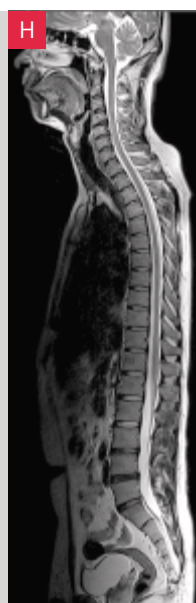
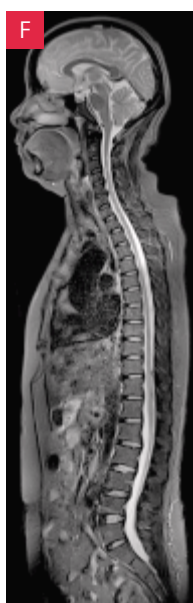


[D] TSE T2 fat sat free breathing, iPAT x 2, 320 resolution.



[E] T1 VIBE fat sat, iPAT x 2, 320 resolution.

[C] FI2d fat suppressed coronal at 450 mm field of view and no distortion correction showed excellent fat suppression over large area.

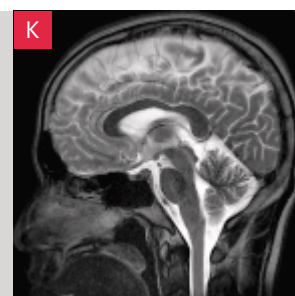


The spine matrix consists of 24 elements and enables iPAT up to factor of 3 in the left-right direction. For sagittal imaging of the spine, it is possible to iPAT in GRAPPA mode to speed up the acquisition time.

[F] T1 TIRM of the entire CNS in 2 steps (480 mm FoV, iPAT x 2) in 2:40 mins.

[G] T1 TSE of the whole spine in 3 steps (400 mm FoV) in 2:41 mins

[H] T2 TSE of the whole spine in 3 steps (400 mm FoV) in 2:42 mins



[I + K] TSE T2 sagittal 1024 x 1024 resolution with iPAT x 2 at 2:03 mins

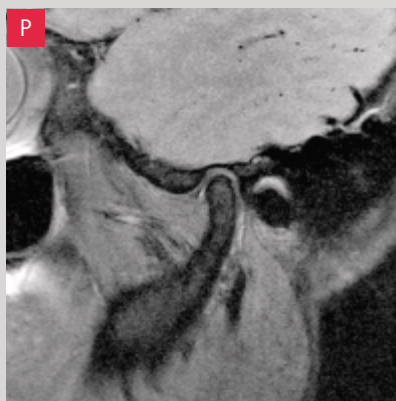
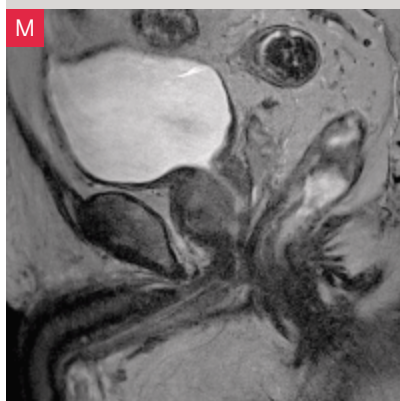
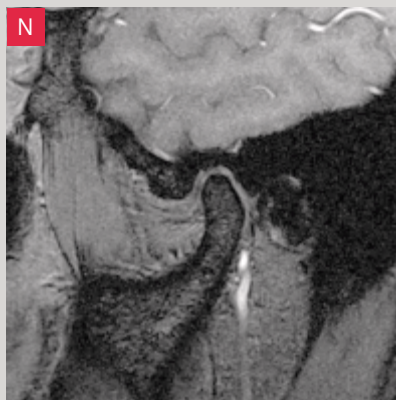


[J] Extreme detail showing the semi circular canal, magnified straight from the sagittal TSE T2, 1024 x 1024 resolution

brain and MRI whole body scans can be combined, saving the patients time and money. The ability to scan the entire body efficiently, with great accuracy and without ionizing radiation opens up innumerable clinical applications. This MRI system is now a 'CT scanner without radiation'. One can imagine it will be a very useful tool for whole body check-up

for which, at present, we are utilizing ultrasound. The inherent superior soft tissue contrast of MRI will make it a natural tool to use for screening the pancreas, uterus, ovaries and the prostate. Prior to the upgrade, the performance of a whole body scan was especially difficult due to the limitation in coverage and the need to change coils for different body

Tim matrix coils offer up to 100% or more signal than conventional CP coils due to the higher number of coil elements and its geometrically optimized design. Examples below shows imaging of the prostate and temporomandibular joint (TMJ), where local dedicated coils are not mandatory anymore.



[L] T2 TSE transverse of the prostate, 20 slices, 3 mm, FoV 160 x 160 mm, 256 x 320, TA: 3:25mins.

[M] T2 TSE sagittal of the prostate, 20 slices, 3 mm, FoV 160 x 160 mm, 357 x 384 resolution, TA: 4:10 mins

14 slices TMJ at 2 mm slice thickness, field of view 100 x 100 mm²

[N] FI2D T1 sag oblique; **[O]** FI2D T1 cor oblique;

[P] TSE pd fat suppression sag oblique; **[Q]** TSE T2 sag oblique

regions. This made the whole process time consuming and the resultant image quality was also less than ideal. With the Tim upgrade, we see a significant improvement, not just in image quality, but also signal-to-noise, shorter set up and scan time. This definitely makes it more effective and efficient in terms of workflow, whilst the clarity and detail obtained from the high-resolution scan enables us to make accurate diagnosis with greater confidence."

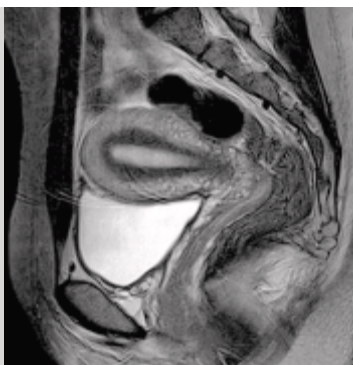
What used to be 'local' imaging is now 'total' imaging, because field of view per scan is now 500 mm: this can be easily expanded to 1810 mm to enable visualization of the entire body from head to foot, thus providing a complete picture. The field of view per scan of 500 mm is currently the largest field of view possible on any 3T systems in the market.

All Tim matrix coils allow application of iPAT (integrated Parallel Acquisition Technique) in all directions throughout the entire field of view of 1810 mm. Currently, the maximum allowable iPAT factor is 16. iPAT plays a very important role in 3T imaging as it helps to reduce distortion in EPI sequences, susceptibility effects, SAR (Specific Absorption Rate) and scan times. Tim matrix coils are so well designed that they can be seamlessly connected to form a larger coil for bigger coverage. Best of all, these coils are extremely light (the body matrix coil weighs a mere 950 g).

This upgrade now equips the system with a TQ-Engine gradient with the strength of 45mT/m (true value per axis) and slew rate of 200 T/m/s. Despite the increase in the gradient power, one would expect a corresponding increase in acoustic noise.

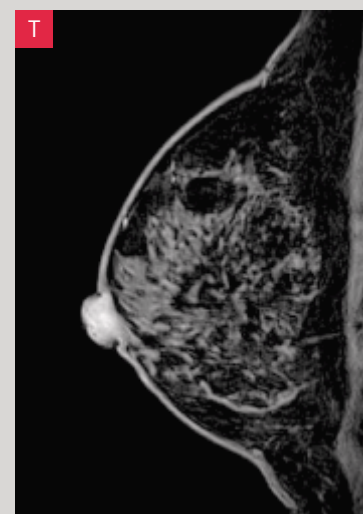
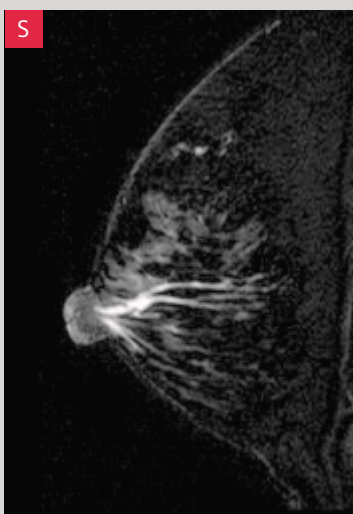
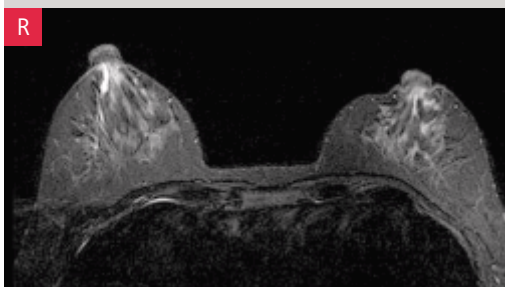
Women's Health

Tim matrix coils provide superb image quality of the uterus due to the superior signal to noise. MRI plays a very important role in the diagnosis of benign uterine pathology due to its excellent soft tissue contrast, multi planar imaging capabilities and most important of all, no ionizing radiation. The possibility of imaging at very high spatial resolution enables clear visualization of the endometrium and retro-vaginal septum without the use of local (vaginal or rectal) coils makes MR the modality of choice.



598 x 1024 resolution

- [R] T1 TIRM tra, 32 slices, 336 x 448 resolution iPATx2 at 4:12 mins
- [S] T2 TSE fat suppressed sag, 23 slices, 240 x 320 resolution at 2:44 mins
- [T] fl3d sag both breasts, iPATx2 (post contrast), 291 x 320 resolution at 3:34 mins



However, the new MAGNETOM Trio, A Tim System features audio comfort which reduces acoustic noise by up to 90%. Assistant Senior Radiographer and MRI chief technician, Mr. Raymond Lee commented that he was very impressed with the reduction of acoustic noise even for the most demanding applications, such as EPI and BOLD imaging. "It was so quiet that sometimes I wasn't even sure if the scan was running!" This has a huge impact on pediatric imaging especially when sedation is given. Acoustic noise is typically a problem on ultra high field imaging as the noise level increases with field and gradient strengths.

The results from the MAGNETOM Trio, A Tim System using Tim matrix coils showed major improvements in image quality compared to the previous version that used coils supplied by third parties. The most significant change in image quality is in spine and abdominal imaging.

Faster gradients, improved signal to noise and iPAT mean that contrast-enhanced MRA is now routinely performed at

512 resolution at a mere 12-second scan time using iPAT factor 3. Such high-resolution whole body MRA has only now become possible.



Hong Kong,
Sanatorium and
Hospital Ltd,
Hong Kong.

The information in this document contains general descriptions of the technical options available, which do not always have to be present in individual cases.

The required features should therefore be specified in each individual case at the time of closing the contract.

Siemens reserves the right to modify the design and specifications contained herein without prior notice. Please contact your local Siemens sales representative for the most current information.

Original images always lose a certain amount of detail when reproduced.

This brochure refers to both standard and optional features. Availability and packaging of options varies by country and is subject to change without notice. Some of the features described are not available for commercial distribution in the US.

Siemens AG
Wittelsbacherplatz 2
D-80333 Muenchen
Germany

Headquarters

Siemens AG, Medical Solutions
Henkestr. 127, D-91052 Erlangen
Germany
Telephone: +49 9131 84-0
www.siemens.com/medical

Contact Addresses

In the USA

Siemens Medical Solutions USA, Inc.
51 Valley Stream Parkway
Malvern, PA 19355
Telephone: +1 888-826-9702
Telephone: +1 610-448-4500
Telefax: +1 610-448-2254

In Japan

Siemens-Asahi
Medical Technologies Ltd.
Takanawa Park Tower 14F
20-14, Higashi-Gotanda 3-chome
Shinagawa-ku
Tokyo 141-8644
Telephone: +81 3 5423 8411

In Asia

Siemens Medical Solutions
Asia Pacific Headquarters
The Siemens Center
60 MacPherson Road
Singapore 348615
Telephone: +65 6490-6000
Telefax: +65 6490-6001

In Germany

Siemens AG, Medical Solutions
Magnetic Resonance
Henkestr. 127, D-91052 Erlangen
Germany
Telephone: +49 9131 84-0

Siemens **Medical**
Solutions that help